Studies on Some Methods for the Analysis of Power Quality Events

Thesis Submitted by

Kiron Nandi

Doctor of Philosophy
(Engineering)

Electrical Engineering Department
Faculty Council of Engineering & Technology
Jadavpur University
Kolkata, India

2025

Jadavpur University
Kolkata – 700032, India

INDEX NO. 166/19/E

1. **Title of the Thesis :**

   Studies on Some Methods for the Analysis of Power Quality Events

2. **Name, Designation & Institution of the Supervisor :**

   Dr. Sovan Dalai
   Professor,
   Electrical Engineering Department,
   Jadavpur University

1. List of Journal Publications :

- **K. Nandi**, A. K. Das, R. Ghosh, S. Dalai and B. Chatterjee, "Hyperbolic Window S-Transform Aided Deep Neural Network Model-Based Power Quality Monitoring Framework in Electrical Power System," in ***IEEE Sensors Journal***, vol. 21, no. 12, pp. 13695-13703, 15 June15, 2021, doi: 10.1109/JSEN.2021.3071935.

- **K. Nandi**, S. Maur, D. Dey, B. Chatterjee and S. Dalai, "Multisynchrosqueezing Transform aided Transfer Learning based Approach for Diagnosis of Single and Mixed Power Quality Events," in ***Electric Power Systems Research***, ***Elsevier***, 2025. (Accepted)

2. List of Patents :

Nil

3. List of Presentations in National/International Conferences :

- **K. Nandi**, R. Ghosh, B. Chatterjee and S. Dalai, "Identification of Multiple Power Quality Disturbances based on Median Filter," ***2022 IEEE Calcutta Conference (CALCON)***, Kolkata, India, 2022, pp. 273-277, doi: 10.1109/CALCON56258.2022.10060289.

- **K. Nandi**, B. Chatterjee and S. Dalai, "Classification of Power Quality Disturbances using Artificial Intelligence: A Review," ***2023 IEEE 3rd Applied Signal Processing Conference (ASPCON)***, India, 2023, pp. 171-175, doi: 10.1109/ASPCON59071.2023.10395948.

- **K. Nandi**, B. Chatterjee, P. Das, S. Dalai and A. K. Das, "Detection of Multiple Power Quality Disturbances using Stockwell Transform and Convolutional Neural Network in Electrical Power System," ***2023 IEEE 3rd Applied Signal Processing Conference (ASPCON)***, India, 2023, pp. 206-210, doi: 10.1109/ASPCON59071.2023.10396286.

Statement of Originality

I, **Kiron Nandi** registered on **20th June, 2019** do hereby declare that this thesis entitled "***Studies on Some Methods for the Analysis of Power Quality Events***" contains literature survey and original research work done by the undersigned candidate as part of Doctoral studies.

All information in this thesis have been obtained and presented in accordance with existing academic rules and ethical conduct. I declare that, as required by these rules and conduct, I have fully cited and referred all materials and results that are not original to this work.

I also declare that I have checked this thesis as per the "Policy on Anti Plagiarism, Jadavpur University, 2019", and the level of similarity as checked by iThenticate software is 03%.

Kiron Nandi

(Signature of Candidate)

Date : 11.12.2025

Certified by Supervisor:

11.12.2025

(Signature with date, seal)

Dr. Sovan Dalai
Professor
Electrical Engineering Department
Jadavpur University
Kolkata-700032

Certificate from the Supervisor

This is to certify that the thesis entitled "***Studies on Some Methods for the Analysis of Power Quality Events***" submitted by **Shri Kiron Nandi**, who got his name registered on **20th June, 2019** for the award of Ph. D. (Engg.) degree of Jadavpur University is absolutely based upon his own work under the supervision of **Prof. Sovan Dalai** and that neither his thesis nor any part of the thesis has been submitted for any degree/diploma or any other academic award anywhere before.

11-12-2025

Signature of the Supervisor
and date with Office Seal

Dr. Sovan Dalai
Professor
Electrical Engineering Department
Jadavpur University
Kolkata-700032

Acknowledgment

The author expresses his sincere appreciation and deep gratitude to his esteemed guide Prof. Sovan Dalai for his invaluable guidance in carrying out the thesis work. The author was allowed to enjoy all the necessary freedom during his work and at the same time the intense supervision by the mentor led the work towards perfection. His moral support, caring personality, untiring endeavor, unparalleled firmness of knowledge and vision, perpetual encouragement and precious advice made the daunting task possible for the author.

The author expresses his deep sense of appreciation to the Head of the Department of Electrical Engineering, Jadavpur University for providing necessary departmental facilities for implementation of this work.

It is the author's pleasure to acknowledge his respected teachers Prof. Biswendu Chatterjee, Prof. Debangshu Dey, Dr. Arpan Kumar Pradhan, Prof. Sivaji Chakravorti and Prof. Kesab Bhattacharya for their advice and encouragement in completing the research work.

The author also wants to acknowledge contributions of Dr. Arup Kumr Das, Mr. Subhajit Maur, Mr. Biswajit Chakraborty and Dr. Abhijit Lahiri in the course of the research work.

The author is thankful to his colleagues Dr. Suhas Deb, Dr. Kaushik Sit, Mr. Rakesh Das, Mr. Sandipan Kumar Paul, Mr. Soumyadeep Maity and Mr. Pradipta Ghosh for providing support in various ways for carrying out the work.

The author would like to express his heart-felt gratitude to all his family members and relatives for their never-ending support and encouragement during the course of the thesis work.

The author also extends thanks to all the members of the High Tension Laboratory of Electrical Engineering Department, Jadavpur University for making it possible to work in a homely atmosphere. Last but not least, the author remains indebted to all the resources that he was fortunate to have during the work.

Niron Nandi

11.12.2025

Dedicated to
My Family
and
Teachers

List of Symbols and Abbreviations

Symbol	Description
$A_c(t)$	Instantaneous amplitude
a_n	Magnitude of n^{th} order harmonic
b_d	Bias vector of decoder
b_e	Bias vector of encoder
d	Reconstruction bandwidth parameter
f_e	Activation function of encoder
f_n	Frequency of n^{th} order harmonic
g_d	Activation function of decoder
$gw(t)$	White gaussian noise
h_i	Feature vector of encoder
L	Window length
m_{noi}	Noise level
η	Frequency-reassignment operator
n_{dt}	Notch depth function
P_p	Polarity mask function
$q(t)$	Sliding window function
u_1	Unit step function
u_2	Unit step function
V_h	Hyperbola
V_{nt}	Notch function
V_{osc}	Oscillation function
$w(t)$	Window function
W_d	Weight matrix of decoder
W_e	Weight matrix of encoder
w_{hyp}	Hyperbolic window
$X(n)$	n^{th} sample of the input signal
$x(n)$	n^{th} peak value of median filter output signal
$x(n)_{min}$	Minimum peak value of median filter output signal
$Y(n)$	n^{th} sample of the output signal
z_i	Reconstructed data
α	Sag decay rate
β	Sag recovery rate
γ	Transient settling time

LIST OF SYMBOLS AND ABBREVIATIONS

γ_{bt}	Backward taper
γ_{ft}	Forward taper
δ	Dirac delta function
ζ_h	Shape parameter
θ_p	Phase angle
λ_c	Positive curvature parameter
ρ	Discrete frequency variable
τ	Dilation factor
$\varphi_c(t)$	Instantaneous phase
$\varphi_c'(t)$	Instantaneous frequency
ω_s	Fundamental frequency

ACO	Ant Colony Optimization
AE	Auto Encoder
ANN	Artificial Neural Network
ANOVA	Analysis of Variance
BP	Back Propagation
CL	Convolution Layer
CNN	Convolutional Neural Network
CVT	Constant Voltage Transformers
CWT	Continuous Wavelet Transform
DAC	Digital to Analog Converter
DenseNet	Dense Convolutional Network
DNN	Deep Neural Network
DT	Decision Tree
DVR	Dynamic Voltage Restorers
EC	Energy Concentration
ELU	Exponential Linear Unit
EPS	Electrical Power System
ES	Expert System
FC	Fully Connected
FL	Fuzzy Logic
FPR	False Positive Rate
FT	Fourier Transform
GA	Genetic Algorithm

GD	Gradient Descent
GNB	Gaussian Naïve Bayes
GNB	Gaussian naïve bayes
HWST	Hyperbolic Window Stockwell Transform
HWST	Hyperbolic Window Stockwell Transform
IF	Instantaneous Frequency
KF	Kalman Filter (KF)
kNN	k-Nearest Neighbor
LCR	Level Crossing Rate
LR	Logistic Regression
MPL	Max Pooling Layer
MSST	Multisynchrosqueezing Transform
M-SVM	Multi-class Support Vector Machine
PQ	Power Quality
PQE	Power Quality Event
PSO	Particle Swarm Optimization
RCT	Relative Computational Time
ResNet	Residual Neural Network
RF	Random Forest
SAE	Stacked Auto Encoder
SST	Synchro Squeezing Transform
SST	Synchro Squeezing Transform
STFT	Short-Time Fourier Transform
STFT	Stockwell Transform
SVM	Support Vector Machine
SVM	Support Vector Machine
T-F	Time-Frequency
THD	Total Harmonic Distortion
TL	Transfer Learning
TVSS	Transient Voltage Surge Suppressor
UPQC	Unified Power Quality Conditioner
VGG	Visual Geometry Group
WT	Wavelet Transform
WVD	Winger Ville Distribution
XGB	XGboost
XWT	Cross Wavelet Transform

Contents

Chapter 5: **Hyperbolic Window Stockwell Transform aided Deep Neural Network Model-based Power Quality Monitoring Framework in Electrical Power System**

Chapter 6: **Multisynchrosqueezing Transform aided Transfer Learning based Approach for Diagnosis of Single and Mixed Power Quality Events**

List of Figures

List of Tables

Chapter 1

Introduction

1.1 Introduction

This research work focuses on the monitoring of multiple Power Quality (PQ) events, which are important for reliable and smooth operation of power utility. An outline of the thesis is described in the following paragraphs before the background and detailed analysis of this work.

Monitoring of Power Quality Events (PQEs) has been carried out in two aspects from the data obtained through the PQEs generation module:

i) Measurement and analysis of PQEs based on signal processing.

ii) Artificial intelligence-based monitoring of PQEs.

The first point reflects the progressive development of signal processing techniques. The second point deals with the artificial intelligence-based monitoring of PQEs through image processing techniques. Both are used in this work for identification and classification of PQEs.

PQ is affected by the occurrence of PQEs in the Electrical Power System (EPS) networks. In order to improve the PQ, the first and foremost requirement is to identify and classify those events. Hence, proper mitigation techniques can be adopted to suppress the detrimental effects of PQEs. It is difficult to identify those events visually. Therefore, a fast and robust technique is required for identification and classification of PQEs. At first, this research work is planning to develop a digital signal processing based technique for analysis of PQEs where minimum human involvement is required. Thereafter, artificial intelligence based automatic method for identifying and classifying PQEs using image processing is introduced. The following are some benefits of using artificial intelligence-based techniques for feature extraction: a) No prior understanding of PQE signal processing is needed. b) The data labeling process has been enhanced. c) Hidden features are extracted while removing the unnecessary ones.

1.2 Background of the Work

1.2.1 Study of Power Quality Events

PQ refers to the reliability and purity of the electricity supply. A deflection from the nominal level of voltage, current and frequency is referred to as PQE. Innovative and expensive equipment in EPS networks has completely changed the load environment. These new types of loads are considered the main sources of PQEs. The incorporation of renewable energy sources into EPS networks has also increased the occurrence of PQEs [1]. These PQEs include flicker, sag, swell, harmonic, notch, transient and noise [2]. Numerous issues have arisen as a result of these events, including the failure of circuit breakers, relays and digital equipment as well as the damage of expensive equipment like computers and delicate microprocessor-based devices. Therefore, PQE detection is essential for both preventative and remedial actions. Thus, according to international standards (IEEE Std 1159-2019), identifying the aforementioned PQEs is crucial [3]. As a result, various features are extracted from the PQE signals. To choose the most suitable features for PQE identification and classification, a sufficient understanding of feature extraction methods is needed. Compared to traditional approaches, automated feature extraction using image processing is more efficient [4]. Thus, automated feature extraction approaches from image processing and artificial intelligence-based classification algorithms have been applied in this research. These techniques are suggested as effective ways to classify PQEs with the least amount of error. Hardware-based controllers may be used in online applications to accomplish these techniques.

Some methods and procedures for classifying PQEs are discussed in [5, 6]. Techniques for detecting and classifying PQEs with noise are addressed in [7]. In EPS, wavelet-based feature extraction methods are covered in [8, 9]. A summary of signal processing and artificial intelligence methods for PQE classification is presented in [10]. Machine learning-based methods are reviewed in [11]. A strong basis for PQE monitoring using image processing was supplied by the extant research. Therefore, this study proposes the use of image processing and artificial intelligence methods to detect and classify PQEs.

1.2.1.1 Causes of Power Quality Events

There are three main causes of PQEs: i) fault conditions and/or load characteristics, ii) switching operations and iii) waveform distortions. Fault conditions cause short-duration voltage changes, including interruptions, sags and swells. Sags and swells can also happen when large loads are turned on or off. Current fluctuations in load are the primary cause of flickers. During flickers, the voltage changes randomly. Transients are mainly caused by lightning or switching operations. The transient is classified as impulsive or oscillatory. Waveform distortions cause issues like harmonics, notches, DC offsets and noises. Harmonics and notches are caused by the non-linear behavior of power electronic devices. Electromagnetic interference from electrical appliances creates noises into the power supply. Several PQE types are shown in Figure 1.1.

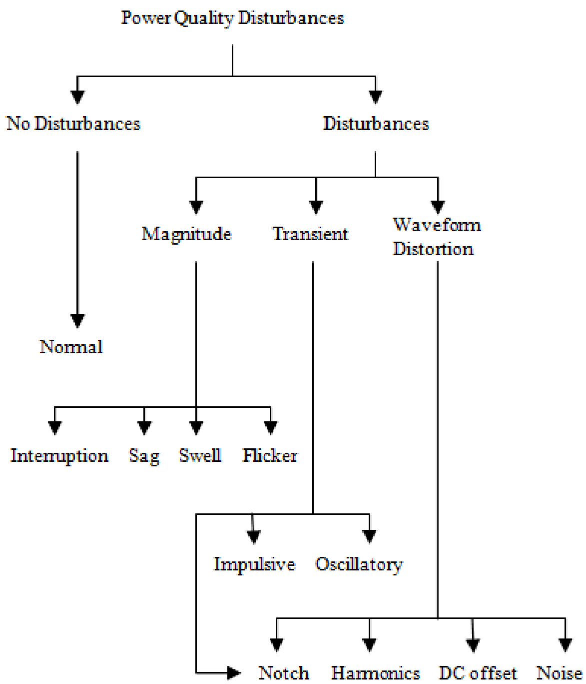

Figure 1.1 Different types of PQEs.

1.2.1.2 Effect of Power Quality Events

PQ ensures that the electrical equipment operates without interruptions, malfunctions or damage. Economic considerations are the main driver behind PQ monitoring. PQEs have a detrimental effect on sensitive electrical equipment, resulting in a shorter equipment lifespan. Short-duration voltage fluctuations cause protective systems to alarm unnecessarily, data processing device to fail and sensitive equipment to get damaged. Long-duration interruptions stop all equipment and ongoing automated processes from working. Transient affect the insulation of equipment. Harmonics cause more energy loss in machines and capacitors, overheating of conductors and cables, accidental activation of protective devices and malfunction of equipment. Noise affects the performance of the delicate devices and leads to more data loss.

1.2.1.3 Corrective Measures of Power Quality Events

PQEs are compensated using various kinds of compensating devices. Constant Voltage Transformers (CVT) and Dynamic Voltage Restorers (DVR) are used to enhance power supply quality by preventing unusual voltage rise and dips. These two devices help to keep the voltage steady at the load terminals. A Transient Voltage Surge Suppressor (TVSS) lowers the overvoltage to a safe level and diverts the surge. Unwanted harmonics and noise are removed from the power supply using harmonic and noise filters. Static VAR Compensators control reactive power in EPS networks to maintain the voltage constant. A Unified Power Quality Conditioner (UPQC) is a combination of series and shunt power converters used to compensate harmonics.

1.2.2 Analysis of Power Quality Events

To analyze PQEs in EPS networks, the first and most important step is identifying them so that suitable mitigation strategies can be applied. If these events are not properly reduced, various electrical devices needed to supply clean and reliable electricity to consumers may malfunction or stop working. PQEs are difficult to identify by visual inspection. Many PQEs can happen at the same time and overlap with each other. Therefore, development of multiple PQEs detection and categorization method is necessary. Several methods and strategies for identifying and classifying single and multiple PQEs are discussed in the literature. Identifying and classifying PQEs involves two main approaches: analysis based on signal processing techniques and artificial intelligence techniques.

1.2.2.1 Analysis based on Signal Processing Techniques

Signal processing techniques involve two primary processes: monitoring power signals and extracting their events. The extracted events are compared with recorded PQE to identify the specific PQE. The literature explores digital signal processing techniques for identifying PQEs.

In recent past, the Fourier Transform (FT) has been used to detect PQEs in stationary periodic signals. The primary drawback of FT is that it only gives information about the frequency. It does not provide any information about when the PQEs occur [12, 13]. Since the majority of PQE signals are transitory and non-stationary, FT is unable to produce meaningful findings. Short-Time Fourier Transform (STFT) [14, 15] and Wavelet Transform (WT) [16, 17, 30, 31] have been introduced to solve this problem. The time-frequency resolution issue is handled with STFT. To detect magnitude fluctuations, STFT focuses on a specific time period using a defined window size. As a result, it is used to various non-stationary and transitory PQE signals to some extent. PQE signals of the harmonics type can be understood more easily with a fixed window size across all frequencies, while PQE signals of the transient type cannot be well resolved in terms of time-frequency. WT solves this issue by using multiresolution analysis. In this process, PQE signals are examined using different frequency components. As a result, WT is widely utilized in PQE research. To detect PQEs, a combination of rule-based and wavelet-based hidden Markov models is presented in [17]. Time-based and frequency-based PQEs are identified using rule-based and wavelet-based models, respectively. However, WT is sensitive in noisy environments.

The enhanced version of continuous WT is known as the S-transform. In [18], a rule-based classification method for classifying PQEs utilizing the S-transform is discussed. PQEs categorization based on probabilistic neural networks and the S-transform is reported in [19]. In [20], PQE classification using logistic model trees and the S-transform is proposed. These methods require fewer features, so they use less memory and processing time. S-transform and a hidden Markov model are employed in [21] to classify PQEs. The number of data signals for training and testing is determined by the hidden Markov model. A discrete orthogonal time-frequency method for analyzing PQEs was introduced in [22]. It indicates a more effective method for detecting PQEs. For voltage sag detection, a modified S-transform based on window selection is employed in [23]. In [24], a hybrid S-transform is presented for the real-time categorization of numerous PQEs. An S-transform using a Kaiser window is proposed in [25] and provides the best frequency detection for multiple PQEs compared to other methods. PQEs are classified in [26] via Gaussian window parameter modification. In [27], a fast generalized S-transform based on adaptive window is presented. Where, window cropping and frequency scaling minimize computing time. To get the best time-frequency spectrum compared to earlier methods, a modified S-transform combined with random forests classifier is proposed in [28]. The S-transform can detect PQEs with good temporal resolution; however, it cannot analyze PQEs at high frequencies with acceptable results.

1.2.2.2 Contributions of the Present Work in Relation to Signal Processing Techniques

Power supply signals corrupted with single and multiple PQEs are identified and classified using signal processing based techniques. Generated PQE signals from the experimental setup are analyzed using median filter [29]. Spikes are removed from the PQE signals using median filter. Thereafter, quantitative indicators are introduced to detect the PQEs. Alternatively, discrete Fourier transform based feature extraction and median filter-based classification techniques are also discussed in this thesis. Results show that the methods can effectively detect the PQEs with 96.7% and 99.61% accuracy, respectively with less computational time compared to the other conventional classifiers and complex mathematical tools. Furthermore, the suggested approach operates satisfactorily under noisy conditions, frequency variations and with practical data collected from local power utilities. The structure of these methods is simple and straightforward, therefore they can be implemented in online EPS networks.

1.2.2.3 Analysis based on Artificial Intelligence Techniques

PQEs are automatically classified using artificial intelligence techniques. Thus, researchers are interested in artificial intelligence based PQE detection systems. The artificial intelligence-based classification process for PQEs is divided into five stages: input, feature extraction, feature selection, classification and identification as shown in Figure 1.2. PQE signals are created at the input stage. In the subsequent phase, distinct features are extracted from the PQEs. To lessen the computational load and time, the less important features are eliminated in the third step after the best features are selected using optimization techniques. Artificial intelligence based automated classification methods are introduced in the next phase. In the last phase, definitive decisions are made. In different literatures, different approaches are used to automatically categorize PQEs in each of the aforementioned stages. Effective tools for artificial intelligence approaches include Artificial Neural Networks (ANNs), Convolutional Neural Networks (CNNs), Support Vector Machines (SVMs), Fuzzy Logic (FL) and Expert System (ES).

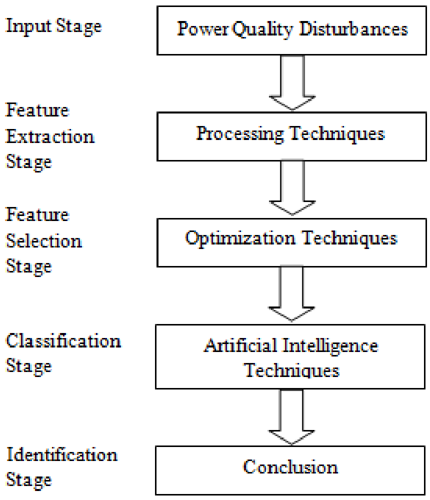

Figure 1.2 Different stages of PQEs classification.

The ANNs are influenced by the biological nervous system. The theory and real-world application of a wavelet-based neural classifier were reported by the authors in [30, 31], respectively. Here, feature extraction is done using WT. The neural classifier receives inputs from extracted features. In [32], multiwavelet-based neural networks are used to identify transients. In [33], independent component analysis is presented as a technique for feature extraction and neural networks are used for classification. In [19], the probabilistic neural network-based classifier is presented. It reflects a satisfactory outcome. In [34], multiresolution analysis is used as a feature extraction method and neural networks are used for automated categorization.

Wavelet energy entropy is utilized in [35] to extract features and backpropagation-based ANNs are employed as a classifier.

Multi-fusion CNNs can automatically identify various PQEs by mixing time and frequency components. This is demonstrated in [36], where 24 distinct classes of PQEs are identified with an accuracy of 99.26%. In [37], deep convolutional networks with a one-dimensional enhanced residual network structure are presented for 99.1% accurate PQE identification and classification, along with improved capacity for generalization. To categorize 24 single and multiple PQEs, a multi-fusion CNN combining CNN-GRU, ResNet-GRU and Inception-GRU networks is employed in [38].

Since, it is not mandatory to have sufficient understanding of PQE signals processing and feature extraction techniques, image processing-based PQE detection has grown in popularity in the present era. In [39], a PQE signal is transformed into an image with the aid of Wigner-Ville distribution approach. CNNs are then used for PQE classification of 9 different classes with 99.67% accuracy. Subsequently, the image's features are automatically extracted using CNNs. A greyscale image that combines spectral and temporal representation of the signal is presented in [40]. After that, CNNs are used to classify 29 different classes of PQE with an accuracy of 97.84%. Here, the greyscale image processing method helps to reduce the calculation time. Image processing and a modified CNN-based algorithm are used in [41] to detect multiple PQEs with an accuracy of 96.55%. Here, the lack of feed-forward networks helps to save substantial computing resources. In [42], a bagged tree classifier achieving 96.3% accuracy for 9 single and multiple PQEs is described. PQEs are identified in [43] using the 3-D plot of S-transform and SVMs.

A fuzzy-expert system with WT and FT is discussed for the automatic classification of PQEs in [44]. The method shows that the fuzzy-expert system classified PQEs efficiently. In [45], fuzzy reasoning with WT is applied for PQEs recognition. In [46], the Kalman filter (KF) combined with discrete WT is proposed for feature extraction. Extracted features are applied to the input of fuzzy-expert system. PQE signals are used as input to the discrete WT to identify the noise. The noise covariance is applied to the KF to maximize the convergence rate. Then the output of KF is fed into the input of the fuzzy-expert system to recognize the PQEs.

The SVMs are convincing tool for automatic classification. Multiclass SVMs classifier is introduced by combining two SVMs. Multiclass SVMs classifier is used for PQEs detection. In [47], improved time-frequency localization is achieved using double resolution S-transform and directed acyclic graph SVMs. Fixed parameter values may reduce the performance of classification for multiple PQEs. This is overcome by using optimized S-transform as in [48] with kernel SVMs. A cubic SVM-based classifier with 99.72% accuracy is used to classify 7 single PQEs in [49]. In [50], quadratic SVMs are presented to classify PQEs automatically.

1.2.2.3.1 Optimization Techniques

Optimization techniques are used to assess the extracted features. To free up more memory, the top features are selected for additional examination, while the remaining features are removed from the system. As a result, the computation time is shortened. The feature extraction procedure is crucial because the accuracy of the approach depends entirely on the features that are selected. The most popular optimization strategies for suitable feature selection and raising classification accuracy are Genetic Algorithm (GA) [51, 52], Particle Swarm Optimization (PSO) [53-55] and Ant Colony Optimization (ACO) [56]. Non-linear optimization problems are solved using GA. GA is used to track the best features for the inputs of the classifier in [51]. The leading features from the wavelet packet transform are chosen by GA. After that, the features are used as inputs to the SVMs based classifier [52]. In [53], for optimal feature selection, an optimization strategy based on PSO is employed. PSO is used in [54] to identify membership functions of fuzzy systems for both single and multiple PQEs. In [55], S-transform and fuzzy-expert system are employed to identify PQEs. Here, Gaussian and trapezoidal membership functions of fuzzy-expert system are obtained from PSO technique. In [56], a hybrid ACO technique followed by fuzzy C-means clustering algorithm is suggested. Extracted features from ACO technique are fed into the input of the time-time transform for event signals pattern classification.

1.2.2.4 Contributions of the Present Work in Relation to Artificial Intelligence Techniques

This work also presents an automatic classification of single and multiple PQE signals. An important part of the automatic PQE classification process is performed by feature extraction algorithms. It is essential that the feature extraction approach and the classification technique work together. In [57], PQEs are transformed into time-frequency grey scale images using S-transform. Thereafter, those images are used as input to the customized CNN architecture for feature extraction as well as for classification purposes. This architecture is effectively detects the PQEs with 99.83% accuracy. In [58], PQE signals are converted into images using hyperbolic window Stockwell transform. After that, deep neural networks are used for feature extraction and the XGboost classifier is used to classify 18 different PQEs with 99.86% accuracy. In chapter 6, a total of 36 (9 single and 27 multiple) PQEs are classified with 99.58% accuracy. Multisynchrosqueezing transform-based image processing, pretrained CNN architectures-based features extraction approaches and an SVM classifier are discussed.

1.2.3 Importance for Analysis of Power Quality Events

It is beneficial for the researchers to have a thorough analysis of PQE identification and classification methods from the literature. A review of the literature reveals that research activities for the identification and classification of PQE occurrences may be split into three categories. First, in order to improve accuracy and reduce processing time, the researchers have concentrated on feature extraction algorithms. Second, researchers are focused on increasing the number of PQEs that the particular algorithm will identify. Third, accurate identification and classification must be maintained while handling noisy data from EPS. Keeping these factors in mind, a discussion of the methods and strategies for identifying and classifying PQEs is provided in this thesis. It reveals that various methods for feature extraction, optimization and classification are effective in identifying and classifying different types and quantities of single and multiple PQEs. However, in the simulated and real-time contexts, image processing and artificial intelligence-based feature extraction approaches are the most effective combination for PQEs identification.

1.3 Organization of Thesis

Different PQEs (sag, swell, flicker, transient, notch, harmonics and noise) are briefly discussed in Chapter 2. These PQEs are included in this thesis work. Due to the lack of real life PQEs data, the data are generated as per IEEE Std 1159-2019 [3] using an experimental setup in Chapter 2.

The main objective of PQ monitoring is to identify both single and multiple PQEs. So that proper mitigation techniques can be implemented. Median filter-based techniques and quantitative indicator-based approaches are discussed in Chapter 3. Median filter-based techniques are used for feature extraction and quantitative indicator-based approaches are used for identification. Alternatively, discrete Fourier transform based feature extraction and median filter-based classification techniques are also covered. The performances of the proposed methods show that the identification process requires less computational time. Hence, these are suitable for online applications in PQ monitoring.

Chapter 4 of this thesis presents an automatic detection method using S-transform and convolutional neural networks for both single and multiple PQEs. The S-transform converts the PQE signals into time-frequency grey scale images. CNNs are used for feature selection and classification.

In Chapter 5, single and multiple PQE signals are analyzed in the time-frequency domain using the hyperbolic window Stockwell transform. A DNN is designed using three autoencoders to extract deep features from the hyperbolic window Stockwell transform matrices. These extract features are used as input to the different classifier. According to the results, the XGboost classifier provides the best classification accuracy. The method also performs well under varying frequencies and noisy conditions. It also shows acceptable results with real-life PQE data. Therefore, this method can enhance the reliability of an EPS networks.

In Chapter 6, a total of 36 PQEs (9 single and 27 multiple) are diagnosed. PQE signals are converted into time-frequency images using the multisynchrosqueezing transform. Thereafter, different pretrained CNN architectures are used to extract features from multisynchrosqueezing transformed images. These extract features are fed into the different classifier. Results show that the VGG16 based automated features extraction with an SVM based classifier gives the best accuracy compared to the existing state-of-the-art techniques. The technique has also been tested in noisy environments and with real-life PQ scenarios.

The summary of the research work and the future scope are presented in the conclusion.

1.4 Originality of the Thesis

The following are the original contributions of the present work as per the best of knowledge of author:

i) Development of median filter-based techniques which are capable of identifying and classifying single as well as multiple PQEs. In these methods, a median filter along with various quantitative indicators is introduced for the identification and discrete Fourier transform aided median filter-based technique is used for diagnosis of PQEs in EPS networks.

ii) Development of an S-transform aided customized CNN scheme for detection of single and multiple PQEs.

iii) Development of a hyperbolic window Stockwell transform aided deep neural network model-based PQ monitoring framework in EPS networks.

iv) Development of a multisynchrosqueezing transform aided transfer learning-based approach for diagnosis of single and multiple PQEs.

Chapter 2

Power Quality Events and Experimental Setup

2.1 Introduction

Power Quality (PQ) is a measure of the power supply's reliability and quality. It guarantees the uninterrupted, error-free and damage-free operation of electrical equipment. Power Quality Event (PQE) is the term used to describe a deviation from the nominal voltage, current and frequency levels. Common PQEs include sag, swell, flicker, transient, notch, harmonics and noise. In general, the power supply signal may be affected by these events. Electrical equipment may malfunction if any of these events exceed specific thresholds. Therefore, PQEs data are needed to study their impact. Due to the paucity of practical PQEs data; they are generated in the laboratory using an experimental setup, as guided by IEEE Std 1159-2019 [3]. Before generating PQE signals, this chapter discusses each PQE and its standard limits.

2.2 Brief Description of Different Power Quality Events

Normal: A power supply signal with a RMS voltage of 230V is called normal RMS voltage. The standard value of normal voltage depends on the country. In India, it is 230V/50Hz.

Transients: Transients are short-duration pulses of high magnitude. They are divided into two types: impulsive or oscillatory. An impulsive transient is a sudden change in voltage or current with a non-power frequency and one-directional polarity. Lightning is the main cause of impulsive transients. It is characterized by rise time and decay times. Figure 2.1 displays a PQE signal with an impulsive transient. An oscillatory transient is a quick change in polarity that reverses back and forth. Switching operations are the main cause of oscillatory transient. It is characterized by magnitude, frequency and duration.

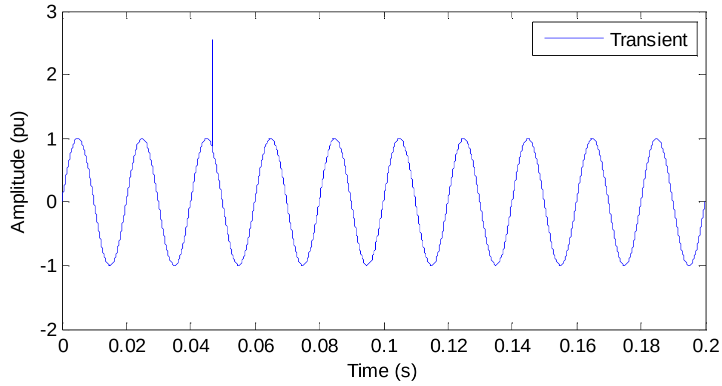

Figure 2.1 Generated PQE signal with impulsive transient.

Sag: Sag is a sudden drop in voltage magnitude ranging from 10% to 90% of the normal voltage level. The duration of sag is from 0.5 cycles to 1 minute. Sag is caused by switching on large loads or heavy motors and by faults in the Electrical Power System (EPS) networks. Figure 2.2 displays the generated PQE signal with sag.

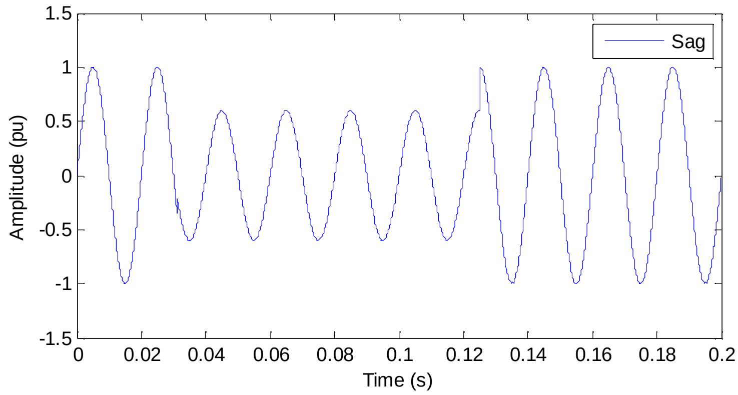

Figure 2.2 Generated PQE signal with sag.

Swell: Swell is a sudden rise in voltage magnitude ranging from 10% to 80% above the normal voltage level.The duration of swell is from 0.5 cycles to 1 minute. Swell is caused by switching off large loads or heavy motors and by connecting large capacitor banks. Figure 2.3 displays the generated PQE signal with swell.

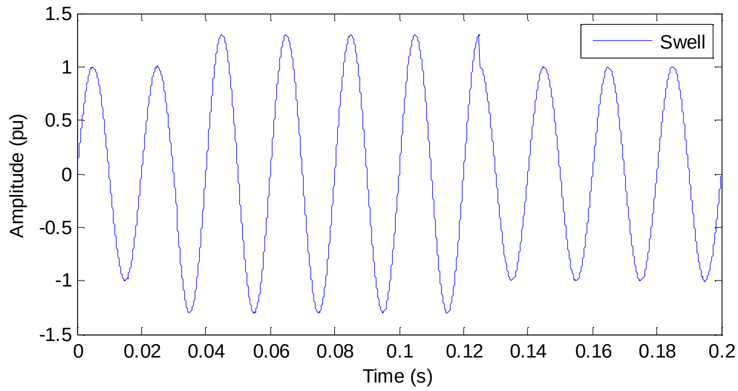

Figure 2.3 Generated PQE signal with swell.

Flicker: Flicker refers to random voltage fluctuations between 0.95 p.u. and 1.05 p.u. of the normal voltage level. Current variations in load are the cause of flicker. Arc furnaces are the prime cause of flicker. Elevator operations also inject flicker into EPS networks. Flicker has frequencies in the range of 6-8 Hz. Figure 2.4 displays the generated PQE signal with flicker.

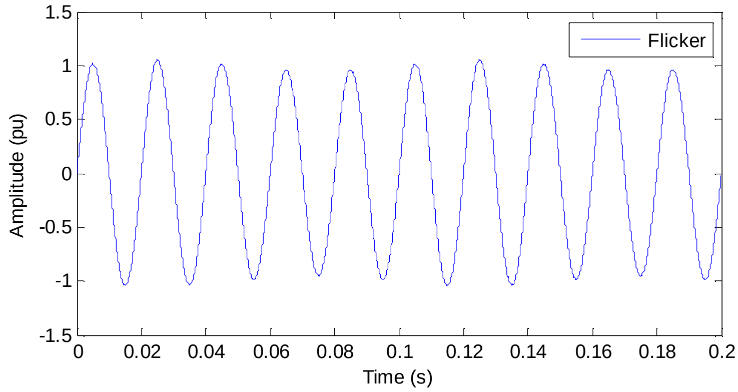

Figure 2.4 Generated PQE signal with flicker.

Harmonics: A voltage or current signal containing integer multiples of the fundamental frequency is known as harmonics. The standard power supply signal frequency, called fundamental frequency, is 50Hz in India. Devices based on power electronics are the main cause of harmonics. Switching mode power supplies, rectified inputs, pulse-width modulated inverters, regenerative drives and rotating machines are the major contributors of harmonics. Harmonic distortions are measured using Total Harmonic Distortion (THD). Figure 2.5 displays the generated PQE signal with harmonics.

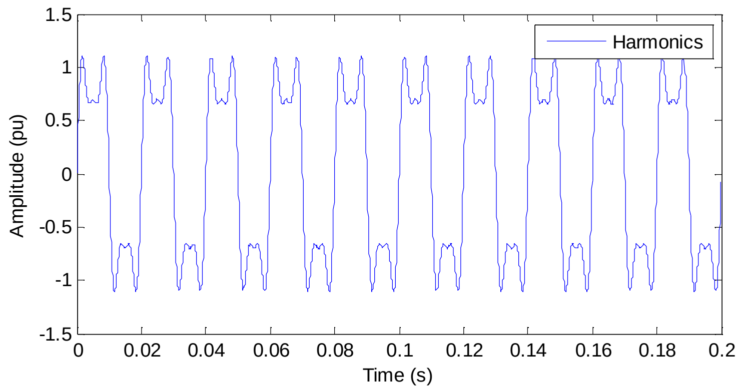

Figure 2.5 Generated PQE signal with harmonics.

Notch: A notch is a periodic sharp change in voltage magnitude. Notches are caused by the non-linear characteristics of power electronics equipment, especially when current is transferred (commutated) from one phase to another. Notch has a high frequency component. Figure 2.6 displays the generated PQE signal with notch.

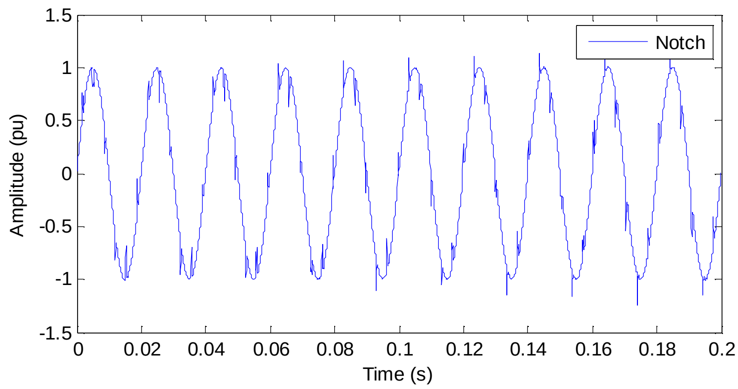

Figure 2.6 Generated PQE signal with notch.

Interruption: An interruption is a drop in voltage magnitude to less than 10% of the normal voltage level. The duration of interruption is less than 1 minute. Interruptions are caused by faults in EPS networks, equipment failures and control malfunctions.

Noise: Noise refers to unwanted electrical signals with frequencies below 200 kHz and magnitudes less than 1% of the normal voltage level. These signals are superimposed on the power supply signal. Noise is caused by power electronic devices, arcing equipment, loads with solid-state rectifiers, switching and improper grounding.

2.3 Generation of Power Quality Events

2.3.1 Mathematical Models

PQE data are obtained from different EPS networks either through long-term continuous monitoring or directly from recorded data at power stations. In this case, only utility engineers can access the restricted PQE data. Therefore, researchers have developed different PQE signals using that specific mathematical model of PQEs because the data collection process is time-consuming and practical data are scarce. The mathematical models of PQEs are created based on IEEE Std 1159-2019 [3] as an alternative to practical PQE data. The mathematical models of single PQEs are stated in Table 2.1 and 2.2. Multiple PQEs are generated by adding two mathematical models representing different single PQEs. The simulated PQEs are somewhat different from practical PQEs data. Therefore, noise (with an SNR value of 30 dB) is added to both single as well as multiple PQEs to make them closely resemble practical data.

Table 2.1: Mathematical models for simulated PQEs generation

PQEs	Causes	MathematicalModels	Parameters
Transient	Capacitor bank charging	$V_{trch} = \sin(\omega_s t + \theta_p) + [\mu_1 \times p \times \sin(2\pi f_{tr} t_1) e^{\gamma t1}$	p≤4 f_{tr}≤5 kHz
	Lightning stroke	$V_{trLs} = \sin(\omega_s t + \theta_p) + [\mu_1 \times p \times e^{\gamma t_1}]$	
	Line energizing	$V_{trLE} = \mu_1 \sin(\omega_s t + \theta_p) + [\mu_1 \times p \times \sin(2\pi f_{tr} t_1) e^{\gamma t_1}$	
Sag	Induction motor starting	$V_{sagst} = [1 - p\{\mu_1(1 - e^{-\alpha_s t_1}) + \mu_1(p_r \sin(\omega_s t_1)\, e^{-\gamma_s t_1} - \mu_2(1 - e^{-\beta_{t_1}})\}]\sin(\omega_s t + \theta_p)$	u_1, u_2 = unit step functions α=sag decay rate β= sag recovery rate 0.1≤ p ≤0.9 γ= transient settling time
	Transformer energizing	$V_{sagTE} = [1 - p\{\mu_1(1 - e^{-\alpha_s t_1})\}] sin(\omega_s t + \theta_p)$	
	0Line fault	V_{sagLF} = [1-p $(\mu_1 - \mu_2) \sin(\mu_1 - \mu_2) \sin(\omega_s t + \theta_p)$	
Swell	Fault due to adjacent phase	$V_{swell} = [1 + p(\mu_1 - \mu_2) \sin(\omega_s t + \theta_t)$	0<θ_p<360° 1.1≤ p ≤1.8

Table 2.2: Mathematical models for simulated PQEs generation

PQEs	**Causes**	**MathematicalModels**	**Parameters**
Flicker	Wind firm and electric furnace	$v_{fl} = [1 + p * \sin(2\pi f_{ft} t + \theta_{fl}) \sin(\omega_s t + \theta_p))$	ω_s= fundamental frequency f_{fl} ≤10Hz p≤0.03 θ_p=phase angle
Harmonics	Non-linear load	$V_{ham} = \sin(\omega_S t + \theta_P) + [\sum a_n \times \sin(2\pi f_n t + \theta_n)]$	f_n=frequency of nth order harmonic n>1 a_n = magnitude of nth order harmonic
Notch	6 pulse 3 phase rectifier	$V_{notch} = \sin(\omega_s t + \theta_p) + [n_{dt} \times V_{osc} \times V_{nt} \times P_p] V_{notch}$	n_{dt}=notch depth function V_{osc}= oscillation function P_p = polarity mask function V_{nt}=notch function
Noise	Electromagnetic interference	$V_{noi} = \sin(\omega_s t + \theta_p) + [m_{noi} \times gw(t)]$	m_{noi}=noise level (%) $gw(t)$=white gaussian noise

2.3.2 Experimental Setup for Power Quality Events Generation

It is observed that simulated PQE data always differ from actual PQE data. Therefore, it is preferable to analyze PQEs using actual data. To achieve this, a specially-designed experimental setup has been developed to more closely resemble with practical data. Using mathematical models and an experimental setup based on [2, 59], PQEs within the power supply signals are produced. Figure 2.7 displays the schematic diagram of the experimental setup. Simulated PQE data are generated using MATLAB© on a computer using the mathematical models. The waveform generator receives digital input from the computer and converts it to analog data. The waveform generator has two sections: the first is a microcontroller and the second is a Digital to Analog Converter (DAC). The microcontroller adjusts the sampling rate of digital data and sends it to DAC. The DAC then convert the digital data into analog data which is sent to the analog data processing stage. A bipolar output is created by properly processing the analog data in the analog data processing stage. However, the output voltage is relatively low. Therefore, to increase the output from the data processing stage, a step-up transformer is used through a driver stage. The primary of the step-up transformer gets sufficient current from the driver stage. The transformer may step up the secondary voltage to almost twice the normal voltage during a swell operation.

To generate transients, some additional hardware components are required. By integrating a pulse transformer into the pulse generator stage of the experimental setup, transients are produced. Simulated transients are generated using MATLAB© in a computer and loaded into the microcontroller via USB. The microcontroller output is connected in series with the secondary of step-up transformer through the pulse generator stage and pulse transformer. Consequently, transients are generated at the output along with other PQEs. Details on the experimental setup are provided in [2, 58].

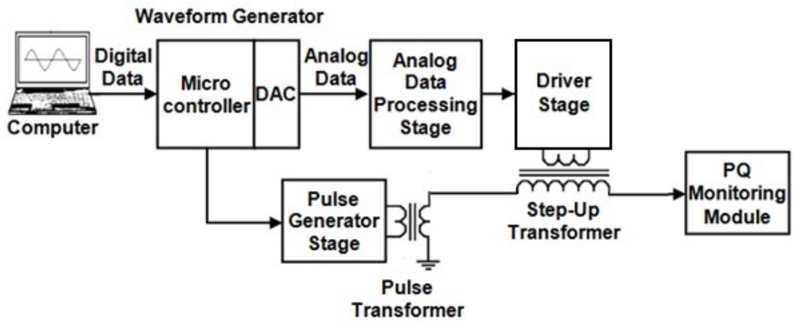

Figure 2.7 A schematic of the experimental set-up.

Figure 2.8 shows the photograph of the experimental setup and Figuer2.9 displays the generated PQE signal (sag) on the oscilloscope.

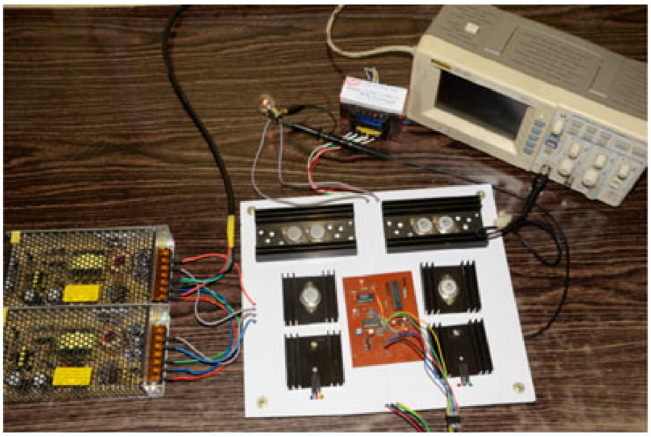

Figure 2.8 Experimental setup for PQEs generation [2].

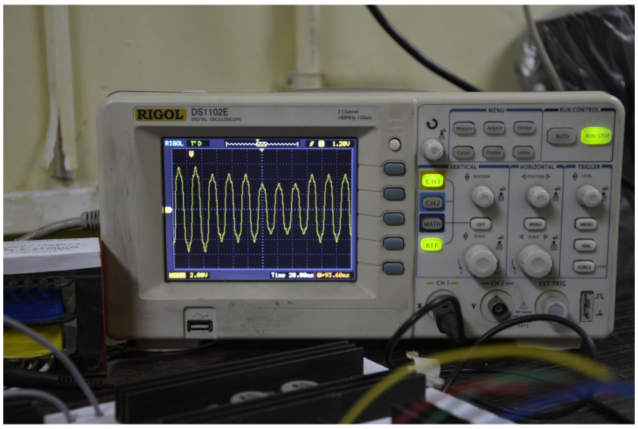

Figure 2.9 Generated PQE signal (sag) on oscilloscope [58].

Figure 2.1 to 2.6 displays the generated single PQE signals, while Figure 2.10 to 2.21 displays the different generated multiple PQE signals obtained from the experimental setup.

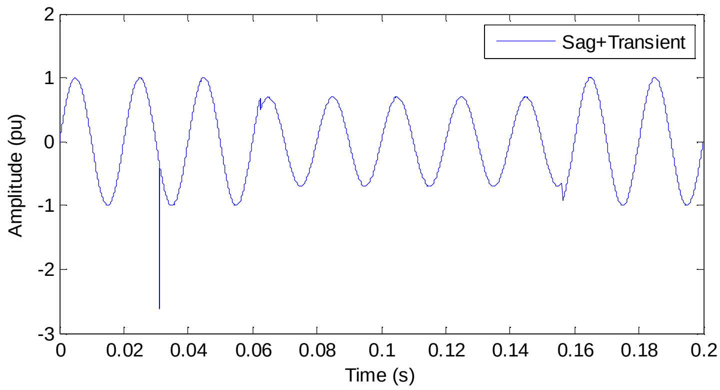

Figure 2.10 Generated PQE signal with Sag and Transient.

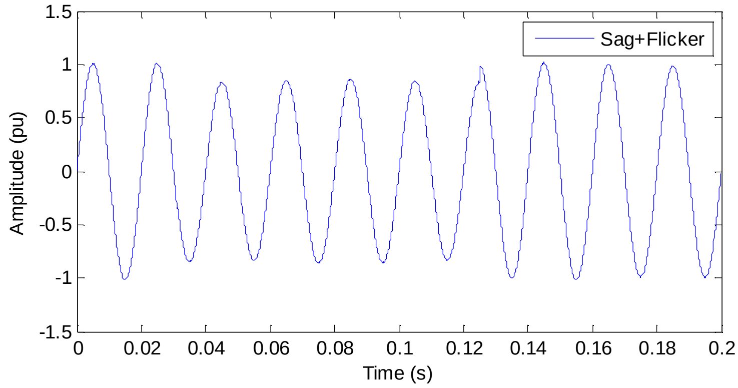

Figure 2.11 Generated PQE signal with Sag and Flicker.

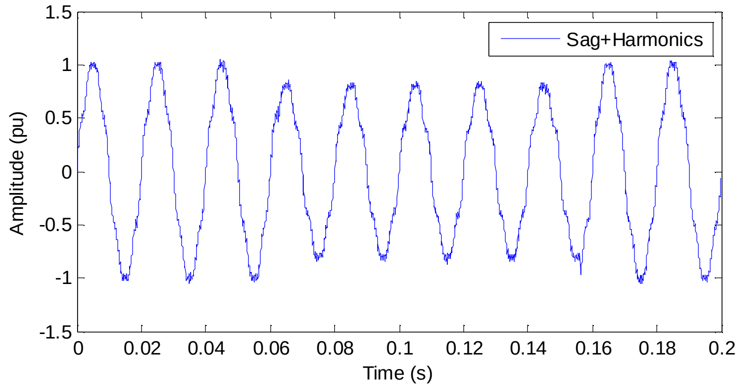

Figure 2.12 Generated PQE signal with Sag and Harmonics.

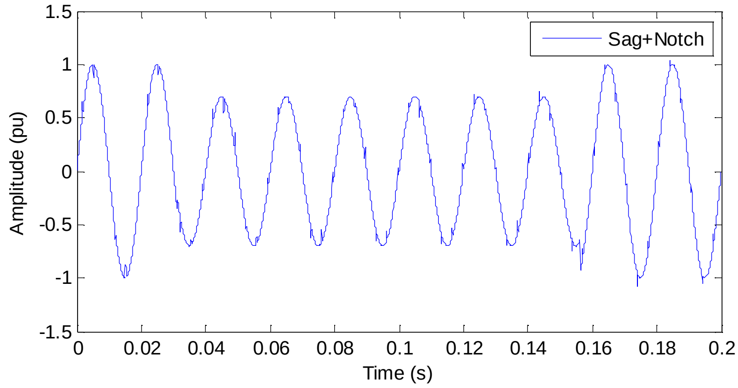

Figure 2.13 Generated PQE signal with Sag and Notch.

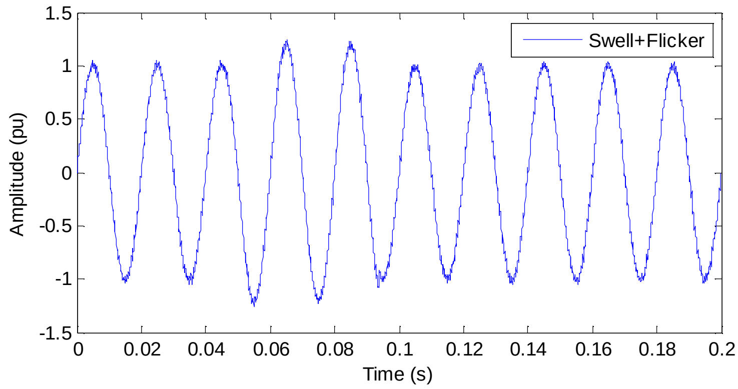

Figure 2.14 Generated PQE signal with Swell and Flicker.

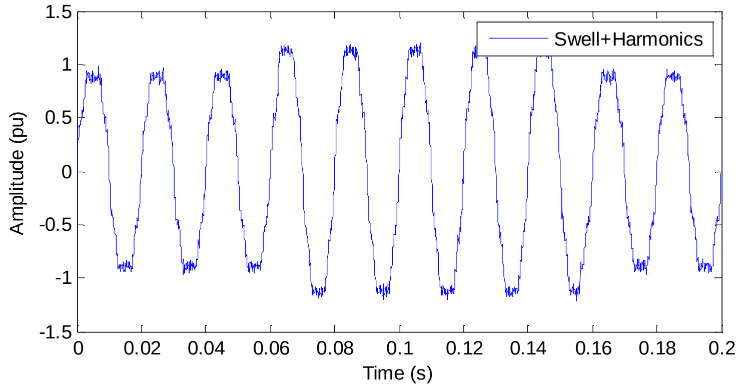

Figure 2.15 Generated PQE signal with Swell and Harmonics.

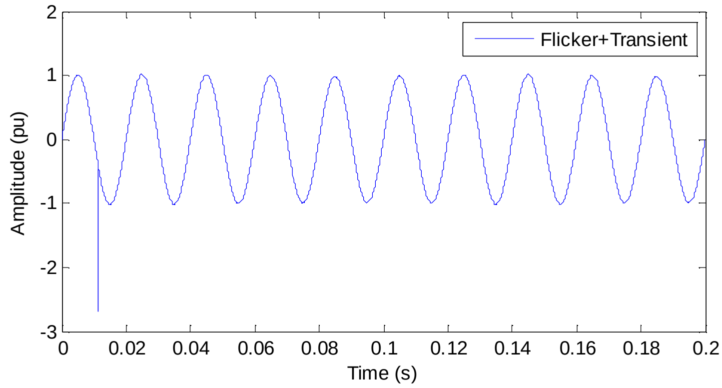

Figure 2.16 Generated PQE signal with Flicker and Transient.

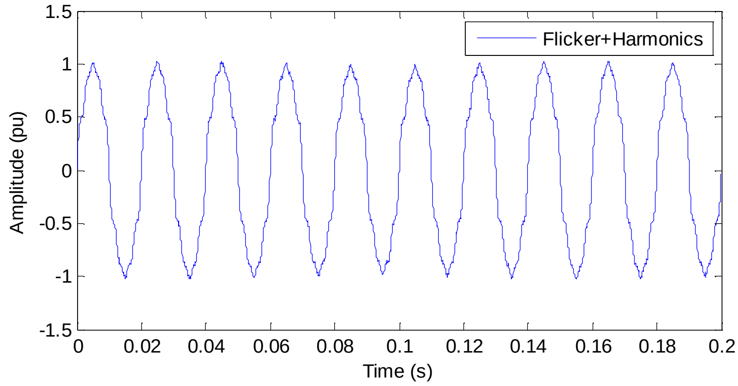

Figure 2.17 Generated PQE signal with Flicker and Harmonics.

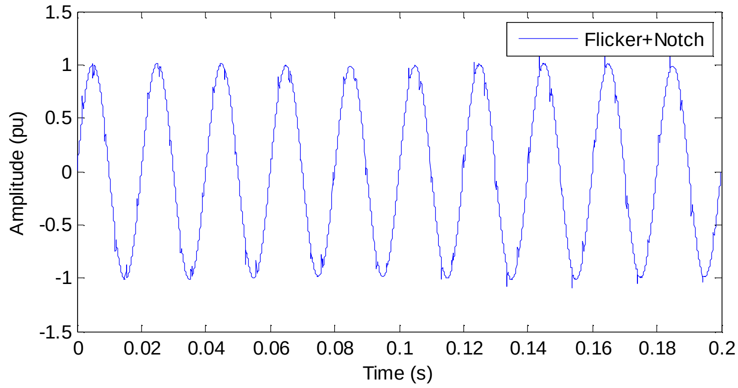

Figure 2.18 Generated PQE signal with Flicker and Notch.

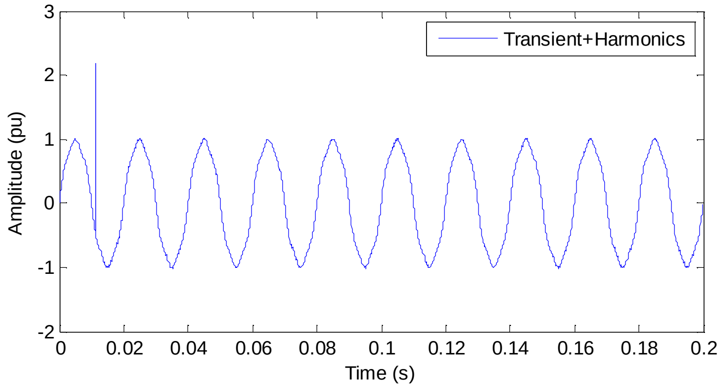

Figure 2.19 Generated PQE signal with Transient and Harmonics.

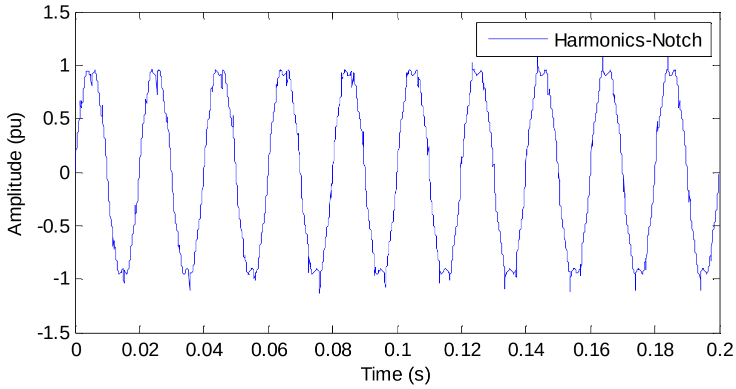

Figure 2.20 Generated PQE signal with Harmonics and Notch.

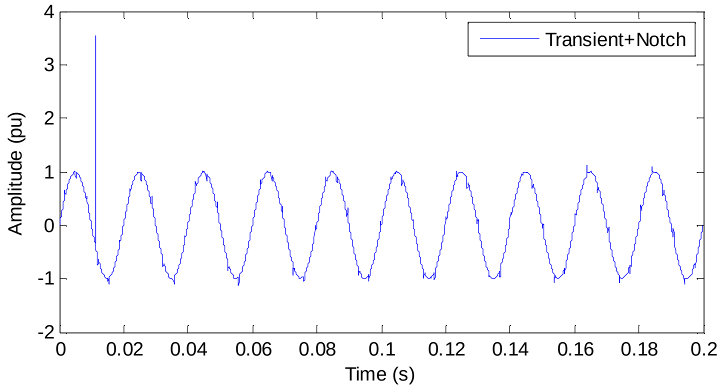

Figure 2.21 Generated PQE signal with Transient and Notch.

2.4 Summary

This chapter discusses the major PQEs and their limits. Those events commonly contaminate the power supply signal in EPS networks. The analysis of PQEs requires PQE data. This chapter also discusses the generation of single and multiple PQE data using the experimental setup.

Chapter 3

Identification of Multiple Power Quality Events based on Median Filter

3.1 Introduction

An important aspect of any electrical power supply system is Power Quality (PQ). The quality of service is significantly reduced by power supply events such as transient, notch, flicker, harmonics, sag and swell. The increasing use of microprocessor-based and power electronics-based technology in appliances and equipment is a major cause of these interruptions. In addition to these, electrical risks such as contact with live components, equipment malfunctions and heavy load switching also reduce PQ. Low PQ not only causes appliance and equipment failures and reduces power supply performance, but also increases system losses and financial costs. Therefore, the first and most important step in improving PQ is to identify the Power Quality Events (PQEs).

Several approaches have been proposed for identifying PQEs. Wavelet transform-based techniques for PQE identification have been widely used in recent past [30, 60]. In [61], PQE monitoring method using S-transforms is proposed. Different feature selection methods using artificial intelligence is described in [62]. In most of the methods, single PQ events are given priority. However, in real-world power systems, multiple PQ events often occur simultaneously. Therefore, identifying multiple PQEs is essential to ensure a stable power supply. In [63], a combination of S-transform and convolutional neural networks is used to identify both single and multiple PQEs. In [64], discrete wavelet transforms, Bayesian optimization and composite convolution techniques for automatic identification is reported. PQE classification using convolutional neural networks is described in [40]. However, these studies use a combination of two or more different techniques, requiring large memory and fast processors to handle the resulting computational complexity.

In this work, power supply signals with single and multiple PQEs are generated using mathematical models (as per IEEE standard 1159-2019 [3]) and a specially designed experimental setup, as discussed in Chapter 2. A signal tracker is developed to continuously monitor the generated signals and extract actual disturbances. A median filter is applied to separate transient signals from other PQEs. Transients are filtered out while the remaining events are retained. Then, individual PQEs are identified using quantitative indicators to draw clear and accurate conclusions.

3.2 Median Filter based Technique

3.2.1 Pre-processing of Power Quality Events

The PQEs used in this work are listed in Table 3.1. These PQEs were generated using mathematical models and experimental setup, as discussed in chapter 2 of this thesis. The generated or captured signals, which contain power supply signals affected by single or multiple PQEs, are processed to remove these events. Each captured signal is sent through a signal tracker that determines its frequency and phase by detecting consecutive zero-crossing points. A best fit sinusoidal signal is generated, minimizing the RMS error between the captured and tracked signals. The difference between the captured and tracked signal represents actual PQEs, as shown in Figure 3.1, where a high-frequency signals is observed as the extracted PQE. In this research, the tracked signal is not affected by nonperiodic repeated zero crossings caused by harmonic distortion or notches. The tracked signal is utilized in this case in order to exclude the fundamental frequency from the captured signal. Figure 3.2 displays few more graphs of extracted PQEs. The extracted PQEs are found to be non-stationary in nature. This motivated the researchers to present quantitative indicators that can distinguish between different types of PQEs.

Table 3.1: Generated PQEs

Events	**Types**
Transient & Noise	Single
Notch & Noise	
Flicker & Noise	
Sag & Noise	
Swell & Noise	
Harmonic & Noise	
Sag, Notch & Noise	Multiple
Sag, Flicker & Noise	
Sag, Transient & Noise	
Flicker, Harmonic & Noise	
Flicker, Notch & Noise	
Flicker, Transient & Noise	
Transient, Harmonic & Noise	
Transient, Notch & Noise	
Harmonic, Notch & Noise	
Swell, Flicker & Noise	
Swell, Harmonic & Noise	
Sag, Harmonic & Noise	

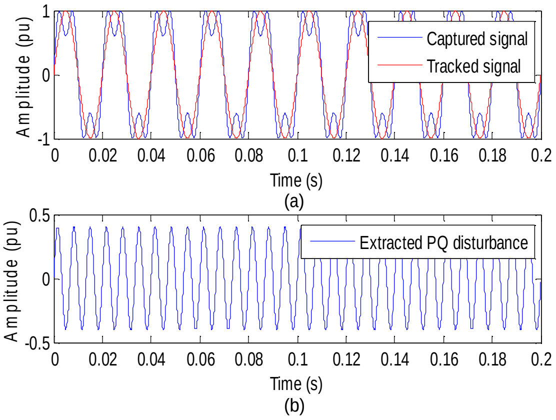

Figure 3.1 (a) Captured signal with PQE (harmonic) and Tracked signal of captured signal, (b) Extracted PQE (harmonic).

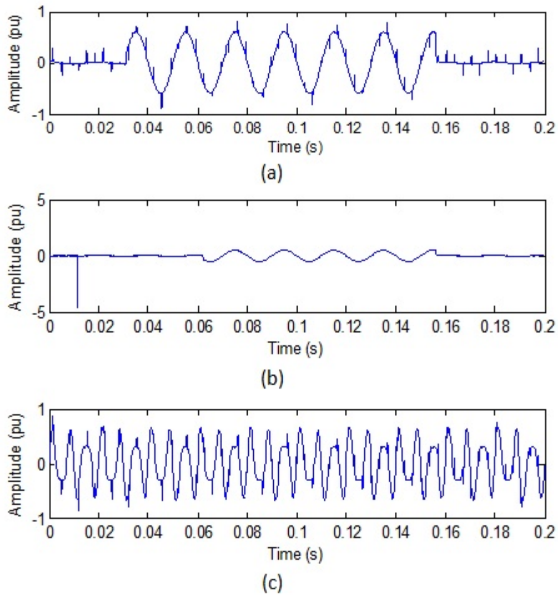

Figure 3.2 Extracted PQEs; (a) Sag and Notch, (b) Sag and Transient, (c) Harmonics and Notch.

3.2.2 Median Filtering

Spikes give false information about the peak value. A median filter is used to detect and remove spikes without affecting the properties of the extracted PQEs. To apply the median filter, a window containing an odd number of input signal data samples is used. The center value in this window is replaced with the median of all the data samples within the window [65].One way to express the filtering procedure is as

$$Y(n) = MED[X(n-M),\dots,X(n),\dots,X(n+M)] \tag{3.1}$$

where, window length, $L = 2M+1$

$X(n)$ and $Y(n)$ are the n^{th} sample of the input and output signals, respectively.

3.2.3 Quantitative Indicators based Method

Figure 3.3 shows a schematic depiction of the proposed approach used to identify events from the extracted PQEs. The median filter reduces oscillations, eliminates impulses and preserves edges. Therefore, a median filter is used to eliminate any transients that may have occurred. When one or more points in a waveform have values that are significantly higher than the rest for a short duration, it is called a transient. To remove transients from the waveform, the median filter uses a window of specific length.

In this study, a captured signal is created with 3200 data samples across 10 cycles, lasting about 200 ms. Here, the sampling frequency is kept at 16 kHz to preserve all important data related to PQEs. Based on these conditions, the median filter is applied to extract PQE signals in an effective manner. A window length of $L = 3$ is used to remove transients, although the choice of L depends entirely on the local characteristics of the signal. The output signal from the median filter does not contain any transient components. As shown in Figure 3.4, the transient component can be obtained by subtracting the median filter output from the median filter input signal.

As shown in Figure 3.5, the median filter output signal is processed again in a second stage using $L = 31$ to eliminate any notches that may be present. A notch is typically defined as a sudden, periodic fluctuation in amplitude that caused by current variations when a device switches from one phase to another in power electronic systems. To accurately conduct quantitative analysis to detect the presence of PQEs, it is emphasized that the median filter is used to remove signals containing transients and notches that are superimposed on other PQEs along with noise.

The next step is to create quantitative indicators for assessing PQEs. This study uses four indicators: (i) maximum value; (ii) Level Crossing Rate (LCR); (iii) number of deviations and (iv) number of peaks at maximum level. The first indicator, maximum value, is used to detect abrupt rising edges in any waveform. If the maximum value of the median filtered signal is high and the signal is nonperiodic, it indicates a transient. If the signal is periodic, it indicates a notch. Events such as flicker, harmonics, sag and swell are represented in the second median filter output signal. In Figure 3.5, the event shown is flicker.

LCR is an important indicator commonly used to monitor the typical noise often present in PQEs. LCR refers to the number of times a PQE signal crosses a defined threshold within the length of the sampled signal. A high LCR value indicates the presence of harmonics. As shown in Figure 3.7, combining LCR with the maximum value can provide useful information about notching.

The number of times the values of two consecutive peaks differ beyond a threshold is called the number of deviations. A high number of deviations indicate the presence of flicker. The number of times condition (3.2) is satisfied can be used to mathematically calculate the number of deviations.

$$|(|x(n)| - |x(n+1)|)| > 50\% \ of \ |x(n)min| \tag{3.2}$$

where, $x(n)_{min}$= minimum peak value of median filter output signal.
$x(n)$= n^{th} peak value of median filter output signal.

The highest number of consecutive peaks that exceed a threshold is considered the number of peaks at maximum level. A large number of peaks at maximum level indicate the presence of sag or swell. Mathematically, the number of peaks at maximum level can be determined by counting how many times condition (3.3) is repeatedly satisfied.

$$|x(n)max| - 25\% \ of \ |x(n)max| < |x(n)| \tag{3.3}$$

where, $x(n)_{max}$= Maximum peak value of median filter output signal.
$x(n)$= n^{th} peak value of median filter output signal.

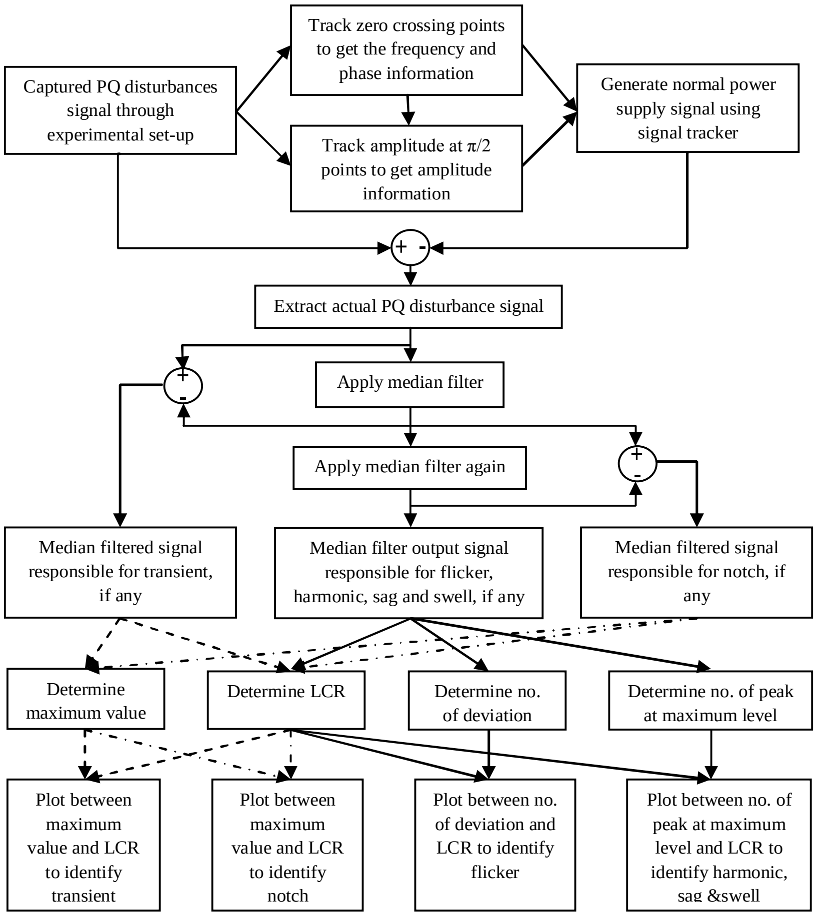

Figure 3.3 A Schematic representation of the proposed method.

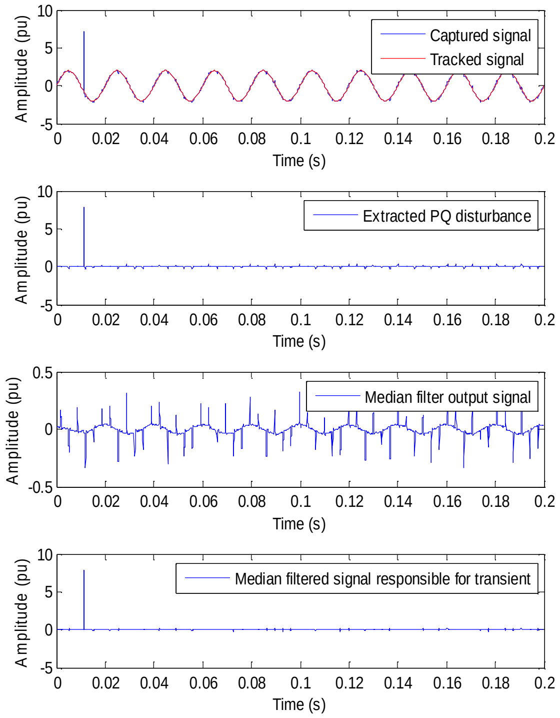

Figure 3.4 Median filtering on extracted PQEs signals (Transient and Notch) to remove Transient by taking window length 3.

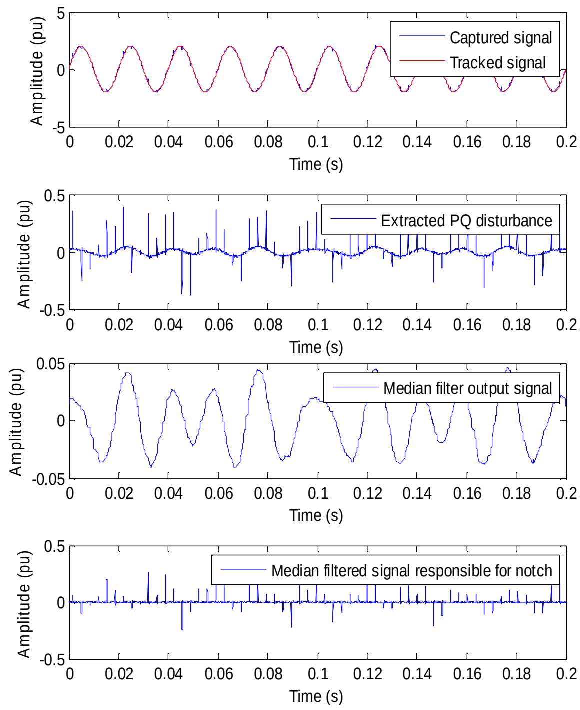

Figure 3.5 Second median filtering on first median filter output signal (Flicker and Notch) to remove Notch by taking window length 31.

As previously mentioned, the median filter in the proposed method helps to distinguish between spiky signals and other PQE signals, enabling the removal of spiky signals and better handling of the remaining ones. Maximum value, LCR, number of deviations and number of peaks at maximum level are thereafter used as quantitative indicators to differentiate events from single and multiple PQEs signals. For LCR, the threshold is set at 0.5% of the maximum absolute value of the tracked signal. This threshold is kept high enough to prevent LCR from being affected by the typical noise present in PQEs.

Rapid voltage fluctuations with amplitudes ranging between 0.95 and 1.05 p.u. are referred to as flicker. The threshold is kept low enough to detect the small amplitude variations in PQEs, such as flicker. In this case, 50% of the minimum peak value of the median filter output signal is chosen as the threshold. On the other hand, the threshold for sag and swell is set high enough to make sure that the number of peaks at maximum level remains unaffected by other PQEs. Here, 25% of the maximum peak value of the median filter output signal is used as the threshold.

The results from the generated or captured PQE studies are shown in Figures 3.6, 3.7, 3.8 and 3.9. The rounded rectangular boxes in the four scatter plots highlight closely packed clusters formed by similar types of PQEs. These plots are used for visual evaluation of acceptability, as only a few instances appear to be misclassified. Figure 3.6 depicts a scatter plot of maximum value and LCR from 18 distinct PQ events, each having 5 samples. Only transient type PQEs are made close cluster among all the other PQEs, while all non-transient PQEs are located far from this cluster. This is indicated by the red, rounded rectangular box in Figure 3.6. It is observed that transient-type PQEs have higher maximum values compared to other PQE types. As mentioned earlier, LCR is used to analyze the periodic nature of the signal. In the cases of transient with notch and transient with harmonic situations, the LCR is influenced by the notch and harmonic components, respectively, due to their periodic nature. Figure 3.7 shows a scatter plot between maximum value and LCR, used to identify notching. All PQEs related to notching form a close cluster, while other PQEs are clearly separated. As notching is a periodic, sharp disturbance, both maximum value and LCR are used together to identify notches. Figure 3.8 displays a scatter plot between the number of deviation and the LCR, which is specifically utilized to diagnose flicker. Flicker-related PQEs exhibit random amplitude variations. Therefore, the number of deviations is high. Finally, Figure 3.9 displays a plot of the number of peaks at maximum level versus LCR to determine sag, swell and harmonics. In sag, the amplitude briefly drops and in swell, it temporarily increases. As a result, PQEs involving sag and swell have higher values for the number of peaks at maximum level compared to other PQEs, as shown in the red, rounded rectangular box in Figure 3.9. The blue, rounded rectangular box in the plot shows higher LCR values for PQEs with harmonics, helping to distinguish them from sag and swell. In this case, the overlapping region represents PQEs that contain both harmonics along with sag or swell.

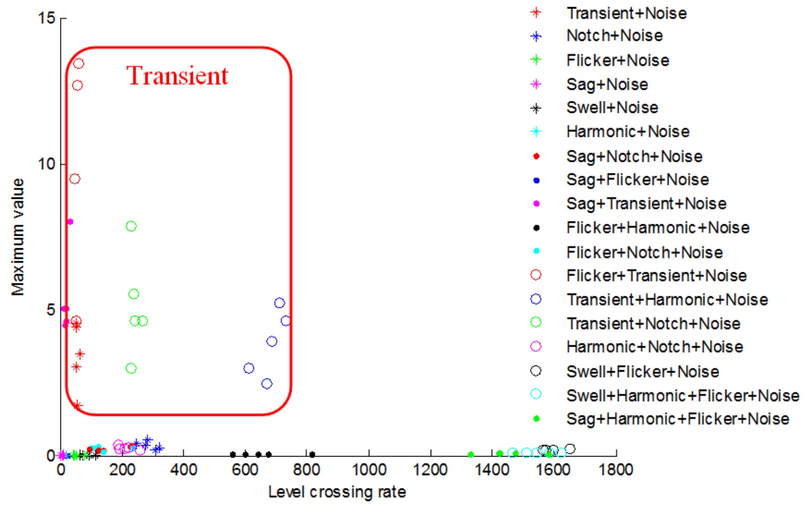

Figure 3.6 Plot between maximum value and LCR to identify Transient.

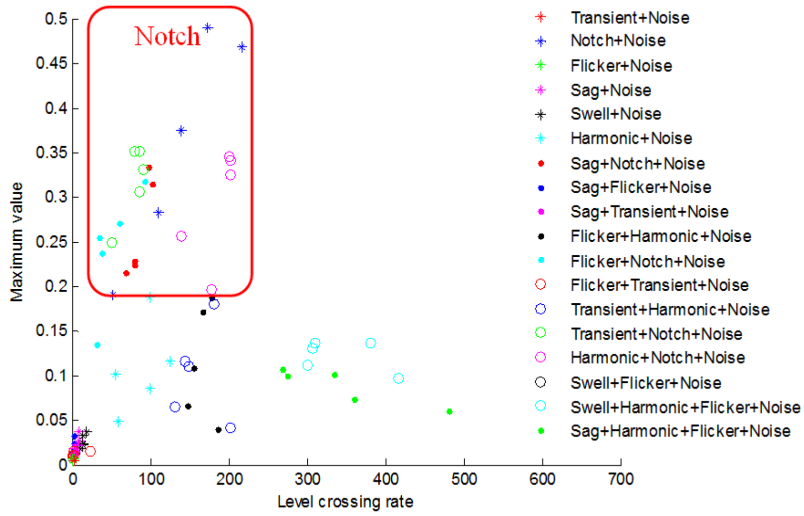

Figure 3.7 Plot between maximum value and LCR to identify Notch.

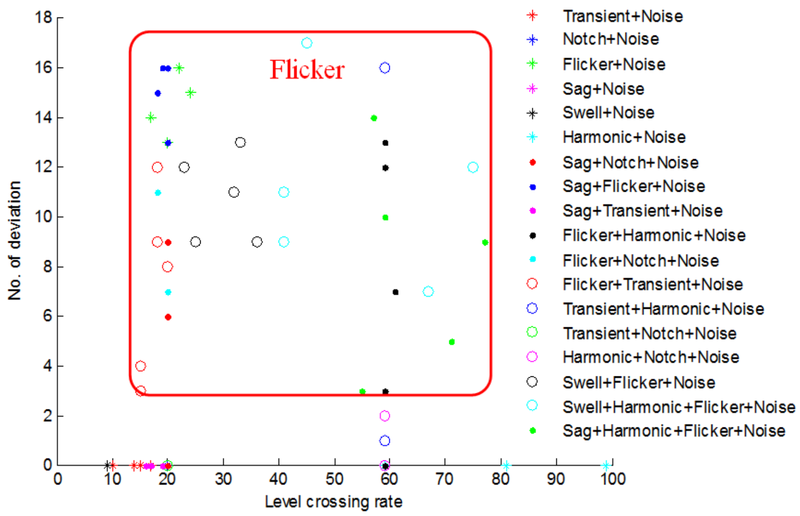

Figure 3.8 Plot between no. of deviation and LCR to identify Flicker.

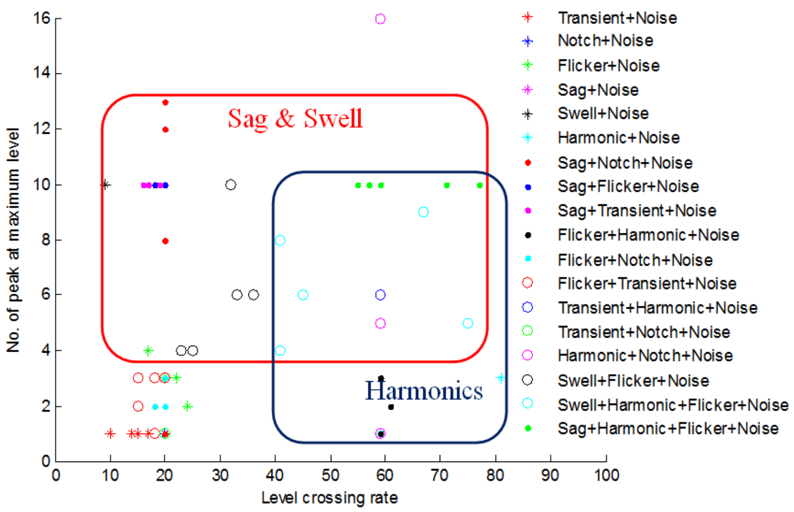

Figure 3.9 Plot between no. of peak at maximum level and LCR to identify Harmonics, Sag & Swell.

3.3 Discrete Fourier Transform based Technique

Alternatively, the generated signal can bypass the signal tracker and be directly fed into the median filter with a window length of L = 33 to discard transient (typically lasting up to 1 ms, as prescribed by IEEE standard 1159-2019 [3]). The median filter output signal is then subtracted from the input signal to obtain the median filtered signal responsible for transient. The presence of a transient is proved if the maximum value of the median filtered signal exceeds a predefined threshold. Here, the threshold is 10% of the peak value as prescribed by IEEE standard 1159-2019 [3] as shown in Figure 3.10. Once the transient is detected, the entire cycle of the generated signal is discarded and a modified version of the generated signal is introduced for further analysis. This is because the median filter is attempts to eliminate the transient superimposed on other PQEs as much as possible. Afterwards, Modified generated signal is forwarded to discrete Furrier transform and median filter based techniques for features extraction and classification.

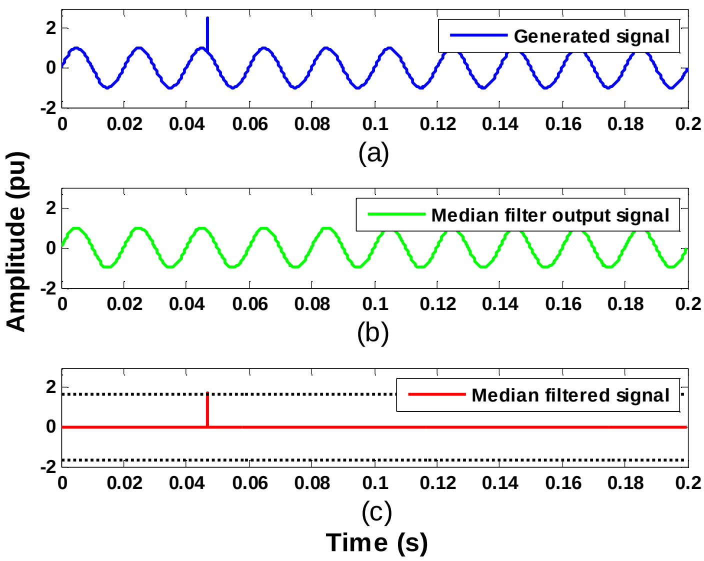

Figure 3.10 Median filtering to segregate transient.

3.3.1 Discrete Fourier Transform based Feature Extraction

A signal is divided into its constituent sinusoids of various frequencies using Fourier analysis. A finite sequence of uniformly spaced samples can be converted into another sequence of complex numbers of the same length. To reduce execution time, this can be done by applying the discrete Fourier transform using fast Fourier transform algorithms [69].

The generated signal (or modified generated signal) is split into l frames. $x_{n+1}^{l} = [x_1, x_2, x_3, \ldots x_N]$ represents the equally spaced discrete data values of one cycle of the fundamental frequency that are contained in each frame. The discrete Fourier transform of x_{n+1}^{l} can be expressed as

$$H_{k+1}^{l} = \sum_{n=0}^{N-1} x_{n+1}^{l}\, e^{-j\frac{2\pi}{N}kn} \quad 0 \leq k \leq N-1 \tag{3.4}$$

The harmonic coefficient H_{k+1}^{l} represents the sine component of the k^{th} harmonic in the l^{th} frame. That is, *k* denotes the harmonics' rank; for example, k = 1 indicates the fundamental component. H_{k+1}^{l} is the same length as x_{n+1}^{l}, which is *N*. The fundamental component's harmonic coefficient and any other harmonic component of the input signal can be used to compute the amplitude and phase.

The amplitude of the harmonic coefficient shows the amount of a specific frequency present in the input signal. The relationship between the amplitude of the harmonic coefficient and input signal can be represented as

$$real\left[H_{k+1}^{l}\right] = A\left(\frac{N}{2}\right) \tag{3.5}$$

where, *A* is the amplitude of the input signal.

This work uses a discrete Fourier transform to estimate the amplitude of the harmonic coefficient for each frame. H_{k+1}^{l}, as stated in equation 3.4, are the harmonic coefficients for the l^{th} frame. H_{i+1}^{l} is the harmonic coefficient of the i^{th} harmonic. In this work, H_{k+1}can be calculated for each frame ranging from 1 to l. The generated signal has 3200 data samples across 10 cycles with a period of roughly 200 ms. The discrete Fourier transform is applied to the generated signal successfully with l = 10. Thus, 320 discrete data samples representing one cycle are included in each frame. However, the choice of l depends entirely on the local characteristics of the signal. The amplitudes of the harmonic coefficients indicate the frequency content of the corresponding harmonics. The generated signal's H_{k+1}^{l}, which includes both sag and harmonic across all 159th harmonics over 10 frames, is shown in Figure 3.11. Sag causes an immediate decline in harmonic coefficients from the 4th to the 8th frames. It is also observed that lower-order harmonics show significant variation, while higher-order harmonics appear smoother. The fundamental component has the highest harmonic coefficient. However, the third and fifth harmonics also show relatively large harmonic coefficients compared to others, as highlighted in blue.

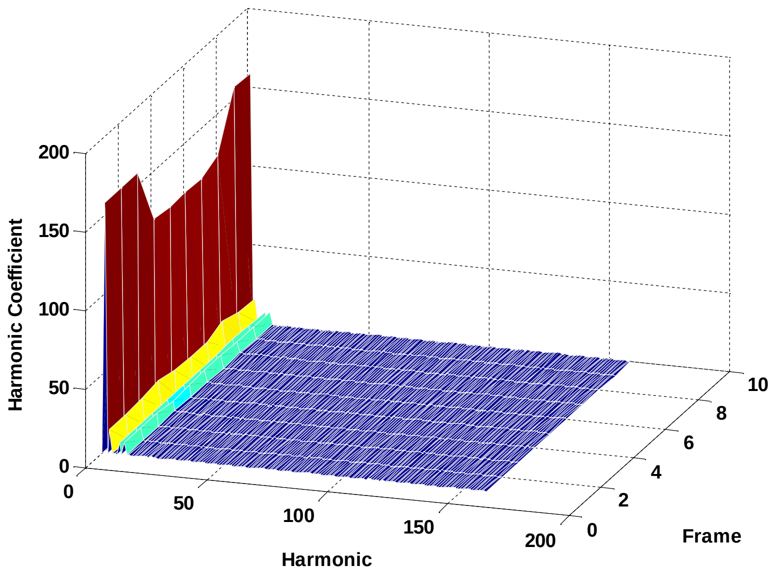

Figure 3.11 The $H_{k+1}^{l}$of generated signal mixed with PQEs (sag + harmonic) for all harmonics of all frames.

3.3.2 Fundamental Frequency Feature Analysis

The fundamental frequency harmonic coefficients of several single PQE-generated signals over all frames are displayed in Figure 3.12. A sudden decrease in harmonic coefficients is observed during sag and a sudden increase during swell, while oscillations in the harmonic coefficients are observed in the case of flicker. Harmonic coefficients are nearly constant in the cases of transient, notch and harmonic. This indicates that the fundamental frequency is not affected by harmonic and notch, whereas sag, swell and flicker are associated with changes in the fundamental frequency. It should be noted that, certain cases, transients can affect the fundamental frequency. Therefore, the entire cycle of the generated signal associated with the transient is removed, as mentioned earlier.

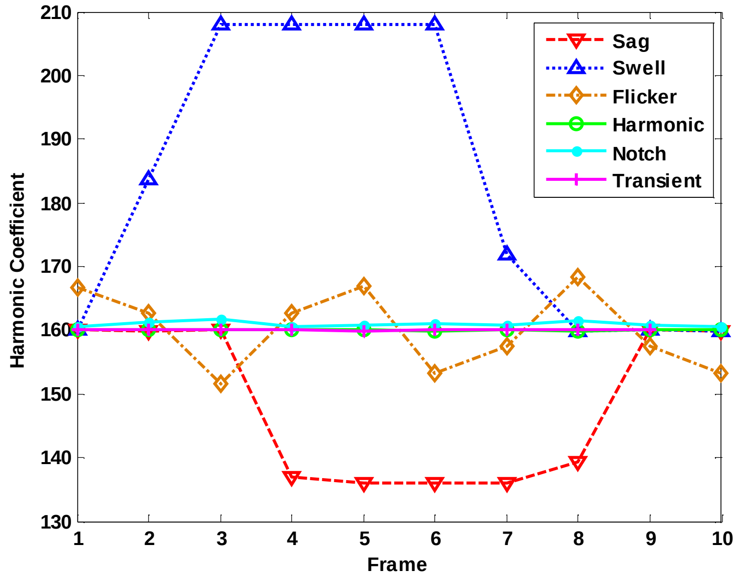

Figure 3.12 Harmonic coefficients of fundamental frequency of different single PQE generated signals of all frames.

Based on the aforementioned information, it can be concluded that harmonic and notch are frequency-based events, while sag, swell and flicker are amplitude-based events. For sag, typical amplitudes range from 0.1 to 0.9 p.u., while for swell, they range from 1.1 to 1.8 p.u. Flicker typically shows amplitude variations between 0.95 and 1.05 p.u., as mentioned in IEEE standard 1159-2019 [3]. This motivates the development of an amplitude-based identification method. However, it becomes challenging when multiple PQEs such as sag, swell and flicker occur together. Thus, an identification method based on a median filter is presented.

A median filter removes sudden fluctuations in the signal while preserving the edges. Therefore, it is used to detect sag, swell and flicker from all frames of fundamental frequency's harmonic coefficients. This approach uses the algorithm presented as follows

Step 1:
If
In the event that none of the harmonic coefficient values across all frames equal to 160. (The optimal fundamental frequency's harmonic coefficient is 160).
Then proceed to step 2 for median filtering.
Otherwise stop and exit.

Step 2:
A median filter is used, with pad value = 160 on both sides of the input sequence and window length, L (where L is an increasing odd integer number in each iteration, starting with 3).

Step 3:
Subtracting the median filter output sequence from the median filter input sequence yields the median filtered sequence.

Step 4:
Repeat step 1 using the output sequence of the median filter.

With the aid of the examples below, this technique may now be used to further demonstrate the median filter's effectiveness in signal processing.

Example 1: Taking L = 3, apply the median filter padded with 160 to the sag and flicker sequences, respectively.
X1 = [160, 144, 144, 160] and X2 = [160, 158, 156, 160]

Y1 = [160, 144, 144, 160] is the median filter output of X1 and it remains unchanged. In contrast, Y2 = [160, 158, 158, 160]. The median filtered sequence, which indicates the existence of flicker, is X2-Y2 = [0, 0, -2, 0].
Conversely, Y1' = [160, 160, 160, 160] and Y2' = [160, 160, 160, 160] would have been the outcomes of a median filter of Y1 and Y2 with L = 5, respectively. Y1 - Y1' = [0, -16, -16, 0] and Y2 - Y2' = [0, -2, -2, 0] are the median filtered sequences in this case. Y1 - Y1' indicate the presence of 10% sag.

Example 2: Taking L = 3, apply the median filter padded with 160 on the sag + flicker sequence below. After that, carry on with the median filter output sequence, taking into account L = L+2 for each iteration until all of the median filter output signal's values become equal to 160.
X = [160, 142, 140, 160]

The median filter output for L = 3 is Y = [160, 142, 142, 160], while the median filtered sequence is X - Y = [0, 0, -2, 0], indicating the existence of flicker.
Conversely, Y' = [160, 160, 160, 160] would have been the outcome of a median filter of Y with L = 5 and the median filtered sequence is Y - Y' = [0, -18, -18, 0], which indicates the presence of sag. In this instance, the negative sign indicates the sag. It is positive in case of swell.

Based on the examples, it can be inferred that the instantaneous dip or rise is identified after random oscillations within the sequence. This means that utilizing a larger window size results in higher smoothing. Similar behaviors can be seen in the event of PQEs, as illustrated in Figure 3.13, when sag is found after flicker.

To separate flicker as much as feasible, a median filter with a modest window length (L = 3) and padded with 160 on both sides of the input signal is used. A sequence of random voltage variations indicates the presence of flicker in a waveform. Subtracting the median filter output signal from its input signal gives the median filtered signal responsible for flicker, as shown in Figure 3.13(b).

Moving forward, the median filter output signal may still contain flicker or may be flicker-free. To remove any remaining flicker, the median filter output signal is processed again using a window length of L = 5. As seen in Figure 3.13(c), the median filtered signal is produced by deducting the median filter output signal from the median filter input signal. However, in this case, no flicker remains in the signal. In each iteration, L is increased by 2 (L = L + 2), as shown in Figure 3.14, until all values in the median filter output signal reach 160. In the case of median filtering, there are no limitations on the signal's amplitude. Therefore, the final median filtered signal indicating flicker is determined by combining the filtered signals that have more than one unique value, where those values are greater than 1% or less than -1% of 160, with the median filtered signal of L = 3. In this case, Figure 3.13(b) itself represents the final median filtered signal indicating flicker. However, by counting the number of values that fall between 1% and

5% of 160 or between -1% and -5% of 160, one may determine whether flicker is present in the resulting median filtered signal. A count of one or more indicates the existence of flicker. The noise that is typically seen in PQEs is suppressed here using a threshold of ± 1%.

For sag detection, the resulting median filtered signal is formed by adding median filtered signals that have only one unique value, which is less than -1% of 160. By combining Figures, 3.13(e), 3.13(f) and 3.13(g), Figure 3.14 shows the resulting median filtered signal responsible for sag. As per IEEE standard 1159-2019 [3], sag can be detected by counting the number of values in the final median filtered signal that fall within the range of -10% to -90% of 160. The existence of sag will be signified if the count is at least 1.

Similarly, to obtain the final median filtered signal for swell, all median filtered signals with only one unique value greater than 1% of 160 are combined. By counting the number of values that are present within the range of 10% to 80% of 160, the presence of swell may be determined from the resultant median filtered signal. If the count is one or more, it confirms the presence of swell.

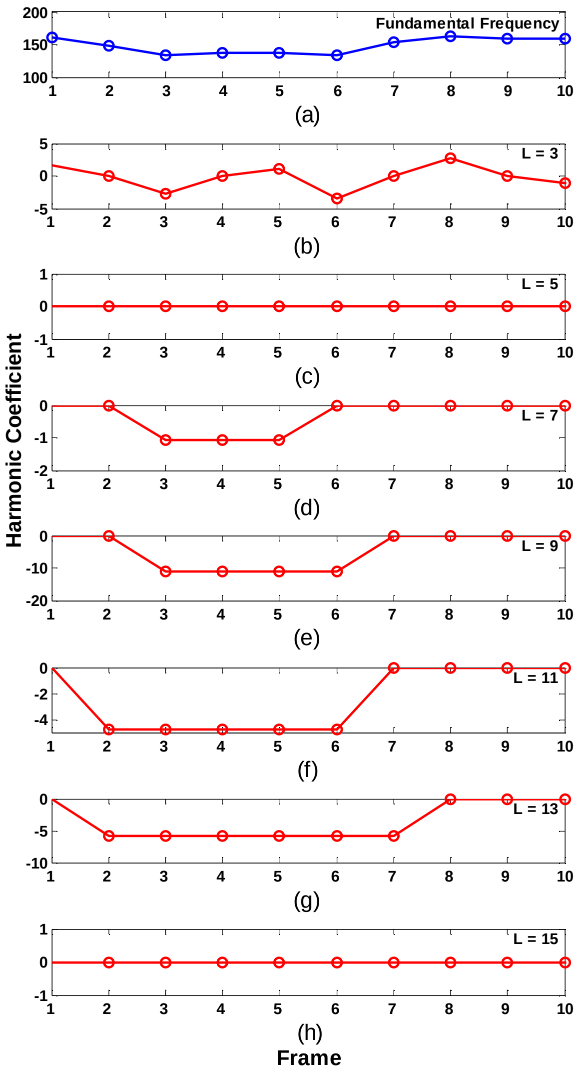

Figure 3.13 Identification of flicker and sag.

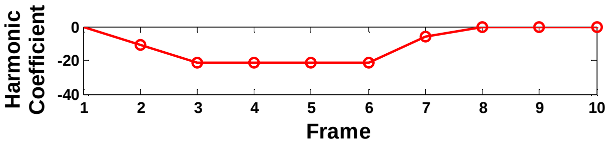

Figure 3.14 Resultant median filtered signal responsible for sag.

3.3.3 Harmonics Component Feature Analysis

The frequencies of harmonics are integer multiples of the fundamental frequency. Harmonics cause waveform distortion due to the nonlinear characteristics of loads and devices in the power system. Total Harmonics Distortion (THD) can be used to determine whether harmonics are present in the signal. In this work, as shown in Figure 3.15(a), the % THD is calculated up to the 11^{th} harmonic of the harmonic coefficients in each frame. A higher value of % THD is seen in comparison to other frames at the time of state transitions in the event of sag and swell. The process of identification might be misled by this. In order to get around this, the impulsions are discarded using a median filter with L = 3. According to IEEE standard 1159-2019 [3], a threshold value of 5% THD is adopted, as seen in Figure 3.15(b). Consequently, median filter output signals that have values greater than 5% THD are considered as harmonics.

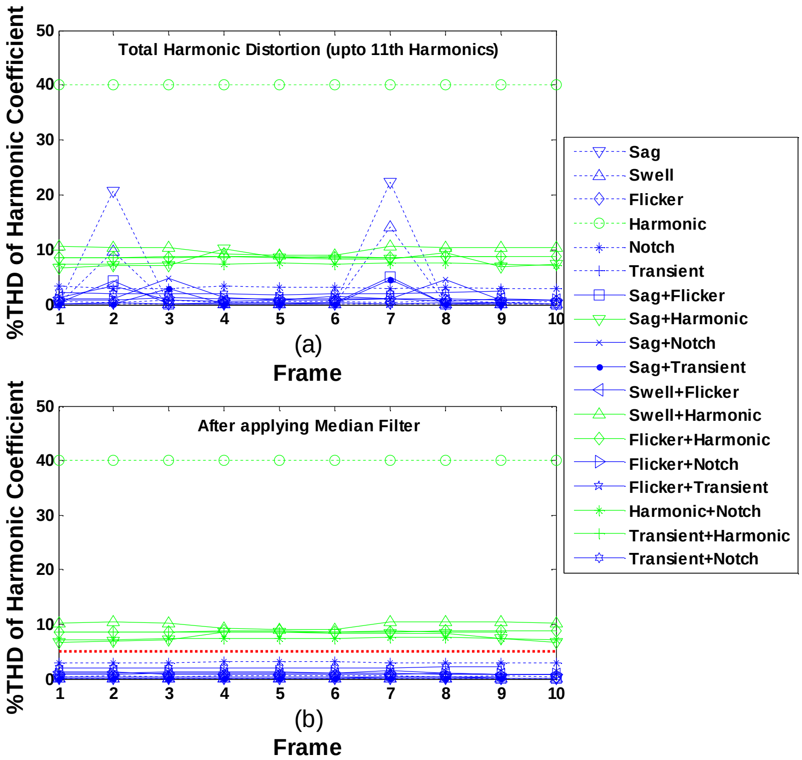

Figure 3.15 Identification of harmonics.

When current is switched from one phase to another, there is a momentary short circuit between the two phases, which results in periodic voltage fluctuations known as notching. As recommended in IEEE standard 1159-2019 [3], the usual notch duration is restricted to 800μs. Therefore, notching corresponds to frequencies approximately 615 Hz and above. In accordance with the above mentioned information, the % THD of harmonic coefficients is computed from the 12^{th} to the 50^{th} harmonic. The notching frequency range may contain an undesired high frequency noise with frequency content generally less than 200 kHz. This might provide false information during the notch identification procedure. To reduce the impact of high-frequency noise, as shown in Figure 3.16(a), the % THD calculated from the 80^{th} to the 159^{th} harmonic is subtracted from the % THD calculated from the 12^{th} to the 50^{th} harmonic. Also, sudden spikes in PQ events related to sag and swell are observed in certain frames due to state transitions. As seen in Figure 3.16(b), this may be fixed with the aid of median filtering with L = 3. The PQ events linked to the notch in Figure 3.16(b) are seen to have a higher % THD of harmonic coefficient than other PQ events, as represented by the pink color.

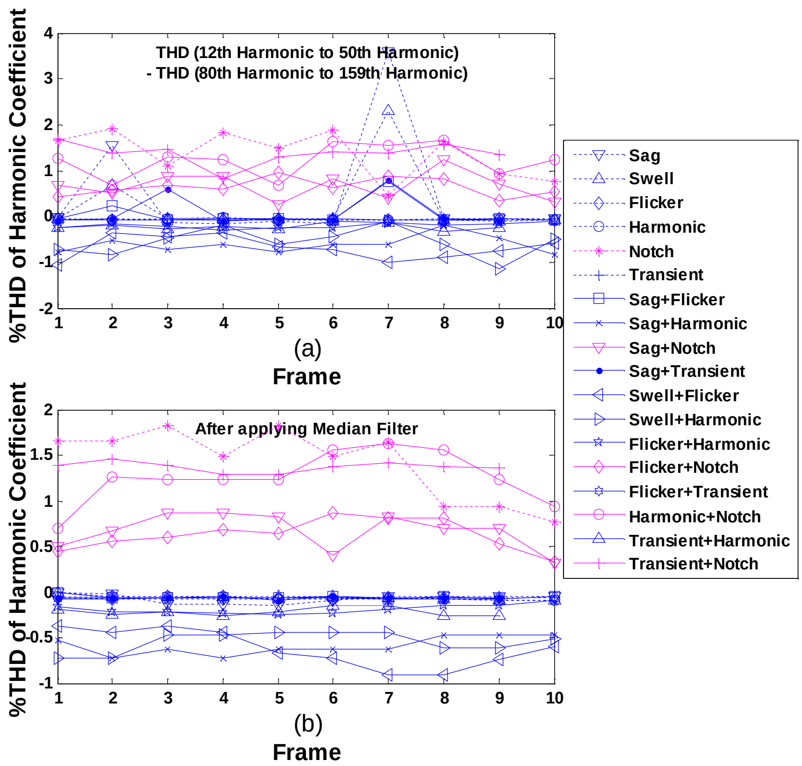

Figure 3.16 Identification of notch.

3.4 Results and Discussions

Because of the use of median filters, the proposed methods for diagnosing PQEs is simple and effective and can be easily implemented in practice. Therefore, the techniques can be useful for online applications. The performances of the developed methods are evaluated based on overall accuracy, Relative Computational Time (RCT) [60] and complexity. Overall accuracy is defined as the ratio of correctly identified events to the total number of events. After testing the performance of suggested methods on 90 samples and 2070 samples, it achieved an overall accuracy of 96.7% and 99.61%, which is acceptable and comparable to the other methods listed in Table 3.2. The method's RCT can be calculated as

$$\mathrm{RCT} = \frac{\text{Computation time for a particular method}}{\text{Minimum computation time considering all methods}} \tag{3.6}$$

Table 3.2 also shows that the proposed methods require the least amount of computation time to detect PQEs. The RCT value indicates that the proposed methods are the least complex compared to the other listed methods.

Table 3.2: Comparison of overall accuracy and RCT for different methods

Methods	**Overall Accuracy (%)**	**RCT (p.u.)**
Discrete wavelet transform and wavelet networks [60]	98.18	3.34
S-transform and probabilistic neural network [66]	93.20	2.73
Wavelet packet decomposition and support vector machines [67]	97.25	2.47
Wavelet transform and neural fuzzy [68]	96.50	2.44
Wavelet transform and neural network [30]	94.37	2.30
Rough set based technique [103]	97.10	1.50
Proposed method-1	96.70	1.06
Proposed method-2	99.61	1.00

3.4.1 Performance under the Ambient Noise

Ambient noise affects the power supply signal. Considering this, the effectiveness of the suggested method-2 is tested in the presence of ambient noise. To do that, the generated signal is mixed with synthetic white Gaussian noise at SNR levels of 20 dB, 30 dB and 40 dB, respectively. Table 3.3 shows the suggested method's detection performance under ambient noise conditions. The findings demonstrate that the suggested method-2 performs well under varying SNR levels.

Table 3.3: Performance of the proposed method under ambient noise

SNR (dB)	**Accuracy (%)**
20	99.32
30	99.61
40	99.61

3.4.2 Performance under the Frequency Variations

In actuality, the dynamic balance between generation and load causes slight variations in the power frequency. Consequently, it is important to examine the effectiveness of the suggested approach under small frequency variations. That is accomplished by altering the fundamental frequency in steps of 0.25 Hz, ranging from 49.5 Hz to 50.5 Hz. Additionally, ambient noise with SNR values of 20 dB, 30 dB and 40 dB is also included. Figure 3.17 shows the changes in identification accuracy for different fundamental frequencies (Proposed method-2). From Figure 3.17, the standard deviations of accuracy across different frequencies are computed. They are 0.27 (20 dB noise), 0.25 (30 dB noise) and 0.24 (40 dB noise), respectively. In this case, the small standard deviations indicate that the suggested method-2 is robust.

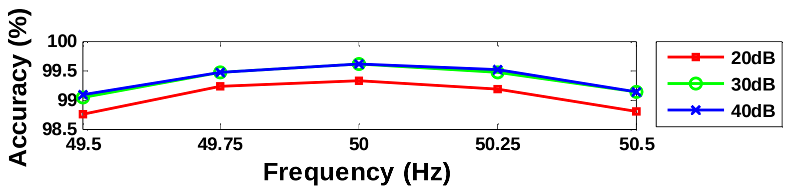

Figure 3.17 Performance of the proposed method under frequency variations.

3.4.3 Validation with Practical Data

The efficacy of the suggested approach is also examined by the identifying PQ events in real-world data. The relevant data is obtained from local electricity providers. In Table 3.4, six types of real-world PQ event data are listed. Figure 3.18 displays real-world data showing a sag event. The real-world data signals having PQ events, as listed in Table 3.4, can be accurately detected using the suggested method-2, achieving 96.36% accuracy. As a result, the suggested method-2 may be successfully implemented to improve the reliability of the Electrical Power System (EPS).

Table 3.4: Practical data with different PQEs from power utilities

PQEs	Types
Sag	Single
Transient	Single
Notch	Single
Sag + Notch	Multiple
Harmonics	Single
Transient + Harmonics	Multiple

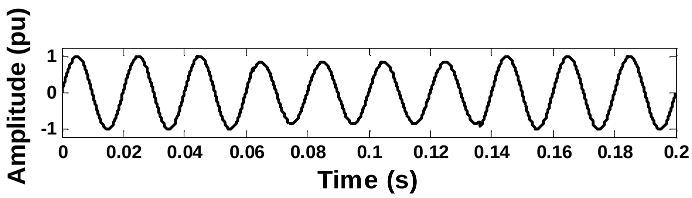

Figure 3.18 Practical voltage signal containing sag.

3.5 Conclusions

The suggested approaches can identify PQEs from single as well as multiple PQE signals. An experimental setup has been developed to artificially generate PQEs in the laboratory. In the first part of this work, a signal tracker establishes the normal level of the generated signal to detect the actual PQEs. Next, the signal with abrupt rising edges is effectively removed using median filter, enabling accurate quantitative analysis and detection of PQEs. Alternatively, in the second part, the median filter is directly applied to the generated signals to remove abrupt rising edges. After that, further analysis is carried out using the discrete Fourier transform and median filters to confirm the presence of PQ events. These simple and straightforward approaches are effective in recognizing PQEs. The proposed approaches, which do not require complex mathematical tools or traditional classifiers, outperform other methods in terms of both accuracy and processing time. Using these techniques can also improve PQ in online applications.

Chapter 4

Detection of Multiple Power Quality Events using Stockwell Transform and Convolutional Neural Network in Electrical Power System

4.1 Introduction

Human society nowadays is heavily dependent on sophisticated electrical equipment and delicate technological gadgets. Due to the widespread use of such advanced devices, a continuous, stable and distortion-free power supply is essential. Electrical Power System (EPS) networks may have issues with Power Quality (PQ) at the transmission and/or distribution stages. Numerous nonlinear loads, unstable loads, atmospheric factors such as lightning, reactive loads, unexpected heavy loads, switching operations, switching surges, faults, etc. can cause Power Quality Events (PQEs). These factors can affect the stability of the system and lead to deviations from standard voltage levels. These PQEs have the potential to irreversibly harm expensive, delicate equipment. Ensuring a smooth, distortion-free and reliable power supply to consumers is becoming increasingly challenging. Thus, it is essential to identify these PQEs to endorse a suitable mitigation plan.

In practice, it is important to emphasize that PQ is impacted not just by a single event but also by the combination of numerous events. As a result, identifying and categorizing various PQEs is essential to improving efficiency. To reduce PQEs in EPS networks, an improved detection method is required due to the increasing complexity of modern power systems. The PQ literature introduces a number of techniques, including the Fourier transform, short time Fourier transform, Hilbert-Huang transform, wavelet transform, Stockwell transform and Wigner-Ville distribution. Among these, the Stockwell transform shows better performance in identifying both single and multiple PQEs [23-24]. It works well against noise as well. As such, it is applied in this study for the Time-Frequency (T-F) encoding of the event signals.

A sophisticated approach for supervised learning is the Convolutional Neural Network (CNN) [36, 37, 70, 71]. It is important to note from the literature that 2-D CNN architecture performs better than 1-D CNN architecture [71]. Consequently, the Stockwell transform is used to convert 1-D time domain single and multiple event signals into 2-D T-F images. The 2-D CNN architecture is then used to classify the 2-D greyscale T-F images.

4.2 Power Quality Events Generation

This study uses MATLAB to construct 18 distinct single and multiple PQEs using the mathematical model as specified in IEEE standard 1159-2019 [3] and as discussed in chapter 2. Table 3.1 provides the details of generated PQEs. It is important to note that, to make the generated PQEs resemble real-life data more closely, white Gaussian noise with an SNR value of 30 dB is added [58]. Figure 4.1 shows the generated signals for Sag + Notch + Noise, Flicker + Transient + Noise and Swell + Harmonic + Noise.

4.3 Methodology

4.3.1 Extracted Event Signal

The generated PQE signals are appropriately handled in this work in order to extract the events from it. The CNN architecture's performance might be compromised by the fundamental component. Therefore, a tracked signal is designed based on the fundamental frequency as discussed in chapter 3. An event signal is extracted by subtracting the tracked signal from the generated PQE signal [29]. Figure 4.2 shows the extracted event signals for Sag + Notch + Noise, Flicker + Transient + Noise and Swell + Harmonic + Noise.

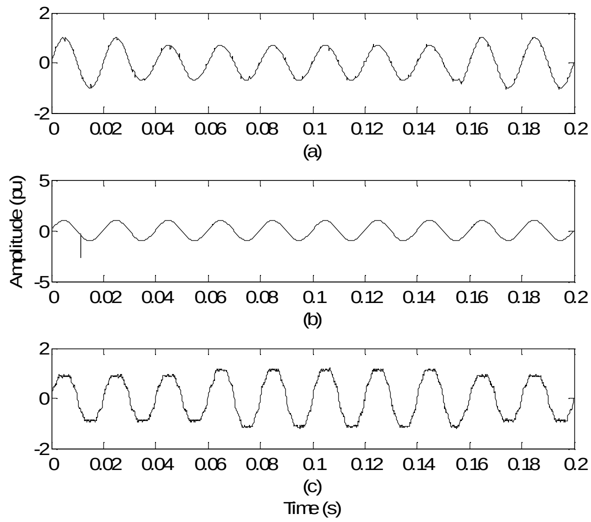

Figure 4.1 Generated PQEs (a) Sag + Notch + Noise, (b) Flicker + Transient + Noise and (c) Swell + Harmonic + Noise.

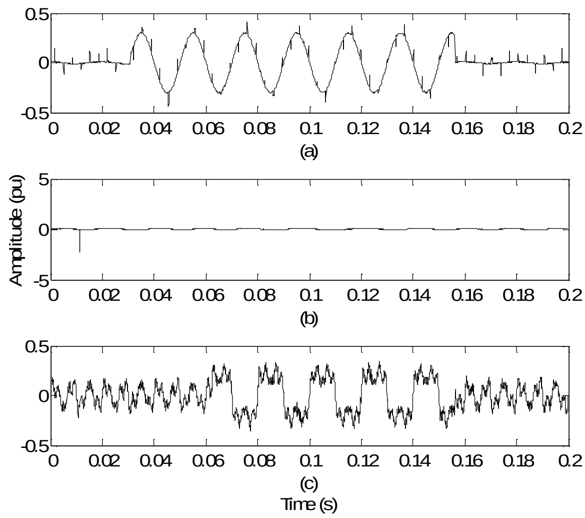

Figure 4.2 Extracted event signals from PODs (a) Sag + Notch + Noise, (b) Flicker + Transient + Noise and (c) Swell + Harmonic + Noise.

4.3.2 Stockwell Transform

R.G. Stockwell was the first to introduce the S-transform. It is a T-F format that makes use of the Fourier and wavelet transforms. With the window function of the signal *f(t)*, the short-time Fourier transform (STFT) may be obtained as,

$$STFT(\tau, f) = \int_{-\infty}^{\infty} f(t)\ w(\tau - t) \exp(-j2\pi ft)\ dt \qquad (4.1)$$

where, τ = time.
f = frequency.
$w(t)$ = window function.

To get S-transforms, the fixed window function of the STFT is substituted by a Gaussian function. The Gaussian function may be written like this,

$$gw(t) = \frac{|f|}{\sqrt{2\Pi}} \exp\left[\frac{-f^2 t^2}{2}\right] \qquad (4.2)$$

Better T-F representation is provided by the S-transform, which solves the fixed window width issue. The S-transform of the signal *f(t)* may be defined as follows from equations 4.1 and 4.2,

$$S(\tau, f) = \int_{-\infty}^{\infty} f(t)\ gw(\tau - t) \exp(-j2\pi ft)\ dt \qquad (4.3)$$

S-transform produces a T-F matrix. The matrix's rows and columns show the signal's frequency and timing information, respectively. As seen in Figure 4.3, signal amplitudes are represented by matrix elements.

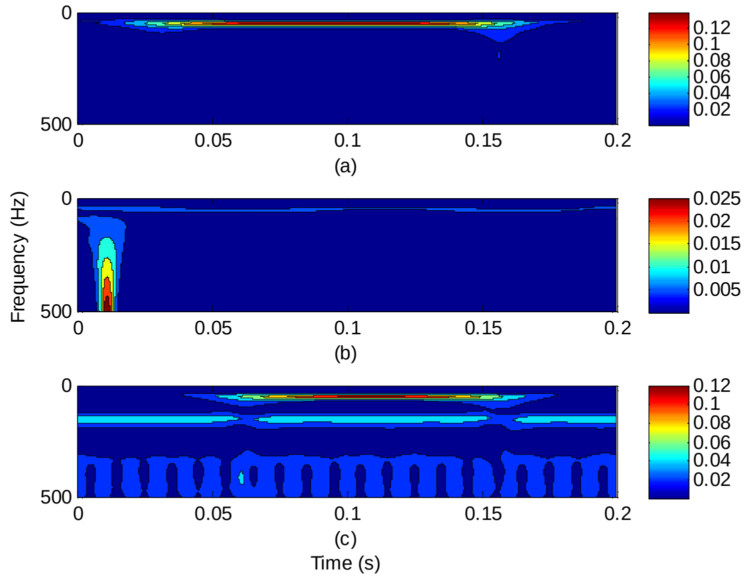

Figure 4.3 Time-Frequency images of extracted event signals (a) Sag + Notch + Noise, (b) Flicker + Transient + Noise and (c) Swell + Harmonic + Noise.

4.3.3 Convolutional Neural Network

In order to classify the image, CNN can transform it into a feature representation field. It is a multilayer network, made up of linked neurons. Input, hidden and output layers make up CNN's fundamental architecture [36, 37, 70, 71]. In this initial layer, the image is sent into the CNN. Various deep learning layers, such as convolution, pooling, Fully Connected (FC), etc., are included in the hidden layers of the network. CNN's essential component is the Convolution Layer (CL). This layer contains a collection of kernels, or learnable filters. To extract features, the input layer's output is transversely convolved using kernels. The most important variables in evaluating CL are size and number of kernels. The extracted feature's dimension from the CL is sufficiently large. As a result, the computational time may increase. The pooling layer is used to minimize the dimension of the convolved features [70-71]. The pooling layer aids in controlling overfitting as well. The two types of pooling methods are max pooling and average pooling. The max pooling technique selects features with the largest value within a pooling window, whereas the average pooling approach selects the average of features. The max pooling approach is used in this work. From the output of the MaxPooling Layer (MPL), a one-dimensional feature vector is created in the FC layer. The features are also used to determine the scores for each class. Ultimately, the probabilistic value in the softmax layer is computed using the FC layer scores. It is possible to determine the probable class based on the probabilistic value.

The aforementioned layers can be combined to create a customized CNN model that performs as needed. As seen in Figure 4.4, the proposed CNN architecture in this research consists of 3 CLs, 3 MPLs, 2 FC layers and a softmax layer. The activation function Exponential Linear Unit (ELU) is used to improve the capacity for feature learning. In ELU, negative features are maintained. There are 18 hidden units in the softmax layer, which corresponds to the 18 distinct PQEs. Table 4.1 provides descriptions of every layer.

Table 4.1: Descriptions of the Proposed CNN Architecture

Layer Name	**Kernel Size**	**No. of Kernels**	**Other Parameters**	**Dimensions**
Input	-	-	-	60×60×1
CL1	3×3	64	-	60×60×64
MPL1	-	-	Pooling Size 2x2	30×30×64
CL2	3×3	64	-	30×30×64
MPL2	-	-	Pooling Size 2x2	15×15×64
CL3	3×3	64	-	15×15×64
MPL3	-	-	Pooling Size 2x2	7×7×64
FC1	-	-	Hidden Unit 2000	1×1×2000
FC2	-	-	Hidden Unit 175	1×1×175
Softmax	-	-	Hidden Unit 18	1×1×18

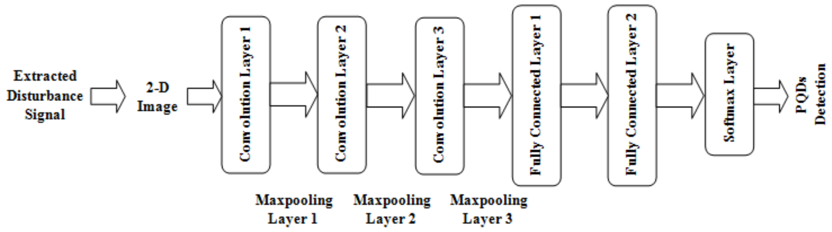

Figure 4.4 Proposed CNN architecture.

4.4 Result and Discussions

4.4.1 Performance Analysis

This study describes the generation of a total 2304 synthetic PQE signals from 18 distinct classes, with 128 signals created for each class. From the generated PQE data, event signals are then taken out and transformed into two-dimensional images. The CNN architecture is then used to automatically extract features from these images and classify both single and multiple PQEs.

As seen in Table 4.2, four statistical parameters accuracy, precision, specificity and F1-score are used to assess the classification ability for reliable performance. The recommended framework's performances for several parameters are very similar to each other. This indicates that the suggested CNN design is robust.

Table 4.2: Performance Parameters of the Proposed Method

Value	Accuracy (%)	Precision (%)	Specificity (%)	F1 score (%)
Mean	99.83	99.83	99.99	99.83
Standard Deviation	0.070	0.070	0.004	0.070

4.4.2 Analysis with Different Kernel Configurations

The size and number of kernel filters in a CL can affect the CNN architecture's capabilities, which make kernels crucial for feature selection. As a result, the performance is observed by varying the size and number of kernels.

4.4.3 Investigation with Different Number of Layers

The kind of classification problem is the sole determinant of the number of layers in a CNN. Layers may be added or removed by researchers until the required performance is attained. As indicated in Table 4.3, this study examines CNNs with three to twelve layers. It should be noted that all CNNs have the same kernel setup, pooling technique and activation function. Figure 4.5 shows the CNN's operational efficiency. It is observed that as the number of layers increases, the average accuracy of the CNN also increases at first. However, CNN's performance decreases beyond the eighth layer. This is because adding more layers improves CNN's ability to learn the training data, but at the same time, it also increases the chance of overfitting. As a result, the CNN6 (8-layer CNN) is taken into consideration for PQ event categorization.

Table 4.3: Different Number of Network Layers in CNN

CNN Identifier	Total No. of Layers	No. of CL	No. of PL	No. of FC
CNN1	3	1	1	1
CNN2	4	1	1	2
CNN3	5	2	2	1
CNN4	6	2	2	2
CNN5	7	3	3	1
CNN6	**8**	**3**	**3**	**2**
CNN7	9	4	4	1
CNN8	10	4	4	2
CNN9	11	5	5	1
CNN10	12	5	5	2

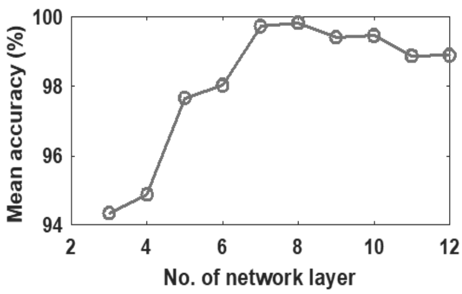

Figure 4.5 Performance analysis with different number of network layers.

4.4.4 Investigation with Different Activation Functions

Non-linearity in a network is introduced via the activation function. The network's capacity is influenced by the type of activation function. As a result, as seen in Figure 4.6, the proposed CNN's capacity is examined using a variety of activation functions, including sigmoid, tanh, ELU and ReLu. The performance of the proposed CNN using the ELU activation function is significantly better than the other activation functions.

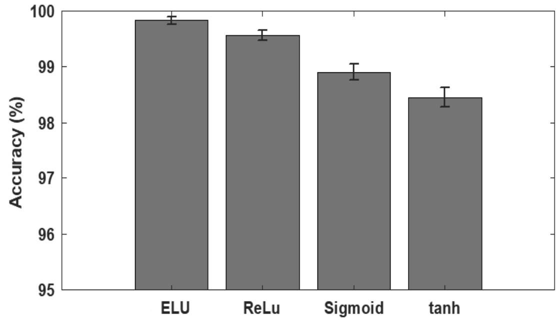

Figure 4.6 Performance analysis with different activation function.

4.4.5 Selection of Optimal Configuration for Fully Connected Layer

CNN performs better with two FCs than it does with one FC. To reach the best possible CNN performance, the optimal number of hidden units in the FCs must be determined. A thorough analysis is carried out for this purpose, as shown in Tables 4.4 and 4.5, respectively. Table 4.4 shows the performance of CNN with one FC, with the number of hidden units in FC varying from 500 to 3000 in steps of 500. The number of hidden units in the second FC is also varied in Table 4.5, ranging from 100 to 225 in steps of 25. The study shows that the best solution is provided by CNN, which uses 2000 hidden units in the first FC and 175 hidden units in the second FC.

Table 4.4: Performance Analysis of CNN with One FC

Parameter	**CNN** **500**	**CNN** **1000**	**CNN** **1500**	**CNN** **2000**	**CNN** **2500**	**CNN** **3000**
Accuracy (%)	99.61	99.65	99.71	**99.73**	99.70	99.68

Table 4.5: Performance Analysis of CNN with Two FC

Parameter	**CNN** 2000-100	**CNN** 2000-125	**CNN** 2000-150	**CNN** 2000-175	**CNN** 2000-200	**CNN** 2000-225
Accuracy (%)	99.76	99.79	99.81	**99.83**	99.82	99.82

4.4.6 Comparative Analysis

Table 4.6 presents a comparison of the proposed procedure with other alternative approaches. CNN is used to automatically classify multiple PQEs using any of the methods listed in the Table 4.6. As shown in Table 4.6, the proposed method achieves the highest classification accuracy of 99.83%. CNN has the benefit of automatically classifying PQEs without requiring prior knowledge of the signals or manual feature extraction.

Table 4.6: Comparative Analysis with Different Methods

Year	**Ref.**	**No. of PQEs**	**Type of Classes**	**Mode**	**Classifier**	**Accuracy (%)**
2023	[36]	12	Multiple	Automatic	CNN	99.60
2018	[37]	16	Multiple	Automatic	CNN	99.52
2019	[39]	9	Multiple	Automatic	CNN	99.67
2022	[41]	6	Multiple	Automatic	CNN	96.55
2019	[96]	16	Multiple	Automatic	CNN	99.75
2023	This work	18	Multiple	Automatic	CNN	**99.83**

4.5 Conclusions

This work presents an automated method for detecting single and multiple PQEs using the Stockwell transform and CNN. MATLAB is used to produce 18 distinct single and multiple PQEs with the assistance of IEEE standard 1159-2019. A basic signal tracker is then used to extract events from the generated PQEs. Consequently, the extracted events are converted into a 2-D T-F grayscale image. To achieve the required performance, a customized CNN architecture is then created for the PQE image classification. The results show that the proposed method accurately detects both single and multiple PQEs with a high accuracy of 99.83%, outperforming other existing methods. Thus, the proposed technique could be useful in detecting PQEs within EPS networks.

Chapter 5

Hyperbolic Window Stockwell Transform aided Deep Neural Network Model-based Power Quality Monitoring Framework in Electrical Power System

5.1 Introduction

Power grid development has been accelerating during the last few decades. For this reason, the network of Electrical Power Systems (EPS) is being expanded with a significant amount of expensive, modern electrical equipment. The EPS network needs high-quality input power to run its electrical equipment in a dependable and seamless manner. However, during transmission, Power Quality (PQ) can degrade, causing various Power Quality Events (PQEs) such as sag, swell, transients, flicker, harmonics, notches and noise, which may disturb the system voltage from its expected normal sinusoidal form [72]. Such issues may be caused by lightning strikes, switching surges, faults in the EPS network and so on [72]. It is also important to note that PQ can worsen when large nonlinear loads are connected [2, 72].

This poor-quality of power, containing multiple events, can lead to equipment tripping and early device failure in the EPS network. This affects the reliability of the EPS network. Therefore, it is essential to detect these PQEs early, so that proper preventive actions can be taken.

Over the years, researchers have created numerous approaches that may identify and classify different PQEs within the transmitted power. To evaluate PQEs using the joint time-frequency plane, a number of signal processing techniques are utilized, including the Wavelet transform, Fourier transform and Stockwell transform. Wavelet transform-based methods have been extensively employed for PQE sensing; nevertheless, the main disadvantage of this approach is that noise may negatively impact its effectiveness. The Stockwell transform has shown better accuracy in identifying PQEs compared to the wavelet transform [24, 28, 73-75]. The Stockwell transform suggests an analysis window with a frequency-dependent width that decreases with frequency. Compared to wavelet transform, Stockwell transform offers a number of clear advantages, including the ability to preserve the signal's absolute phase information at all frequencies and its robustness against noise [24, 28, 74-75]. For this reason, methods based on Stockwell transforms have been employed extensively for PQ detection.

It should be noted that in practice, the voltage waveform is altered not only by a single event, but also by the combination of many PQEs. Hence, detecting multiple PQEs occurring at the same time is vital for ensuring EPS network reliability.

Although many time-frequency techniques have been used successfully for PQE detection, they often require manual extraction of features from the 2D time-frequency spectrum [2, 24, 28, 72-75]. Any classification technique may be influenced by the extracted features [76]. Manual feature extraction may introduce irrelevant features, reducing the performance of classifiers. Deep learning has opened up new possibilities recently, allowing for the direct learning of appropriate features from input data. Compared to the conventional manual feature extraction approach, it has a number of benefits. It can reduce the need for manual labeling, eliminate redundant features and uncover hidden patterns that traditional methods may miss [76]. Because of these advantages, deep learning-based feature learning has been used successfully in fields such as gearbox failure detection [77], locomotive adhesion monitoring [78] and biomedical engineering [76]. Thus, a method of analyzing PQE signals in the combined time-frequency domain using the Hyperbolic Window Stockwell Transform (HWST) has been presented in this study. Next, features were extracted from the time-frequency HWST spectrum using a Deep Neural Network (DNN) based on Stacked AutoEncoders (SAE).

Several experiments were carried out to simulate both single and multiple PQE signals. Then, the signals are converted to the time-frequency domain and the proposed DNN learns the relevant features. Finally, several standard classifiers were used to detect and classify different PQEs using these automatically extracted features.

5.2 Power Quality Events Generation

The generated signal, as discussed in chapter 2 of this thesis and the numerical model, defined in IEEE Std. 1159-2019 have been used to generate 18 classes of PQEs. Table 3.1 contains the generated PQEs. Figure 5.1 shows the PQE signal for the events Sag + Noise and Swell + Flicker + Noise.

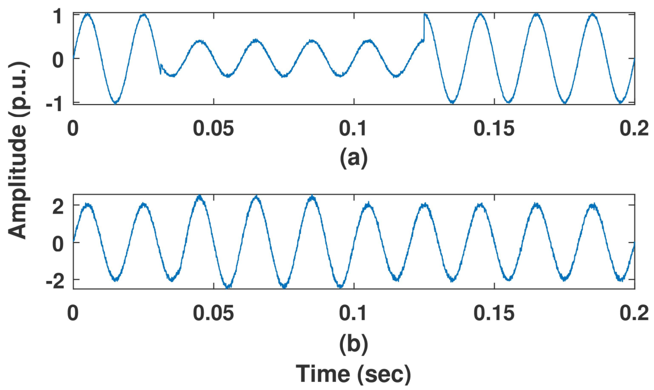

Figure 5.1 PQ signal for event (a) Sag + Noise, (b) Swell +Flicker + Noise.

5.3 Analysis of Power Quality Events in Time- Frequency Plane Employing Hyperbolic Window Stockwell Transform

5.3.1 Hyperbolic Window Stockwell Transform

Hyperbolic Window Stockwell Transform (HWST), which is a modification of traditional Stockwell transform uses modified hyperbolic window instead of generalized gaussian window [79-80]. It is important to note that the hyperbolic window function is a pseudo-Gaussian window function. It exhibits some distinct advantage such as, frequency dependent asymmetry. At lower frequencies, the hyperbolic window function is asymmetric in nature, whereas at higher frequencies, the hyperbolic window becomes more like a symmetric Gaussian window [79]. Normally symmetric window provides better resolution compared to asymmetric window. Thus, at higher frequency where the window is narrow and time resolution is good, a symmetric window can be used. On the other hand, at lower frequencies, where the window is wider and frequency resolution is less critical, an asymmetric window is more suitable as it helps events from appearing too early in the Stockwell transform. Therefore, HWST has an edge over conventional Stockwell transform. Considering this advantage, it is useful for improving local spectral characteristics of nonstationary signals like PQE signals. A discrete form of HWST of a *p(t)* signal can be mathematically expressed as,

$$HWST_p(n, j) = \sum_{r=0}^{N-1} P(r+n) HW(r, n) e^{i2\pi rj} \tag{5.1}$$

In equation 5.1, $P(r+n)$ is discrete Fourier transform of *p(t)* and $HW(r,n)$ = discrete Fourier transform of hyperbolic window w_{hyp}, which can be further expressed as,

$$w_{hyp} = \frac{2f}{\sqrt{2\pi}(\gamma_{ft}+\gamma_{bt})} e^{\left(-\frac{f^2 V_h{}^2}{2}\right)} \quad 0 < \gamma_{ft} < \gamma_{bt} \tag{5.2}$$

In this equation 5.2, V_h, γ_{ft} and γ_{bt} represent hyperbola, forward taper and backward taper respectively. The hyperbola V_h, has been further expressed as,

$$V_h(\tau - t) = \left[\frac{\gamma_{ft}+\gamma_{bt}}{2\gamma_{ft}\gamma_{bt}}\right](\tau - t - \zeta_h) + \left[\frac{\gamma_{ft}+\gamma_{bt}}{2\gamma_{ft}\gamma_{bt}}\right]\sqrt{(\tau - t - \zeta_h)^2 + \lambda_c} \tag{5.3}$$

In equation 5.3, λ_c is the positive curvature parameter in the hyperbola V_h and τ is dilation factor [79]. The parameter ζ_h is a shape parameter, which ensure that the peak of hyperbola V_h occurs at $(\tau - t) = 0$. The value of ζ_h is controlled by γ_{ft}, γ_{bt} and λ_c. Considering the fact, the parameters i.e. γ_{ft}, γ_{bt} and λ_c controls the shape of adjustable hyperbolic window w_{hyp}.

5.3.2 Hyperbolic Window Parameter Selection using Random Search Optimization Technique

To analyze a PQ signal using HWST, choosing the right window parameter is very important. Therefore, setting a fixed value for the hyperbolic window parameter may not be technically accurate. Hence, this paper proposes an adaptive hyperbolic window based on the Energy Concentration (EC) measurement of the HWST matrix. The task is to find the optimal value of the hyperbolic window parameter such that the EC of the HWST matrix in the time-frequency plane is maximized. The EC measurement of HWST matrix can be mathematically expressed as,

$$ECM(\gamma_{ft}, \gamma_{bt}, \lambda_c) = \frac{1}{\int_{-\infty}^{\infty}\int_{-\infty}^{\infty} \overline{HWST_p^{\gamma_{ft}, \gamma_{bt}, \lambda_c}}(n, j)\, dn\, dj} \tag{5.4}$$

where, $\overline{HWST_p^{\gamma_{ft}, \gamma_{bt}, \lambda_c}}(n, j)$ = normalized HWST matrix.

In this paper, the hyperbolic window parameters have been tuned through random search optimization technique. The condition for random search optimization can be given as,

$$0 \le \gamma_{ft} \le 1;\ \gamma_{ft} < \gamma_{bt} \le 1;\ 100 \le \lambda_c \le 1000$$

It is noteworthy the value of γ_{ft} and γ_{bt} has been kept low in order to keep the window narrow whereas a larger value λ_c has been chosen so that the change in shape of the window from asymmetrical to symmetrical can occur rapidly with increasing of frequency.

The output of hyperbolic window s-transform of PQE signal is a two-dimensional matrix namely HWST matrix. An image contour plot of two-dimensional HWST matrix represents the HWST spectrum of the PQ signal. The HWST spectrum for PQEs like Sag + Noise and Flicker + Harmonics + Noise is shown in Figure 5.2. In this spectrum, the x-axis represents time (in seconds), while the y-axis represents frequency (in Hz). The color intensity at any point in the spectrum indicates the magnitude of the HWST matrix at that point. The obtained HWST matrices have been subsequently fed to deep neural network for automatic feature extraction. A detailed description of the automatic feature extraction process is provided in the next section.

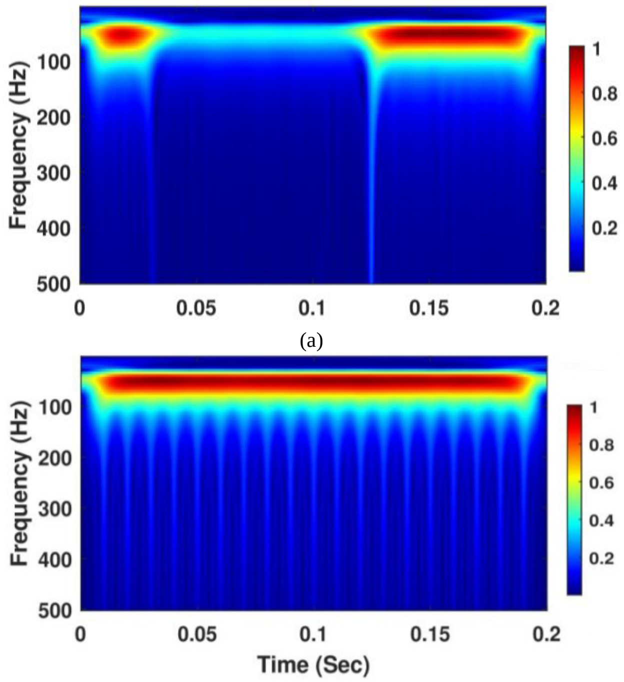

Figure 5.2 HWST spectrum for PQE (a) Sag + Noise (γ_{ft}, γ_{bt} and λ_c=0.52, 0.54 and 534.5) and (b) Flicker + Harmonics+ Noise (γ_{ft}, γ_{bt} and λ_c=0.57, 0.60 and 527).

5.4 Deep Feature Extraction from Time-Frequency Hyperbolic Window Stockwell Transform Matrix of Power Quality Events

The way of feature extraction has a pivotal role in any classification approach. Due to its several advantages, unsupervised deep learning-based feature extraction has gained importance in various domains of engineering [76-78]. In this work, a Deep Neural Network (DNN) has been designed based on a Stacked AutoEncoder (SAE) in order to extract deep features from the time frequency HWST spectrum of PQEs.

5.4.1 Theoretical Background of Autoencoder

AutoEncoder (AE) is an unsupervised feature learning method based on deep learning framework. An AE model has three parts i.e. encoder, hidden layers and decoder [76, 81]. The encoder maps the input data $\{x_i\}_{i=1}^{m}$ into 1-d feature vector $\{h_i\}_{i=1}^{m}$ using the encoder activation function given as,

$$h_i = f(W_e x_i + b_e) \tag{5.5}$$

In the equation 5.5, f is the activation function that encodes the input dataset into a hidden feature vector. W_e represent the weight matrix of encoder whereas b_e is bias vector of encoder. It is noteworthy that activation function plays an important role in learning deep features. In this work, ReLu or rectified linear unit has been used as activation function. ReLU has some advantages over traditional activation functions such as sigmoid and hyperbolic tangent, as it does not suffer from gradient diffusion or vanishing problems [77].It is also important to note that the dimension of encoded deep feature vector h_i is equal to the number of neurons in the hidden layer of the AE model.

The encoded representation of input data h_i can be reconstructed through another activation function g defined as follows,

$$z_i = g(W_d h_i + b_d) \tag{5.6}$$

In the above equation, z_i is reconstructed data whereas, W_d and b_d represents weight matrix of decoder and bias vector of decoder, respectively. The cost function of AE model can be expressed as,

$$C(W, b) = argmin \frac{1}{m} \sum_{i=1}^{m} (\frac{1}{2} \|x_i - z_i\|)^2 \tag{5.7}$$

The cost function tries to minimize losses between input data and reconstructed data. Therefore, an AE model can represent the knowledge of 2-d matrix or 1-d signal in compressed form through the encoded deep features. The schematic diagram of deep AE model has been shown in Figure 5.3.

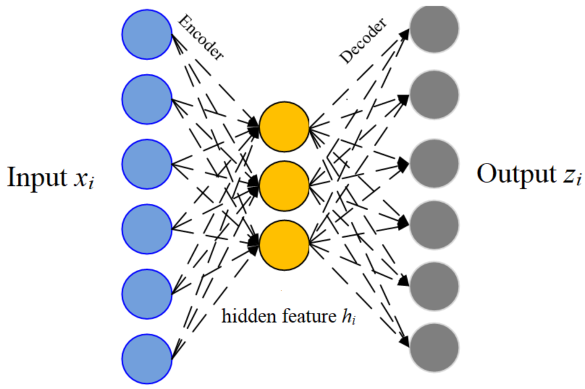

Figure 5.3 Autoencoder model.

5.4.2 Proposed DNN Framework

In this work, SAE model has been adopted for deep feature learning from HWST matrices of PQEs. In a SAE network, multiple autoencoder are stacked together. Number of layers in a SAE network is the number of stacked AEs in that network. The first AE in a SAE network maps the input data into hidden feature vector. Thereafter, the output of first AE model has been given as input to the next AE and this procedure is continued till last layer [77, 82]. The output obtained from last AE or last layer is the extracted deep features of the network. It should be mentioned here in a SAE network the neuron value of a layer is always less than the neuron value of preceding layers i.e. neurons of AE_1> neurons of AE_2 …. > neurons of AE_n (n is the number of layers in a SAE network). Therefore, the size of extracted deep features of a SAE network is the neuron value of last layer. SAE yields some distinct advantages such as, addition of number of layers may results in increasing the discrimination capability of learned features. Therefore, much detailed information can be extracted from input data, which in turn provides better features from all explanatory variables [82]. Considering the fact, a deep neural network has been designed in this work stacking three AE models.

One of the problems in feature learning from deep neural network is the risk of overfitting. Overfitting often occurs when the input dataset is small and it can negatively impact the model's performance. To minimize this issue, a dropout technique has been adopted in the proposed deep neural network. In the dropout technique, some neurons in the hidden layer are randomly dropped during training process but their weights are retained. These neurons can become active again when the next input sample is processed. By setting the output of certain hidden neurons to zero, they are excluded from the forward propagation temporarily. In the proposed deep neural network, the dropout rate has been taken as 0.2. This technique is well-established and has been adopted in several studies [77, 83] to effectively reduce overfitting.

Proposed framework of the deep neural network for deep feature extraction from HWST matrices has been shown in Figure 5.4. In this proposed framework, three AEs have been stacked together. In this proposed DNN, 2-d HWST matrices have been given as input in the input layer. After training the network, 50 deep features can be extracted from each HWST matrix. The complete architecture of proposed DNN can be expressed as $HWST_p(n, j)$. Where, dimension of input layer of proposed DNN is (n x j). Whereas first, second and third layers of the network consists 200, 100 and 50 neurons respectively. Complete training procedure of proposed DNN model has been described below.

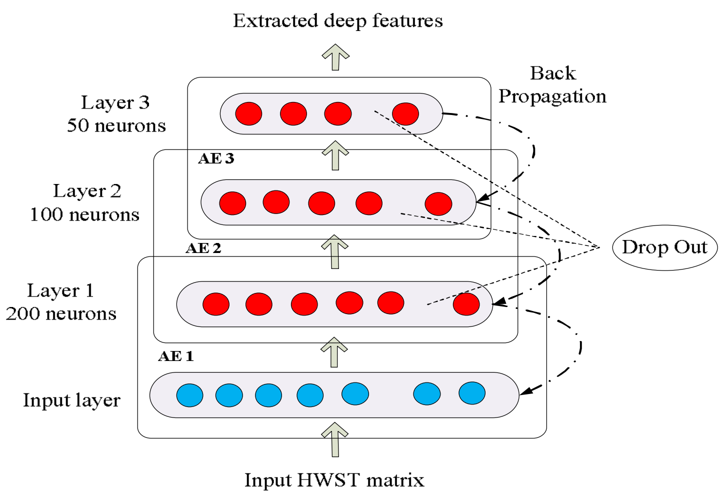

Figure 5.4 Proposed DNN framework.

Initialize the weight and bias of the AE models in the DNN. Pretrain the DNN with unlabeled training dataset $\{x_i\}_{i=1}^{m}$ layer by layer. Employ Back

Propagation (BP) technique to update the weights and fine tune the parameters of DNN in supervised manner. In BP technique, Gradient Descent (GD) optimization technique has been used to minimize the loss between input data and reconstructed data through optimizing the cost function given in equation 5.7.

In this work, 50 deep features have been extracted for each PQE converted HWST matrix from the last layer of proposed DNN. Thereafter, these extracted deep features have been given as input to some benchmark classifiers for PQE classification.

5.5 Results and Analysis

5.5.1 Performance Analysis of Proposed Framework

In this work, both single and multiple PQEs have been generated through the procedure given in chapter 2. Total 2070 PQ signals, 115 for each event has been acquired to the sense the PQE. The following steps have been performed for the sensing of PQEs.

Step 1: In the first step PQEs are analyzed in joint time frequency domain through HWST. During this process, the hyperbolic window parameters are tuned using random search optimization so that the EC of the time-frequency HWST matrix is maximized. The output of HWST of PQEs returned a time-frequency HWST matrix of size 100 x 2400. To reduce computational complexity, the matrix is divided into 20 blocks along the frequency axis and 480 blocks along the time axis. Therefore, total 9600 blocks are formed by accumulating the signal power in each block. Finally, a 20 x 480 HWST matrix is reconstructed from these blocks. This method has been adopted in the literature [84], to resize the time-frequency matrix without loss of information. Thereafter, these matrices are fed to propose DNN for automated deep feature extraction. It is noteworthy prior to automated deep feature extraction, the dataset has been split into 2:1 train-test ratio i.e. two-thirds of the dataset is used for training and the remaining one-third is reserved for validation.

Step 2: To extract deep feature from HWST spectrum of PQEs, a DNN framework has been developed by stacking three AE models. The HWST matrices generated from PQEs are used as input to the DNN and trained layer by layer. To train a DNN, it is necessary to select a suitable learning rate. If the learning rate is too high, it will allow the DNN to learn quickly. In that case loss of DNN model is too high and it oscillates over the epochs. A low leaning rate may allow the network to learn more optimally. In this work, the learning rate of proposed DNN has been set at 0.005. This value was chosen through trial and error. The performance of the proposed DNN has been shown in Figure 5.5. According to Figure 5.5(a) the best training performance of the proposed DNN was achieved at epoch 200, so the epoch size was set to 200. For selecting the dropout rate, the DNN's performance was tested with dropout rates ranging from 0.1 to 0.5 at each layer. Based on the analysis presented in Figure 5.5(b), a dropout rate of 0.2 was selected for each layer. It is important to note that time taken to train the proposed DNN model employing HWST matrix is about 7 minutes on a 2.5 GHz Intel core i5 system. Finally, after training, 50 deep features were extracted for each HWST matrix and these extracted deep features were used as input to some benchmark classifiers for classification purposes.

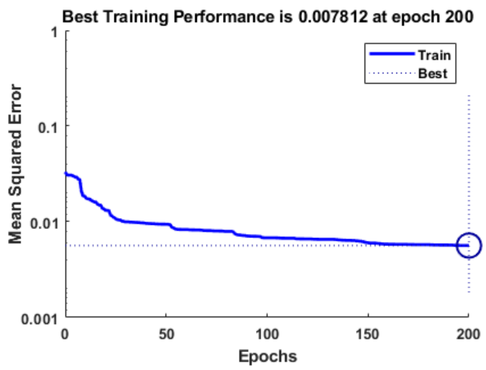

(a)

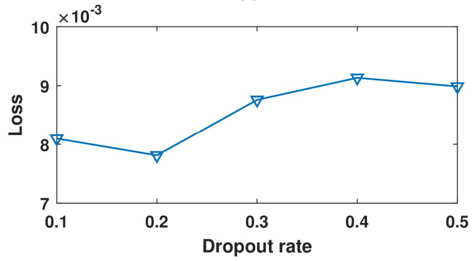

(b)

Figure 5.5 Performance of proposed DNN with (a) epoch variation and (b) with dropout rate.

Step 3: In this study, six well known classifiers i.e., Logistic Regression (LR), Multi class Support Vector Machine (M-SVM), Gaussian Naïve Bayes (GNB), k-Nearest Neighbor (kNN), Decision Tree (DT), Random Forest (RF) and XGboost (XGB) have been used to classify the PQEs based on extracted deep features. It should be noted that these classifiers are widely used in various practical applications. Also, in some studies**,** these classifiers have been used for deep feature classification [76, 85]. More information about these classifiers can be found in references [86-92]. The extracted deep features from the test dataset have been used to validate the performance of the classifiers. The performance of the classifier can be assessed through four parameters: accuracy, precision, sensitivity and False Positive Rate (FPR). These performance metrics are calculated from the confusion matrix produced by each classifier**.** The performance report of the proposed method for different classifiers has been presented in Table 5.1.

Table 5.1: Performance report for different classifier

Classifier	**Accuracy (%)**	**Precision (%)**	**Specificity (%)**	**FPR (%)**
GNB	98.99	99.00	99.93	0.060
LR	98.99	99.00	99.93	0.060
DT	99.28	99.29	99.95	0.051
kNN	99.42	99.43	99.96	0.043
MSVM	99.57	99.58	99.97	0.026
RF	99.71	99.71	99.98	0.017
XGB	**99.86**	**99.86**	**99.99**	**0.011**

Based on this report it can be said that XGboost (XGB) gives the best performance in sensing the PQE. The performance of RF, M-SVM and kNN is also quite satisfactory whereas the performance of DT, LR and GNB has been found to be lower. For the RF classifier, optimal accuracy has been achieved with 200 trees, whereas for M-SVM, optimal accuracy has been achieved with a radial base function. In the kNN classifier, number of nearest neighbors (k) has been set to 8. It is noteworthy that the optimal hyperparameters of the classifiers have been tuned using random search optimization. The confusion matrix for the XGB classifier used for PQE detection has been shown in Figure 5.6.

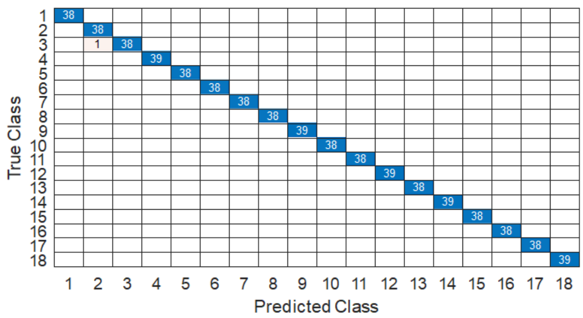

Figure 5.6 Confusion matrix for PQE sensing for XGB classifier.

5.5.2 Performance Analysis of Proposed DNN

To investigate the efficacy of proposed DNN, layer wise performance has been analyzed. To do this, features have been extracted from layer 1, layer 2 and layer 3 of proposed DNN and subsequently fed to the classifier for PQ classification. Classification results for RF and XGB classifier has been presented through Table 5.2. According to the result presented in Table 5.2, the deep feature extracted from the 3rd layer of proposed DNN yield the best performance, which indicates that the 3-layer SAE has better feature extraction capability from PQE converted HWST matrix.

Table 5.2: Layer wise classification analysis of proposed DNN

Layer	**Classifier**	**Accuracy (%)**
1st layer	RF	98.99
	XGB	99.28
2nd layer	RF	99.42
	XGB	99.57
3rd layer	RF	99.71
	XGB	99.86

5.5.3 Computational Complexity Calculation

The computational complexity of the HWST depends on the number of input signal '*m*' which can be expressed as *O(mlog(m))* [97]. The computational complexity of 3-layer DNN is given as *O(em(ab+bc))*. Here '*e*' is the number of epochs and '*a*', '*b*' and '*c*' are the number of neurons in layer1, layer2 and layer3 of proposed DNN respectively. For classifier, the time complexity of GNB classifier is *O(md)* [98], where '*d*' is the dimension of extracted deep features. For the LR classifier the time complexity is *O(d)* and for DT it is *O(mlog(m) d)*. For kNN classifier the time complexity is expressed as *O(kmd)*. Here '*k*' is the number of nearest neighbors [98]. The time complexity for SVM classifier is *O(m2)* and for RF it is *O(mlog(m) dt)*, where '*t*' is number of trees [98]. For XGB classifier the time complexity has been given by *O(tlog(m)hy)*, where '*t*' is number of trees, '*h*' is height of the trees and '*y*' is non-missing entries in training data. In this work, extraction of deep features using HWST and proposed DNN took almost 513 seconds and classification using GNB, LR, DT, kNN, SVM, RF and XGB took 45.5 seconds, 34 seconds, 51 seconds, 59.3 seconds, 64.1 seconds, 78.4 seconds and 67.2 seconds respectively on a 2.5 GHz Intel core i5 system with 8 GB RAM using MATLAB R2020a.

5.5.4 Performance Analysis against Background Noise

In real life operation, PQ signals are contaminated with background noise. Considering the fact, the efficacy of the proposed method has been investigated in a noisy background. In order to do that, simulated data has been contaminated with synthetic white gaussian noise of SNR value of 20 dB, 30 dB and 40 dB respectively. The performance of the proposed method at noiseless and noisy background for the XGB and RF classifier has been presented through Table 5.3. Result shows, the method has delivered acceptable performance under noisy background of different SNR value.

Table 5.3: Performance investigation of the proposed method under noisy background

SNR (dB)	**Classifier**	**Accuracy (%)**
20	RF	99.42
	XGB	99.57
30	RF	99.57
	XGB	99.86
40	RF	99.71
	XGB	99.86

5.5.5 Performance under Variable Frequency

In a practical scenario, there exist small variations in power system frequency. It is noteworthy that, this frequency variation occurs due to a change in the dynamic balance between generation and load. Therefore, it is worthwhile to investigate the performance of the proposed framework under small frequency variation. In order to do that, the fundamental frequency of the PQ signal has been varied from 49 Hz to 51 Hz, with a step change of 0.25 Hz under 20 dB, 30 dB and 40 dB noise conditions. The variation of classification accuracy with signal frequency has been portrayed through Figure 5.7. From the result presented in Figure 5.7, it can be calculated that the standard deviation of accuracy under variable frequency is 0.31% (with 40 dB noise), 0.29% (with 30 dB noise) and 0.24% (with 20 dB noise). Hence the standard deviation in accuracy of the proposed framework under variable frequency is very low, which signifies the robustness of the proposed framework.

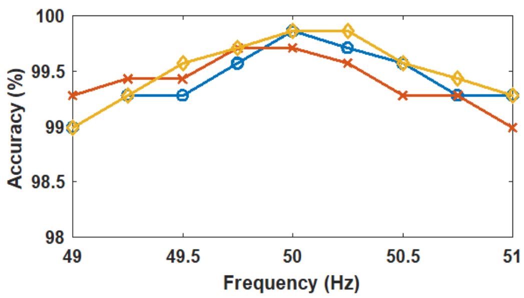

Figure 5.7 Performance of proposed method with frequency variation (with XGB classifier).

5.5.6 Validation with Real Life Data

The effectiveness of the proposed framework is also investigated with real life PQ data. It is noteworthy that, six different types of real-life PQ signals were imported from a local power utility. Detailed information about the imported real-life PQ signals is presented in Table 5.4. The recorded voltage waveform for sag is shown in Figure 5.8.

Table 5.4: Information of real-life PQ data

PQEs	**No. of imported real life data**
Sag	20
Transient	15
Notch	20
Sag + Notch	15
Harmonics	25
Transient + Harmonics	15

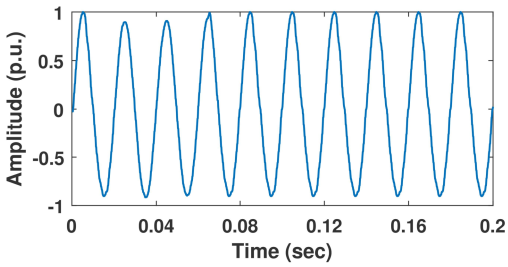

Figure 5.8 Real-life sag voltage signal.

The imported real-life PQ signals are analyzed in time-frequency space through HWST. Then, the resulting HWST matrices are divided into time-frequency blocks, resized 60×120 and fed into the pretrained proposed framework for PQE classification. It has been observed that the proposed framework achieved an accuracy of 96.36% using the XGBclassifier. The result of the proposed framework with the XGB classifier for real life data is shown in Table 5.5. Therefore, implementing the proposed framework can effectively improve the reliability of the EPS network.

Table 5.5: Performance of proposed framework with real-life data

Classifier	**Accuracy (%)**	**Precision (%)**	**Specificity (%)**	**FPR (%)**
XGB	96.36	96.63	99.26	0.74

5.5.7 Comparative Study

In Table 5.6, the result of proposed method has been compared with several different scenarios. In the first case raw PQEs are given as input to the proposed neural network for deep feature extraction. Whereas, in the rest of cases time-frequency matrices obtained from existing time-frequency methods i.e. Short Time Fourier Transform (STFT) [93], Wavelet Transform (WT) [94], Cross Wavelet Transform (XWT) [72] and classical Stockwell Transform (ST) [74] are given as input to the proposed deep neural network respectively. It is important to note that, for all cases, the dataset was split in a 2:1 train-test ratio. According to the result presented in Table 5.6, it has been observed that deep features extracted from the HWST time-frequency spectrum achieved the best performance with the XGB classifier in terms of accuracy, compared to extracted deep feature from raw PQEs and other time-frequency spectra. This demonstrates the effectiveness of HWST based time-frequency analysis in PQE detection.

Table 5.6: Comparative study with other methods

DSP applied	Framework + Classifier	Accuracy (%)
Raw PQ signal	DNN + XGB	92.90
STFT		97.39
WT		97.53
ST		98.84
XWT		99.13
HWST		99.86

A comparative study of the proposed method has been conducted with existing methods reported in literature. According to Table 5.7, it can be observed that our proposed method delivered results that are almost comparable in detecting single and multiple PQEs. It has been observed that work presented in [96] achieved slightly higher accuracy compared to proposed method. However, the proposed framework can classify a greater number of PQEs than the method in [96]. Also, the proposed method is based on a DNN framework, where features are extracted from the time-frequency spectrum in an automated manner. Also, it has evident that proposed method is very much efficient under noisy background, under dynamic frequency variation and with real life data. Hence, proposed method can be implemented for the classification of different single and combined PQEs in an EPS network.

Table 5.7: Comparative study with existing methods

Paper	DSP Method	Extracted feature	No. of PQEs	Accuracy (%)
[95]	TQWT	Handpicked	14	97.29
[66]	ST	Handpicked	11	97.40
[55]	ST	Handpicked	12	99.20
[24]	Hybrid ST	Handpicked	11	94.36
[75]	Rule-based ST	Handpicked	13	99.37
[28]	MOFDST	Handpicked	13	99.61
[39]	WVD	Automated	9	99.67
[91]	MRST	Handpicked	16	99.69
[96]	CWT	Automated	16	99.75
Proposed Work	**HWST**	**Automated**	**18**	**99.86**

5.6 Conclusions

In this article, a methodology has been proposed to accurately detect both single and multiple PQEs. For this purpose, a setup was developed in the laboratory, through which synthetic single and multiple PQ signals were converted into analog signal. Next, these PQ signals were analyzed in the time-frequency domain using HWST. A DNN was then designed by stacking three AEs to extract deep features from the HWST matrices of the PQ signals. These automatically extracted features were then fed as input to several standard machine learning classifiers. According to the results, the proposed framework performed well with all classifiers. However, XGB achieved best performance. The prime advantage of the proposed framework is that feature extraction process from the HWST spectrum of PQEs is completely automated. The proposed method also performed well in the presence of background noise and dynamic frequency variations. Furthermore, its performance with real-life PQ data was found to be highly comparable. Therefore, it can be concluded that implementing the proposed framework with the XGB classifier can improve the reliability of an EPS network.

Chapter 6

Multisynchrosqueezing Transform aided Transfer Learning based Approach for Diagnosis of Single and Mixed Power Quality Events

6.1 Introduction

Power Quality Events (PQEs) must be accurately detected to provide consumers with a clear power source for their sensitive electrical devices. PQEs have been analyzed using a variety of signal processing approaches in recent years [99-106]. In [2], detrended fluctuation analysis successfully detects both single and multiple PQEs. In the combined Time-Frequency (T-F) plane, several PQE signals have been successfully analyzed using the Wavelet Transform (WT), Hilbert-Huang transform, Wigner-Ville distribution, Short Time Fourier Transform (STFT) and Stockwell transform [28, 39, 58, 72, 75, 91, 94-95, 104-106]. T-F representations produced by WT, Hilbert-Huang transform, Wigner-Ville distribution and STFT of a non-stationary signal are frequently hazy due to the Heisenberg uncertainty principle [107]. Therefore, it is challenging to extract accurate PQE information from the hazy T-F representation. When compared to other traditional techniques, the Stockwell transform can offer superior T-F resolution. However, the window shape must be optimized during the Stockwell transform of the PQE signal in order to achieve greater T-F resolution [28, 58]. Some evolutionary optimization techniques should be used for this, even if they may make computations more complex. Given the circumstances, the PQE signal in the combined T-F frame has been analyzed in this study using the MultiSynchroSqueezing Transform (MSST). MSST has the benefit of being able to generate a focused and clear T-F representation of a time-varying signal.

The feature extraction technique is crucial to the development of a PQE detection algorithm. The majority of PQE detection techniques rely on customized feature extraction. These customized feature extraction approaches are relatively simple but may require some expertise in signal processing. Deep learning techniques can be used to address the customized feature extraction challenge. Deep learning has the advantage of automatically learning rich information from input data. Deep learning techniques have therefore been used for PQE detection in [36, 39-40, 58, 91, 106].

An efficient deep learning technique for automatically extracting features from input data is the Convolutional Neural Network (CNN) [39]. To train a CNN model effectively, however, a lot of data is needed and it takes significant processing time. Considering this problem, this article uses CNN with a Transfer Learning (TL) technique to identify both single and multiple PQEs in Electrical Power System (EPS) networks. This method involves encoding the T-F spectrum image using the T-F representation of the PQE signal that was received during the MSST procedure. Following that, the image plot of the T-F representation is fed into the pretrained deep architectures to automatically extract features. In the end, statistically rich deep features are fed into certain benchmark classifiers in order to identify PQEs.

6.2 Power Quality Event Generation

In this chapter, 9 distinct forms of PQE data (pure sinusoidal, transient, sag, swell, flicker, harmonics, notch, spike and interruption) have been simulated using the numerical models specified in IEEE Std. 1159-2019.

A number of publications have stated that several PQEs can occur at the same time [2, 72]. In light of this problem, this study concatenates two or more numerical models of the relevant single PQE to create multiple PQEs. For analytical purposes, 27 multiple PQEs were generated for this chapter. The names of the single and multiple PQEs are listed in Table 6.1. It should be noted that a total of 200 PQE signals have been simulated for each PQE. Additionally, white Gaussian noise with SNR values of 10 dB, 15 dB, 20 dB, 25 dB, 30 dB, 35 dB and 40 dB was added to each simulated PQE signal to increase the amount of data and produce a PQE database that is more likely to be practical. A total of 57,600 {200 (simulated PQE signals per class) × 36 (number of classes) × 8 (1 simulated data + 7 additive noise levels)} PQE signals form the overall PQE database. The time-domain plot of the PQEs Sag + Noise, Harmonics + Noise, Transient + Noise, Sag + Harmonics + Noise, Notch + Transient + Noise and Sag + Harmonics + Transient + Noise is shown in Figure 6.1 (a-f), respectively.

Table 6.1: Description of PQEs

PQE	Label	Type
Pure sinusoidal+ Noise	PQE1	Single
Sag + Noise	PQE2	
Harmonic + Noise	PQE3	
Notch + Noise	PQE4	
Swell + Noise	PQE5	
Flicker + Noise	PQE6	
Transient + Noise	PQE7	
Impulse/Spike + Noise	PQE8	
Interruption + Noise	PQE9	
Sag + Flicker + Noise	PQE10	Multiple
Sag + Notch + Noise	PQE11	
Sag + Harmonic + Noise	PQE12	
Sag + Transient + Noise	PQE13	
Harmonic + Notch + Noise	PQE14	
Flicker + Notch + Noise	PQE15	
Flicker + Harmonic + Noise	PQE16	
Interruption + Harmonic + Noise	PQE17	
Flicker + Transient + Noise	PQE18	
Swell + Harmonic + Noise	PQE19	
Swell + Flicker + Noise	PQE20	
Swell + Notch + Noise	PQE21	
Swell + Transient + Noise	PQE22	
Notch +Transient + Noise	PQE23	
Transient + Harmonic + Noise	PQE24	
Spike + Transient + Noise	PQE25	
Sag+ Flicker+ Transient + Noise	PQE26	
Sag +Notch+ Transient + Noise	PQE27	
Sag +Harmonic+ Transient + Noise	PQE28	
Swell+ Flicker+ Transient + Noise	PQE29	
Swell +Notch+ Transient + Noise	PQE30	
Swell +Harmonic+ Transient + Noise	PQE31	
Flicker + Harmonic + Transient + Noise	PQE32	
Flicker + Notch + Transient + Noise	PQE33	
Harmonic + Notch + Transient + Noise	PQE34	
Flicker + Harmonics + Interrupt + Noise	PQE35	
Spike + Transient + Swell + Noise	PQE36	

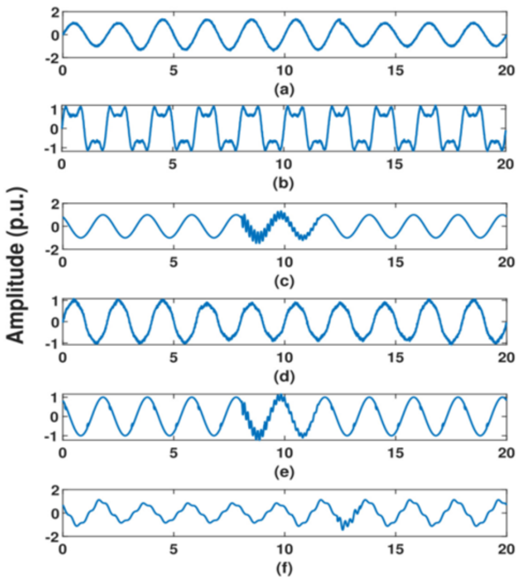

Figure 6.1 Generated PQEs (a) Swell + Noise, (b) Harmonics + Noise, (c) Transient+ Noise, (d) Sag +Harmonics + Noise, (e) Notch +Transient + Noise and (f) Sag + Harmonics + Transient + Noise.

6.3 Methodology

6.3.1 Theoretical Background

An efficient method for analyzing multicomponent non-stationary signals is T-F analysis. The T-F representation that is produced by T-F analysis of a signal allows for the observation of its time-varying characteristics. Assume that *s(t)* is a multicomponent non-stationary signal. At this point, *s(t)* may be stated mathematically as

$$s(t) = \sum_{c=1}^{C} s_c(t) = \sum_{c=1}^{C} A_c(t) e^{i\varphi_c(t)} \tag{6.1}$$

The instantaneous amplitude and instantaneous phase of the signal *s(t)* are denoted by $A_c(t)$ and $\varphi_c(t)$, respectively, in equation 6.1. The Instantaneous Frequency (IF) is the first derivative of $\varphi_c(t)$ i.e., $\varphi_c'(t)$. The multicomponent signal *s(t)* may thus be mathematically represented using the T-F representation as follows:

$$TFR(t,\omega) = \sum_{c=1}^{C} A_c(t)\delta(\omega - \varphi_c'(t))e^{i\varphi_c(t)} \quad (6.2)$$

δ(.) in the previously described equation stands for the "Dirac delta function", which in discrete signal processing degenerates to the "Kronecker delta function" [107]. The T-F representation only produces high energy concentrations at the IF trajectories, according to equation 6.2 [107-108]. STFT and WT are the standard methods for T-F analysis of a signal. A 1-D signal (in the time domain) can be transformed into a 2-D T-F domain using STFT and WT. The T-F representation image is the image plot of the 2-D T-F domain. Time-varying aspects of a signal can be identified from its T-F representation, which is produced using STFT and WT. However, the "Heisenberg uncertainty principle" states that it is challenging to derive accurate information about a signal's time-varying characteristics from the T-F representation obtained by a traditional method.

To address the limitations of the traditional T-F strategy, other sophisticated techniques have been proposed. One of the most sophisticated T-F analysis techniques is the Synchro Squeezing Transform (SST). The T-F representation produced by the traditional method is enhanced by SST. SST was initially used with continuous WT and then with STFT-based T-F representations [108]. The focus of this study has been on STFT-based SST. Based on the local IF estimation in the 2-D T-F representation, the SST concentrates the representation's energy on each component's local IF trajectory. The mathematical expression for the local IF estimate $\tilde{\omega}(t, \omega)$ is as follows [108-109]:

$$\tilde{\omega}(t,\omega) = \frac{\delta_t F(t,\omega)}{iF(t,\omega)} F(t,\omega) \neq 0 \quad (6.3)$$

F(t,ω) is the STFT of *s(t)* in equation 6.3 and it may be further stated as

$$F(\omega,t) = \int_{-\propto}^{+\propto} q(v-t)s(v)e^{-i\omega(v-t)}\,dv \quad (6.4)$$

In this case, the sliding window function is *q(t)*. The "gaussian window function" is used in this work, can be expressed mathematically as

$$q(t) = e^{=0.5t^2} \quad (6.5)$$

Consequently, the mathematical expression for the SST of signal *s(t)* is as follows [108-109]:

$$SST(t,\eta) = \int_{-\propto}^{+\propto} F(t,\omega)\delta(\eta - \tilde{\omega}(t,\omega))\, d\omega \tag{6.6}$$

η denotes the "frequency-reassignment operator" in the equation 6.6, which assembles the spread T-F coefficients. Therefore, SST can be used to sharpen the hazy T-F representation produced by STFT around the IF trajectories of each component. The signal's components may now be reconstructed using equation 6.7, which is written as

$$s_c(t) \approx \frac{1}{q(0)} \int_{|\omega - \varphi_c'(t)| < d} SST(t,\omega) d\omega \tag{6.7}$$

The "reconstruction bandwidth parameter" of SST is denoted by d in equation 6.7. In the 2-D T-F representation, this parameter is used to correct the mistakes that occur during local IF estimation. To get a sharp T-F representation of a signal, d should be kept low. The publication [107-108] provides further information about SST.

6.3.2 Multisynchrosqueezing Transform

The difference between the real and estimated IF will be large if the signal is significantly non-stationary [109]. When the PQE signal is significantly non-stationary, this might lead to a hazy T-F representation (produced using SST). Multiple SST operations can be performed to overcome this SST constraint. After several SST operations, the estimated IF has been shown to be substantially closer to the real IF. Therefore, it is possible to increase the T-F representation's sharpness and concentration by performing several SST operations. The Multisynchrosqueezing Transform (MSST) is the term used to describe this multiple SST operation method. A mathematical expression for the MSST operation of the signal *s(t)* for N iterations is as follows [107]:

$$MSST^{[N]}(t,\eta) = \int_{-\propto}^{+\propto} F(t,\omega)\delta(\eta - \tilde{\omega}^{[N]}(t,\omega))\, d\omega \tag{6.8}$$

The estimated IF following N times SST procedure is represented by $\tilde{\omega}^{[N]}(t,\omega)$ in the equation 6.8. Mathematically, the discrete version of MSST operation is stated as

$$MSST^{[N]}(d,\rho) = \sum_{j=0}^{L-1} F[d,j]\,\delta[\rho - \tilde{\omega}^{[N]}[d,j]] \tag{6.9}$$

where, d = discrete time variable.
L = number of samples in a signal.
ρ = discrete frequency variable.

6.3.3 Tuning of Iteration Number in MSST

The optimum number of iterations during the MSST operation must be determined to provide a focused and sharpened T-F representation of a non-stationary signal. However, because the degree of non-stationarity varies among PQE signals, it is theoretically incorrect to analyze all PQE signals using a fixed value for the iteration number. As a result, this study presents an adaptive MSST that adjusts the iteration number according to the Rényi entropy measurement. It should be noted that the most concentrated T-F representation is obtained when the Rényi entropy has the lowest value [109].

6.3.4 T-F Representation with MSST

The features of various single and multiple PQE signals in the T-F representation are observed in this work using adaptive MSST. The MSST operation on the PQE signal produced a 2D complex MSST matrix as its output and the absolute MSST matrix's image plot serves as a T-F representation image. The MSST image in this case refers to the PQE signal transformed into T-F representation images. The MSST images for the PQEs "Sag + Noise," "Harmonics + Noise," "Transient + Noise," "Sag + Harmonics + Transient + Noise," and "Notch + Transient + Noise" are shown in Figure 6.2(a–e), respectively. Figure 6.2 shows that MSST images have good T-F resolution, which is helpful for identifying various PQE types. Thus, TL with CNN has been used to extract useful features from the MSST images. A quick explanation of TL is given in the next section.

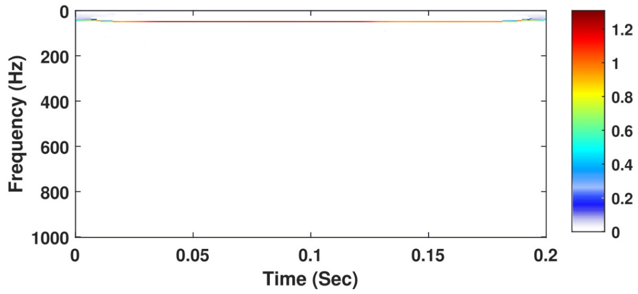
Frequency (Hz)
Time (Sec)

(a)

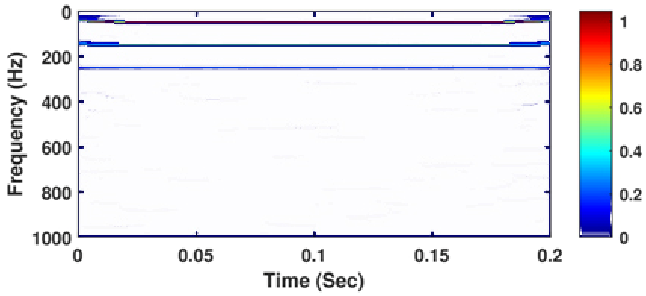
Frequency (Hz)
Time (Sec)

(b)

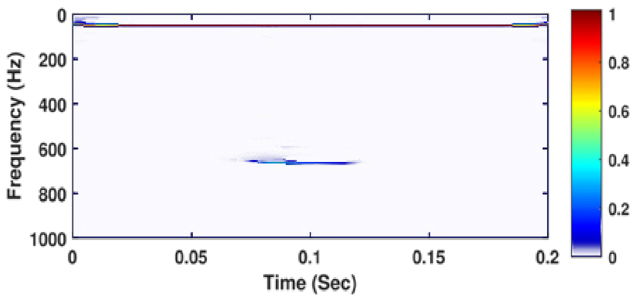
Frequency (Hz)
Time (Sec)

(c)

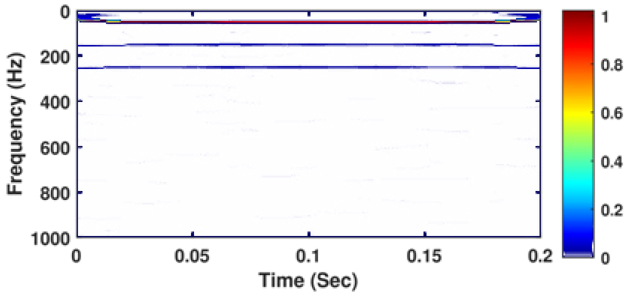

(d)

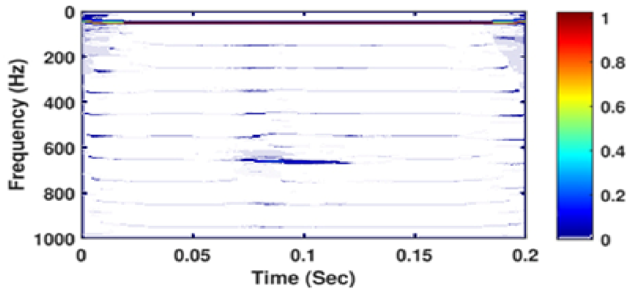

(e)

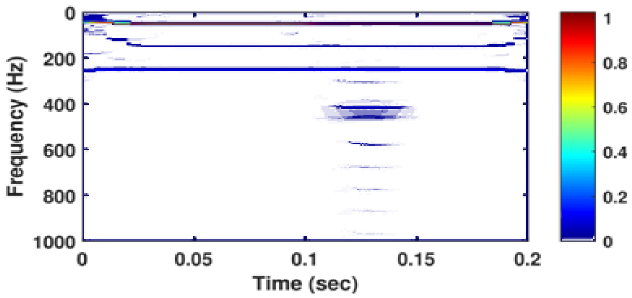

(f)

Figure 6.2 MSST images correspond to PQEs (a) Swell + Noise, (b) Harmonics + Noise, (c) Transient+ Noise, (d) Sag +Harmonics + Noise, (e) Notch +Transient + Noise and (f) Sag + Harmonics + Transient + Noise.

6.3.5 Automated Deep Feature Extraction using TL

The T-F representation of the PQE signal is used to manually extract features in the classical machine learning technique. Decision-making in this classical method necessitates both quantitative and qualitative analysis [85, 110]. CNN has become increasingly popular in recent years for tasks such as feature extraction, object identification and image classification [85, 110]. It makes use of convolution operations, which are capable of automatically and adaptively learning spatial characteristics in images. The "convolution layer," "pooling layer," and "fully connected layer" form a basic CNN block. The last layer maps the learned features for classification purposes, whereas the previous two layers are in charge of feature extraction [85].

CNN is incredibly helpful for tasks involving images, but training a CNN model from scratch has several drawbacks, which are as follows:

• Training a network from scratch requires a large amount of data and with a limited amount of data; there is a chance that the CNN model may overfit the training data [111-112]. Nevertheless, there is very little PQE data collected for this study.

• The weights in a deep CNN model are initialized at random. These weights are modified following each iteration of the network's training process based on the labeled data and the loss function. It is computationally expensive to update all the weights repeatedly [111-112].

Considering these drawbacks, this work uses the TL approach to train machine learning models for the identification of single and multiple PQEs utilizing T-F representation images as input. As the name implies, TL applies previously learned information from a pretrained model to a new task. TL is widely used in many engineering problems and is highly favored in machine learning research [111-112]. It should be noted that TL-based approaches work quite well with small datasets. Additionally, this method is quicker than training a network from scratch [111-112].

This study uses the TL technique to extract features from MSST images that have been transformed from PQE signals. Four pre-trained deep CNN architectures have been used for this purpose, including "VGG16" [113], "ResNet50" [111], "DenseNet201" [112] and "InceptionV3" [112]. Every deep CNN architecture produces outstanding results and has been thoroughly trained using the ImageNet dataset. Due to their several layers and millions of learnable parameters, these deep CNN architectures require a significant amount of time to train [108-111]. Even though medical and infrared images differ greatly from natural images, CNN architectures trained on the ImageNet dataset have been effectively used for tasks relating to medical and infrared imaging in a number of publications [108-109]. Inspired by these successes, this work applies the deep CNN architecture's learnings from the ImageNet dataset to the MSST image dataset transformed from PQE signals for automated feature extraction. A summary of the suggested TL-based feature extraction from the PQE signal-transformed T-F representation image is shown in Figure 6.3. The following is a quick explanation of the pre-trained deep CNN architectures utilized in this study.

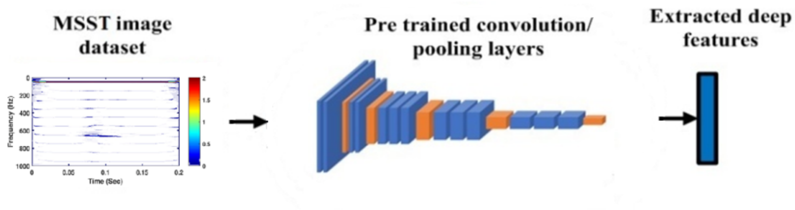

Figure 6.3 Automated deep feature extraction based on TL.

VGG16: The Oxford Visual Geometry Group (VGG) developed the deep CNN known as "VGG16" [113]. The network is a 16-layer series system. VGG16 has a very basic architecture made up of 13 CL, 5 PL and 3 FCL. The publication [113] provides a detailed explanation of the VGG16 architecture.

ResNet50: Residual learning forms the basis of the Deep Residual Neural Network (ResNet) [111]. It is a widely used architecture designed to address various deep learning challenges. In residual learning, residual blocks create a direct pathway from the input to the output, which helps to overcome the vanishing gradient problem. The 50-layer residual network, known as "ResNet50," is used in this work.

DenseNet201: Huang et al.’s Dense Convolutional Network (DenseNet) was a top-performing architecture in the 2017 ILSVRC competition. In conventional deep networks, each layer is connected only to the next layer. DenseNet introduces a new structure called a dense block, which allows feature reuse across the entire network [112]. This reduces the number of learnable parameters and helps to mitigate the vanishing gradient problem. DenseNet has four variants: "DenseNet121," "DenseNet169," "DenseNet201," and "DenseNet264". The 201-layer variant, "DenseNet201," is used in this work.

InceptionV3: The main objective of "InceptionV3", developed by Szegedy et al. in 2015 [114], is to design a deep architecture with reduced computational complexity. By using factorized convolutions, it lowers the number of learnable parameters. InceptionV3 consists of 48 layers and has been extensively trained on the ImageNet dataset.

6.3.6 Classifier used

Four popular classifiers have been employed in this task: Gaussian naïve bayes (GNB), Support Vector Machine (SVM), Random Forest (RF) and K-Nearest Neighbor (KNN). Since the idea behind the aforementioned classifiers has been widely accepted and utilized throughout time, in-depth explanations are not included in this thesis. [88], [112], [28] and [112] provide descriptions of GNB, SVM, RF and KNN, respectively.

6.4 Result and Discussions

6.4.1 Performance Analysis

This research proposes an enhanced deep learning-based framework that uses a T-F representation image as input to automatically recognize single and multiple PQEs. Within this system, PQE signals are converted into T-F representation images after being processed using MSST. The encoded T-F representation images are then sent to the appropriate pre-trained CNN model for automatic deep feature extraction after being resized to meet the models' specifications (listed in Table 6.2). It should be noted that this study uses the Keras library to automatically extract features from the CNN model pre-trained on a large dataset. Following deep feature extraction, a one-way analysis of variance (ANOVA) test is applied to further examine the statistical significance of the features extracted. Based on the probabilistic value (*p*-value), the ANOVA test can identify discriminative features [111]. Following the ANOVA test, the top 100 discriminative deep features are selected for the classification procedure.

Table 6.2: Brief information about automated feature extraction from the pre-trained networks

Architecture	Year proposed	Image input size	Layer from which features have been extracted	No. of feature extracted
VGG16	2014	224×224×3	“fc6”	4096
ResNet50	2015	224×224×3	“avg_pool”	2048
DensNet201	2017	224×224×3	“avg_pool”	1920
InceptionV3	2015	299×299×3	“avg_pool”	2048

Four benchmark classifiers (SVM, RF, KNN and GNB) are employed for classification in this study. To train the classifier, an optimal hyperparameter needs to be determined. Apart from Naïve Bayes, all classifiers' hyperparameters are tuned using the configuration shown in Table 6.3. The best hyperparameters are selected for this study using a 4-fold cross-validation approach. It is important to note that the classification performance is evaluated using three metrics: accuracy, specificity and F1-score. The evaluation metrics for each fold are calculated using the corresponding confusion matrix. The mean value of the evaluation metrics are reported in Table 6.4. The best effective pretrained CNN model for automatic feature extraction from T-F MSST spectrum images encoded with PQE signals is "VGG16," as shown in Table 6.4. This is explained by the fact that the most informative and discriminative features are obtained using "VGG16." It should be noted that the "VGG16-SVM" feature extractor-classifier model produces the best results. Additionally, it is observed that "ResNet50" "DenseNet201" and "InceptionV3" perform nearly identically. The "VGG16-SVM" feature extractor-classifier model's class-wise performance is presented in Table 6.5. The confusion matrix of this classification has been shown in Figure 6.4.

Table 6.3: Configuration setup adopted for classification process

Classifier	Optimizer used	Parameters tuned	Setup
SVM	Random search	C	2-5 to 210
		γ	2-15 to 24
k-NN	Grid search	No. of neighbors	3 to 9 (in step of 1)
NB	-	-	Gaussian probability density function
RF	Grid search	No. of decision tree	50-500 (in step of 50)

Table 6.4: Performance analysis of four architectures and four classifiers (16 combinations) for PQE signal converted MSST images

Architecture	**Classifier**	**Accuracy (%)**	**Specificity (%)**	**F1 score (%)**
VGG16	k-NN	99.54	99.98	99.54
	SVM	**99.58**	**99.98**	**91.50**
	GNB	99.43	99.98	99.43
	RF	99.57	99.98	99.57
ResNet50	k-NN	99.44	99.98	99.44
	SVM	99.49	99.98	99.49
	GNB	99.41	99.97	99.41
	RF	99.52	99.98	99.52
DenseNet201	k-NN	99.36	99.97	99.36
	SVM	99.38	99.97	99.38
	GNB	99.28	99.97	99.28
	RF	99.42	99.98	99.42
InceptionV3	k-NN	99.12	99.96	99.12
	SVM	99.14	99.96	99.14
	GNB	99.03	99.96	99.03
	RF	99.19	99.97	99.19

Table 6.5: Class wise performance for "VGG16-SVM" feature extractor-classifier model

Class identifier	Accuracy (%)	Precision (%)	Recall (%)	F1 score (%)	Specificity (%)
PQD1	100.00	100.00	100.00	100.00	100.00
PQD2	100.00	100.00	100.00	100.00	100.00
PQD3	100.00	100.00	100.00	100.00	100.00
PQD4	100.00	100.00	100.00	100.00	100.00
PQD5	99.87	99.61	95.69	97.61	99.99
PQD6	99.94	98.94	98.88	98.91	99.97
PQD7	99.94	98.63	99.19	98.91	99.96
PQD8	99.94	99.31	98.50	98.90	99.98
PQD9	99.94	99.31	98.50	98.90	99.98
PQD10	99.50	99.55	82.38	90.15	99.99
PQD11	99.13	99.46	69.06	81.52	99.99
PQD12	99.09	99.45	67.56	80.46	99.99
PQD13	99.38	98.29	79.06	87.63	99.96
PQD14	99.38	99.13	78.38	87.54	99.98
PQD15	99.50	99.18	82.69	90.18	99.98
PQD16	99.75	100.00	91.00	95.29	100.00
PQD17	99.56	100.00	84.19	91.41	100.00
PQD18	99.75	99.26	91.69	95.32	99.98
PQD19	99.63	99.22	87.38	92.92	99.98
PQD20	99.81	99.27	93.88	96.50	99.98
PQD21	99.75	99.26	91.69	95.32	99.98
PQD22	99.63	100.00	86.69	92.87	100.00
PQD23	99.25	99.49	73.38	84.46	99.99
PQD24	99.31	99.51	75.56	85.90	99.99
PQD25	99.44	100.00	79.81	88.77	100.00
PQD26	99.50	100.00	82.00	90.11	100.00
PQD27	99.38	100.00	77.69	87.44	100.00
PQD28	99.56	100.00	84.19	91.41	100.00
PQD29	99.44	99.53	80.19	88.82	99.99
PQD30	99.44	99.53	80.19	88.82	99.99
PQD31	99.50	100.00	82.00	90.11	100.00
PQD32	99.38	100.00	77.69	87.44	100.00
PQD33	99.31	99.51	75.56	85.90	99.99
PQD34	99.56	100.00	84.19	91.41	100.00
PQD35	99.19	100.00	70.81	82.91	100.00
PQD36	99.31	100.00	75.19	85.84	100.00

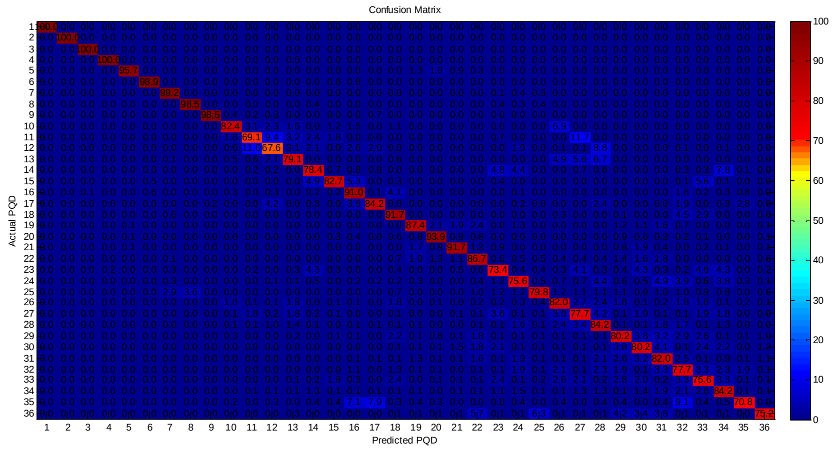

Figure 6.4 Normalized confusion matrix heatmap for all the 36 classes.

6.4.2 Computational Time Calculation

The computing time of the framework is crucial for real-world deployment. It takes around 8640 seconds in total to transform the PQE signal dataset into an MSST image dataset (approximately 0.15 seconds for each signal). It took 1613 seconds (approximately 28 ms for a single image) to extract deep features from the MSST image dataset using VGG16. Training the classifiers (SVM, k-NN, RF and GNB) takes approximately 38, 33, 46 and 28 seconds, respectively. Additionally, it has been noted that the suggested framework can identify a PQE in less than 1 second (for a single signal in 2.5 GHz Intel core i5 system with 8 GB RAM) following data acquisition, making it very appropriate for real-world use.

6.4.3 Performance under Noisy Background

In the actual world, background noise can taint PQE signals. In light of this, the effectiveness of the suggested approach has been examined using PQE data that has been tainted by background noise. To do this, the suggested framework for PQE identification is given PQE data that has been tainted by white Gaussian noise with SNR values of 10 dB, 20 dB, 30 dB and 40 dB. The results show that the performance of the suggested framework slightly decreases with the degree of noise pollution in Table 6.6. However, the framework's performance under noisy background is still satisfactory. Therefore, using the suggested approach in a noisy environment is feasible.

Table 6.6: Performance of the proposed method under noisy environment

SNR value (dB)	**Accuracy (%)**
10	99.40
20	99.44
30	99.58
40	99.62

6.4.4 Performance Analysis with Other T-F Analysis

This section presents a comparison of the performance of the suggested TL technique using MSST-based T-F representation image with other T-F representation images. Several benchmark T-F analyses, including the "Short Time Fourier Transform" (STFT), "Continuous Wavelet Transform" (CWT), "Winger Ville Distribution" (WVD), "Stockwell Transform" (ST), "Hyperbolic Window Stockwell Transform" (HWST) and "Synchro Squeezing Transform" (SST), have been used to obtain the T-F representation images of PQE signals for this purpose. The PQE signal-converted T-F representation images are then input into four CNN models that have already been trained for automatic feature extraction. Four machine learning classifiers are then used to classify the features that have been extracted. Notably, the ANOVA test is used to examine the extracted features in this case as well and the classifier is given the top 500 discriminative features. The best feature extractor-classifier model's performance using the STFT, CWT, WVD, ST, HWST and SST T-F representation images is shown in Table 6.7. The optimum combination using MSST performs 0.7%, 0.57%, 0.49%, 0.15%, 0.09% and 0.13% better, respectively, according to the study shown in Table 6.7. For PQE identification, the MSST T-F representation-aided TL technique is hence more effective than other T-F representation-based approaches.

Table 6.7: Performance comparison with other T-F representation

T-F image	Best combination	Accuracy (%)
STFT	VGG16-RF	98.88
CWT	ResNet50-SVM	99.01
WVD	ResNet50-RF	99.09
ST	VGG16-RF	99.43
HWST	VGG16-RF	99.49
SST	VGG16-SVM	99.45
MSST	**VGG16-SVM**	**99.58**

6.4.5 Performance Analysis with Real-Life Power Quality Event Data

To determine the efficacy, the method's performance is verified using actual PQE data. Six distinct real-life PQE data sets were gathered from nearby utilities for this study. Table 6.9 reports the suggested method's validation performance. The performance is considered satisfactory based on the validation report. As a result, the suggested approach can potentially be applied in real-world scenarios to diagnose PQEs.

Table 6.8: Real-life PQE data from local utilities

PQEs	No. of collected data
Sag	20
Sag + Notch	15
Harmonics	25
Notch	20
Transient	15
Transient + Harmonics	15

Table 6.9: Validation performance using real-life PQE data

Accuracy (%)	Precision (%)	Specificity (%)	F1 score (%)
98.18	98.13	99.64	98.29

6.4.6 Comparative Analysis with Existing State of-the-Art Techniques

Table 6.10 presents a comparison between the suggested framework and current state-of-the-art methods. The performance of PQE identification utilizing the suggested framework is very similar to state-of-the-art methods, according to the results shown in Table 6.10. In comparison to state-of-the-art methods, the suggested framework also has the benefit of being able to identify more single and multiple PQEs. Additionally, the suggested solution eliminates the need for human feature extraction by automating the feature extraction process. As a result, the suggested approach is ideal for monitoring PQEs in EPS networks in real-life scenarios.

Table 6.10: Comparisons of proposed technique with other state-of-art techniques

Paper	**Year**	**No. of PQEs classified**	**Feature extraction mode**	**Accuracy (%)**
[100]	2018	14	Manual	99.46
[101]	2021	10	Manual	99.67
[72]	2015	22	Manual	99.09
[95]	2018	14	Manual	97.29
[75]	2016	13	Manual	99.37
[28]	2018	13	Manual	99.61
[105]	2019	16	Manual	99.81
[106]	2019	13	Automatic	99.46
[39]	2019	9	Automatic	99.67
[91]	2019	16	Automatic	99.69
[58]	2021	18	Automatic	99.86
[40]	2020	29	Automatic	97.84
[36]	2020	24	Automatic	99.26
This work	**-**	**36**	**Automatic**	**99.58**

6.5 Conclusions

An automated, precise and reliable technique for diagnosing single and multiple PQEs in an EPS network is presented in this work. PQE signals that correlate to 9 single PQEs and 27 mixed PQEs have been synthesized for this purpose. After that, the MSST procedure is used to encode the PQE signals into T-F spectrum images. The T-F images have now been put into a few pretrained CNN architectures for automatic deep feature extraction, including "VGG16," "ResNet50," "DenseNet201," and "InceptionV3." In the end, the features have been classified using a few benchmark machine learning classifiers. The following is a presentation of the work's noteworthy contributions.

• The suggested approach has an acceptable accuracy of 99.58% in identifying 36 distinct PQEs, both single and mixed.

• The suggested approach works well in noisy environments.

• When compared to other T-F spectrum images, MSST-based T-F spectrum images (i.e., MSST images) provided better deep feature extraction performance. This indicates that, in comparison to other T-F spectrum images, MSST images contain more relevant information about the PQE.

• This technique uses pretrained CNN models for deep feature extraction, which significantly reduces the high computational cost of creating a CNN model from scratch.

• The suggested method's accuracy has been determined to be significantly comparable with the cutting-edge approaches. Additionally, the suggested approach performs satisfactorily when tested on data from actual PQE occurrences.

Thus, it can be concluded that the suggested plan may be used to diagnose PQEs in EPS networks.

Chapter 7

Conclusions

7.1 Conclusions

The research presented in this thesis focuses on several techniques that can be used to identify and classify Power Quality Events (PQEs). It is possible that multiple PQEs may take place at the same time and overlap with each other. As a result, techniques for identifying and classifying multiple PQEs are discussed. It has two parts: analysis using signal processing techniques and analysis using artificial intelligence techniques. The methods presented in the study were chosen with the aim of reducing the overall computation time for PQE monitoring. Additionally, the suggested techniques perform satisfactorily in noisy background**s**, frequency fluctuations and with real-world data obtained from nearby power providers. The following paragraphs provide a summary of the salient points of this thesis.

Long-term power signal monitoring in a power station provides real-time PQE data. However, utility professionals are the only ones with access to this data. As a result, real-world data is always restricted. Simulated data is an alternative option for PQE research. However, as practical experience has shown, simulated data is always different from real-world data. Therefore, it is usually preferable that the study be conducted using data from real-world situations. However, in practice, it is not possible to produce real-world data with events exactly the way that one desires. Therefore, in Chapter 2, an experimental setup for PQE generation is built to address the difficulty.

In Chapter 3, the objective is to develop strategies for PQE analysis based on digital signal processing and requiring little human intervention. A signal tracker is introduced to extract actual events from the PQE signals generated by the specially designed experimental setup. Afterwards, a median filter is successfully applied to remove signals having sharp rising edges, so that the quantitative analyses can be processed appropriately to establish the presence of PQEs. In addition, Chapter 3 also discusses the successful use of a discrete Fourier transform and median filter-based approach to analyze generated PQE signals and determine whether events are present. Though these approaches appear to be simple and straightforward, their effectiveness in recognizing events is comparable to other methods used in recent times. The results show that the suggested methods provide efficient performance with 96.7% and 99.61% accuracy and less computational time without using conventional classifiers or complex mathematical tools. Therefore, the methods may be implemented in online applications to enhance Power Quality (PQ).

The next part of the work introduces artificial intelligence-based automated identification and classification of PQEs using image processing. Feature extraction techniques perform a crucial role in the automatic PQE classification method. Collaboration between the classification method and the feature extraction technique is vital. The S-transform is used in Chapter 4 to convert PQEs into time-frequency greyscale images. After that, the modified CNN architecture uses those images as input for both feature extraction and classification. The result shows that the proposed method effectively detects single as well as multiple PQEs with an acceptable accuracy of 99.83%. In Chapter 5, the hyperbolic window Stockwell transform is used to convert PQE signals into images. Afterwards, a deep neural network is designed using the stacking of three autoencoder**s** in order to extract deep features from the PQE signals converted by hyperbolic window Stockwell transform matrices. These automatically extracted features are then fed as input to several benchmark machine learning classifiers. According to the results, the XGBoost classifier delivers the best performance in classifying 18 different single and multiple PQEs with 99.86% accuracy. The proposed method also performs satisfactorily under background noise, frequency variation and with real-life PQEs data. Chapter 6 discusses a multisynchrosqueezing transform-based image processing and a pretrained CNN architecture-based feature extraction approach. The selection of significant features is done using one-way analysis of variance. Thereafter, several benchmark classifiers are used to classify the selected features. A total of 36 PQEs (9 single and 27 multiple) are categorized in this study. The results indicate that the features extracted by VGGNet16 and classified by the support vector machine can detect PQEs with an accuracy of 99.58%. Another advantage of the suggested method is that it detects a greater number of single and multiple PQEs than existing approaches. The marginal drop in accuracy is justified by the significant increase in the number of PQE signals, making it a more effective and scalable solution for real-world circumstances. The faster processing time, combined with acceptable accuracy, makes these techniques more suitable for practical applications, especially those requiring real-time performance.

7.2 Future Scope

To properly identify and classify multiple PQEs, the study described in the thesis uses carefully selected feature extraction and classification techniques. However, the field of multiple PQE identification and classification still has a lot of room for future research. For instance, it is possible to improve PQE monitoring by using a minimum number of features for event identification while maintaining accuracy, dependability and effectiveness. The computational load is reduced when a minimum number of features are chosen, which allows more attention to be given to the early detection of PQEs in future research. It is also necessary to look at the performance of different classifiers to determine an event. The increasing use of renewable energy sources such as wind and solar creates new types of PQEs due to their intermittency and variability. Therefore, other feasible multiple PQE combinations, which might include more than three concurrently occurring events, can be investigated in addition to the events included in this thesis. The various PQE monitoring approaches presented in this thesis are easily implementable in stand-alone modules based on microcontrollers for the Electrical Power System (EPS) networks. The development and refinement of advanced mitigation techniques that are both proactive and adaptive to dynamic grid conditions are essential for future power system resilience.

References

[1] O. Ellabban, H. Abu-Rub, and F. Blaabjerg, “Renewable energy resources: current status, future prospects and their enabling technology,” Renewable and Sustainable Energy Reviews, vol. 39, pp. 748–764, Nov. 2014.

[2] S. Das, A. K. Pradhan, A. Kedia, S. Dalai, B. Chatterjee, and S. Chakravorti, “Diagnosis of power quality events based on detrended fluctuation analysis,” IEEE Transactions on Industrial Electronics, vol. 65, no. 9, pp. 7322-7331, Sept. 2018.

[3] “IEEE recommended practice for monitoring electric power quality,” IEEE Std 1159-2019 (Revision of IEEE Std 1159-2009), pp. 1-98, Aug. 2019.

[4] H. Shareef, A. Mohamed, and A. A. Ibrahim, “An image processing based method for power quality event identification,” International Journal of Electrical Power & Energy Systems, vol. 46, pp. 184–197, March 2013.

[5] M. K. Saini and R. Kapoor, “Classification of power quality events–a review,” International Journal of Electrical Power & Energy Systems, vol. 43, no. 1, pp. 11–19, Dec. 2012.

[6] D. Granados-Lieberman, R. Romero-Troncoso, R. Osornio-Rios, A. Garcia-Perez, and E. Cabal-Yepez, “Techniques and methodologies for power quality analysis and disturbances classification in power systems: a review,” IET Generation, Transmission & Distribution, vol. 5, no. 4, pp. 519–529, April 2011.

[7] O. P. Mahela, A. G. Shaik, and N. Gupta, “A critical review of detection and classification of power quality events,” Renewable and Sustainable Energy Reviews, vol. 41, pp. 495–505, Jan. 2015.

[8] A. Augustine, R. D. Prakash, R. Xavier, and M. C. Parassery, “Review of signal processing techniques for detection of power quality events,” American Journal of Engineering and Applied Sciences, vol. 9, no. 2, pp. 364–370, April 2016.

[9] S. Avdakovic, A. Nuhanovic, M. Kusljugic, and M. Music, “Wavelet transform applications in power system dynamics,” Electric Power Systems Research, vol. 83, no. 1, pp. 237–245, Feb. 2012.

[10] S. Khokhar, A. A. B. M. Zin, A. S. B. Mokhtar, and M. Pesaran, “A comprehensive overview on signal processing and artificial intelligence techniques applications in classification of power quality disturbances,” Renewable and Sustainable Energy Reviews, vol. 51, pp. 1650–1663, Nov. 2015.

[11] O. A. Alimi, K. Ouahada, and A. M. Abu-Mahfouz, “A review of machine learning approaches to power system security and stability,” IEEE Access, vol. 8, pp. 113512–113531, 2020.

[12] T. Tarasiuk, “Comparative study of various methods of DFT calculation in the wake of IEC standard 61000-4-7,” IEEE Transactions on Instrumentation and Measurement, vol. 58, no. 10, pp. 3666-3677, Oct. 2009.

[13] U. Dwivedi, D. Shakya, and S. Singh, “Power quality monitoring and analysis: an overview and key issues,” International Journal of Systems Signal Control and Engineering Application, vol. 1, no. 1, pp. 74-88, 2008.

[14] F. Jurado and J. R. Saenz, “Comparison between discrete STFT and wavelets for the analysis of power quality events,” Electric Power Systems Research, vol. 62, no. 3, pp. 183-190, July 2002.

[15] Y. H. Gu and M. H. J. Bollen, “Time-frequency and time-scale domain analysis of voltage disturbances,” IEEE Transactions on Power Delivery, vol. 15, no. 4, pp. 1279-1284, Oct. 2000.

[16] S. Nath, P. Sinha, and S. K. Goswami, “A wavelet based novel method for the detection of harmonic sources in power systems,” International Journal of Electrical Power & Energy Systems, vol. 40, no. 1, pp. 54-61, Sept. 2012.

[17] H. Dehghani, B. Vahidi, R. A. Naghizadeh, and S. H. Hosseinian, “Power quality disturbance classification using a statistical and wavelet-based hidden Markov model with Dempster–Shafer algorithm,” International Journal of Electrical Power & Energy Systems, vol. 47, pp. 368-377, May 2013.

[18] A. Rodríguez, J. A. Aguado, F. Martín, J. J. López, F. Muñoz, and J. E. Ruiz, “Rule-based classification of power quality disturbances using S-transform,” Electric Power Systems Research, vol. 86, pp. 113-121, May 2012.

[19] N. Huang, D. Xu, X. Liu, and L. Lin, "Power quality disturbances classification based on S-transform and probabilistic neural network," Neurocomputing, vol. 98, pp. 12-23, Dec. 2012.

[20] Z. Moravej, A. A. Abdoos, and M. Pazoki, "New combined S-transform and logistic model tree technique for recognition and classification of power quality disturbances," Electric Power Components and Systems, vol. 39, no. 1, pp. 80-98, 2011.

[21] S. Hasheminejad, S. Esmaeili, and S. Jazebi, "Power quality disturbance classification using S-transform and hidden Markov model," Electric Power Components and Systems, vol. 40, no. 10, pp. 1160- 1182, 2012.

[22] M. J. B. Reddy, R. K. Raghupathy, K. P. Venkatesh, and D. K. Mohanta, "Power quality analysis using discrete orthogonal S-transform (DOST)," Digital Signal Processing, vol. 23, no. 2, pp. 616-626, March 2013.

[23] J. Li, Y. Yang, H. Lin, Z. Teng, F. Zhang, and Y. Xu, "A voltage sag detection method based on modified S transform with digital prolate spheroidal window," IEEE Transactions on Power Delivery, vol. 36, no. 2, pp. 997-1006, April 2021.

[24] S. He, K. Li, and M. Zhang, "A real-time power quality disturbances classification using hybrid method based on S-transform and dynamics," IEEE Transactions on Instrumentation and Measurement, vol. 62, no. 9, pp. 2465-2475, Sept. 2013.

[25] C. Liang et al., "A Kaiser window-based S-transform for time-frequency analysis of power quality signals," IEEE Transactions on Industrial Informatics, vol. 18, no. 2, pp. 965-975, Feb. 2022.

[26] I. W. C. Lee and P. K. Dash, "S-transform-based intelligent system for classification of power quality disturbance signals," IEEE Transactions on Industrial Electronics, vol. 50, no. 4, pp. 800-805, Aug. 2003.

[27] M. Biswal and P. K. Dash, "Estimation of time-varying power quality indices with an adaptive window-based fast generalised S-transform," IET Science, Measurement & Technology, vol. 6, no. 4, pp. 189–197, July 2012.

[28] M. V. Reddy and R. Sodhi, "A modified S-transform and random forests based power quality assessment framework," IEEE Transactions on Instrumentation and Measurement, vol. 67, no. 1, pp. 78-89, Jan. 2018.

[29] K. Nandi, R. Ghosh, B. Chatterjee, and S. Dalai, "Identification of Multiple Power Quality Disturbances based on Median Filter," 2022 IEEE Calcutta Conference (CALCON), Kolkata, India, 2022, pp. 273-277.

[30] S. Santoso, E. J. Powers, W. M. Grady, and A. C. Parsons, “Power quality disturbance waveform recognition using wavelet-based neural classifier. I. theoretical foundation,” IEEE Transactions on Power Delivery, vol. 15, no. 1, pp. 222-228, Jan. 2000.

[31] S. Santoso, E. J. Powers, W. M. Grady, and A. C. Parsons, “Power quality disturbance waveform recognition using wavelet-based neural classifier. II. application,” IEEE Transactions on Power Delivery, vol. 15, no. 1, pp. 229-235, Jan. 2000.

[32] S. Kaewarsa, K. Attakitmongcol, and T. Kulworawanichpong, “Recognition of power quality events by using multiwavelet-based neural networks,” International Journal of Electrical Power & Energy Systems, vol. 30, no. 4, pp. 254-260, May 2008.

[33] M. A. A. Lima, D. D. Ferreira, A. S. Cerqueira, C. A. Duque, M. V. Ribeiro, and J. M. De Seixas, “Separation and recognition of multiple PQ disturbances using independent component analysis and neural networks,” 2008 13th International Conference on Harmonics and Quality of Power, Wollongong, NSW, Australia, 2008, pp. 1-6.

[34] M. Oleskovicz, D. V. Coury, O. D. Felho, W. F. Usida, A. A. F. M. Carneiro, and L. R. S. Pires, “Power quality analysis applying a hybrid methodology with wavelet transforms and neural networks,” International Journal of Electrical Power & Energy Systems, vol. 31, no. 5, pp. 206-212, June 2009.

[35] H. Zhengyou, G. Shibin, C. Xiaoqin, Z. Jun, B. Zhiqian, and Q. Qingquan, “Study of a new method for power system transients classification based on wavelet entropy and neural network,” International Journal of Electrical Power & Energy Systems, vol. 33, no. 3, pp. 402-410, March 2011.

[36] J. Cai, K. Zhang, and H. Jiang, “Power Quality Disturbance Classification Based on Parallel Fusion of CNN and GRU,” Energies, vol. 16, no. 4029, pp. 1-12, May 2023.

[37] H. Liu, F. Hussain, Y. Shen, S. Arif, A. Nazir, and M. Abubakar, “Complex power quality disturbances classification via curvelet

transform and deep learning," Electric Power Systems Research, vol. 163(A), pp. 1-9, 2018.

[38] X. Xiao and K. Li, "Multi-label classification for power quality disturbances by integrated deep learning," IEEE Access, vol. 9, pp. 152250-152260, 2021.

[39] K. Cai, W. Cao, L. Aarniovuori, H. Pang, Y. Lin, and G. Li, "Classification of power quality disturbances using Wigner-Ville distribution and deep convolutional neural networks," IEEE Access, vol. 7, pp. 119099-119109, 2019.

[40] M. A. Ahajjam, D. B. Licea, M. Ghogho, and A. Kobbane, "Electric power quality disturbances classification based on temporal-spectral images and deep convolutional neural networks," 2020 International Wireless Communications and Mobile Computing (IWCMC), Limassol, Cyprus, 2020, pp. 1701-1706.

[41] C. Iturrino-García et al., "An innovative single shot power quality disturbance detector algorithm," IEEE Transactions on Instrumentation and Measurement, vol. 71, pp. 1-10, 2022.

[42] Abdullah, M. U. Khan, S. Aziz, A. Usman, and T. Jalil, "Soft computing approach for classification of complex power quality events," 2021 International Conference on Artificial Intelligence (ICAI), Islamabad, Pakistan, 2021, pp. 223-228.

[43] P. Zhang, Q. Feng, R. Chen, D. Wang, and L. Ren, "Classification and identification of power quality in distribution network," 2020 5th International Conference on Power and Renewable Energy (ICPRE), Shanghai, China, 2020, pp. 533-537.

[44] Y. Liao and J.-B. Lee, "A fuzzy-expert system for classifying power quality disturbances," International Journal of Electrical Power & Energy Systems, vol. 26, no. 3, pp. 199-205, March 2004.

[45] T. X. Zhu, S. K. Tso, and K. L. Lo, "Wavelet-based fuzzy reasoning approach to power-quality disturbance recognition," IEEE Transactions on Power Delivery, vol. 19, no. 4, pp. 1928-1935, Oct. 2004.

[46] A. A. Abdelsalam, A. A. Eldesouky, and A. A. Sallam, "Classification of power system disturbances using linear Kalman filter and fuzzyexpert system," International Journal of Electrical Power & Energy Systems, vol. 43, no. 1, pp. 688-695, Dec. 2012.

[47] J. Li, Z. Teng, Q. Tang, and J. Song, “Detection and classification of power quality disturbances using double resolution S-transform and DAG-SVMs,” IEEE Transactions on Instrumentation and Measurement, vol. 65, no. 10, pp. 2302-2312, Oct. 2016.

[48] Q. Tang, W. Qiu, and Y. Zhou, “Classification of complex power quality disturbances using optimized S-transform and kernel SVM,” IEEE Transactions on Industrial Electronics, vol. 67, no. 11, pp. 9715-9723, Nov. 2020.

[49] S. Aziz, M. U. Khan, Abdullah, A. Usman, and A. Mobeen, “Pattern analysis for classification of power quality disturbances,” 2020 International Conference on Emerging Trends in Smart Technologies (ICETST), Karachi, Pakistan, 2020, pp. 1-5.

[50] Abdullah, M. U. Khan, W. Ali, M. F. Shahzad, and S. Aziz, “A signal analysis approach towards detection and classification of power quality disturbances," 2020 First International Conference of Smart Systems and Emerging Technologies (SMARTTECH), Riyadh, Saudi Arabia, 2020, pp. 71-76.

[51] B. K. Panigrahi and V. R. Pandi, “Optimal feature selection for classification of power quality disturbances using wavelet packet-based fuzzy k-nearest neighbour algorithm," IET Generation, Transmission & Distribution, vol. 3, no. 3, pp. 296-306, March 2009.

[52] K. Manimala, K. Selvi, and R. Ahila, “Optimization techniques for improving power quality data mining using wavelet packet based support vector machine,” Neurocomputing, vol. 77, no. 1, pp. 36-47, Feb. 2012.

[53] C. -Y. Lee and Y. -X. Shen, “Optimal feature selection for power-quality disturbances classification,” IEEE Transactions on Power Delivery, vol. 26, no. 4, pp. 2342-2351, Oct. 2011.

[54] R. Hooshmand and A. Enshaee, “Detection and classification of single and combined power quality disturbances using fuzzy systems oriented by particle swarm optimization algorithm," Electric Power Systems Research, vol. 80, no. 12, pp. 1552-1561, Dec. 2010.

[55] H. Behera, P. Dash, and B. Biswal, “Power quality time series data mining using S-transform and fuzzy expert system,” Applied Soft Computing, vol. 10, no. 3, pp. 945-955, June 2010.

[56] B. Biswal, P. M. Dash, and S. Mishra, “A hybrid ant colony optimization technique for power signal pattern classification,” Expert Systems with Applications, vol. 38, no. 5, pp. 6368-6375, May 2011.

[57] K. Nandi, B. Chatterjee, P. Das, S. Dalai, and A. K. Das, "Detection of Multiple Power Quality Disturbances using Stockwell Transform and Convolutional Neural Network in Electrical Power System," 2023 IEEE 3rd Applied Signal Processing Conference (ASPCON), India, 2023, pp. 206-210.

[58] K. Nandi, A. K. Das, R. Ghosh, S. Dalai, and B. Chatterjee, “Hyperbolic window S-transform aided deep neural network model-based power quality monitoring framework in electrical power system,” IEEE Sensors Journal, vol. 21, no. 12, pp. 13695-13703, June 2021.

[59] R. H. G. Tan and V. K. Ramachandaramurthy, “Numerical model framework of power quality events,” European Journal of Scientific Research, vol.43, no.1, pp.30-47, 2010.

[60] M. A. S. Masoum, S. Jamali and N. Ghaffarzadeh, “Detection and classification of power quality disturbances using discrete wavelet transform and wavelet networks,” IET Science, Measurement and Technology, vol. 4, iss.4, pp 193-205, Jul 2010.

[61] R. Kumar, A. Saxena, R. Kumar, S. Marwaha, J. Singh and G. K. Singh, “A Comprehensive Overview on Modified Versions of Stockwell Transform For Power Quality Monitoring,” in IEEE Access, vol. 10, pp. 91963-91975, 2022.

[62] M. N. Dehaghani, T. Korõtko and A. Rosin, “AI Applications for Power Quality Issues in Distribution Systems: A Systematic Review,” in IEEE Access, vol. 13, pp. 18346-18365, 2025.

[63] C. Cui, Y. Duan, H. Hu, L. Wang and Q. Liu, “Detection and Classification of Multiple Power Quality Disturbances Using Stockwell Transform and Deep Learning,” in IEEE Transactions on Instrumentation and Measurement, vol. 71, pp. 1-12, 2022.

[64] M. Wang, Z. Deng, Y. Zhang and Z. Zhu, “An Automatic Identification Framework for Complex Power Quality Disturbances Based on Ensemble CNN,” in IEEE Access, vol. 11, pp. 56550-56560, 2023.

[65] L. Yin, R. Yang, M. Gabbouj and Y. Neuvo, “Weighted median filters: A tutorial,” IEEE Transactions on Circuits and Systems-II: Analog and Digital Signal Processing, vol.43, no. 3, pp. 157–192, 1996.

[66] S. Mishra, C. N. Bhende, and B. K. Panigrahi, “Detection and classification of power quality disturbances using S-transform and probabilistic neural network,” IEEE Transactions on Power Delivery, vol. 23, no. 1, pp. 280–287,2008.

[67] W. Tong, X. Song, J. Lin, and Z. Zhao, “Detection and classification of power quality disturbances based on wavelet packet decomposition and support vector machines,” in Proc. 8th Int. Conf. Signal Process., pp. 1–4, 2006.

[68] J. Huang, M. Negnevitsky, and D. T. Nguyen, “A neural fuzzy classifier for recognition of power quality disturbances,” IEEE Transactions on Power Delivery, vol. 17, no. 2, pp. 609–616, 2002.

[69] K. Wang, N. An, B. N. Li, Y. Zhang, and L. Li, “Speech emotion recognition using fourier parameters,” *IEEE Trans. on Affective Computing*, vol.6, no. 1, pp. 69-75, Jan.-Mar. 2015.

[70] S. K. Khare and V. Bajaj, “Time-frequency representation and convolutional neural network-based emotion recognition,” IEEE Transactions on Neural Networks and Learning Systems, vol. 32, no. 7, pp. 2901-2909, July 2021.

[71] O. Yildirim, M. Talo, B. Ay, U. B. Baloglu, G. Aydin, and U. R. Acharya, “Automated detection of diabetic subject using pre-trained 2D-CNN models with frequency spectrum images extracted from heart rate signals,” Computers in Biology and Medicine, vol. 113, 2019.

[72] S. Dalai, D. Dey, B. Chatterjee, S. Chakravorti and K. Bhattacharya, "Cross-Spectrum Analysis-Based Scheme for Multiple Power Quality Disturbance Sensing Device," in IEEE Sensors Journal, vol. 15, no. 7, pp. 3989-3997, July 2015.

[73] M. Biswal and P. K. Dash, “Measurement and classification of simultaneous power signal patterns with an S- transform variant and fuzzy decision tree,” IEEE Trans. Ind. Inf., vol. 9, no. 4, pp. 1819–1827, Nov. 2013.

[74] M. F. Faisal, A. Mohamed, A. Hussain, and M. Nizam, “Support vector regression-based S transform for prediction of single and multiple power quality disturbances,” Eur. J. Sci. Res., vol. 34, no. 2, pp. 237–251, 2009.

[75] M. V. Reddy and R. Sodhi, “A rule-based S-transform and adaboost based approach for power quality assessment,” Electr. Power Syst. Res., vol. 134, pp. 66–79, May 2016.

[76] K. Samanta, S. Chatterjee and R. Bose, "Cross-Subject Motor Imagery Tasks EEG Signal Classification Employing Multiplex Weighted Visibility Graph and Deep Feature Extraction," in IEEE Sensors Letters, vol. 4, no. 1, pp. 1-4, Jan. 2020.

[77] G. Liu, H. Bao, B. Han, "A Stacked Autoencoder-Based Deep Neural Network for Achieving Gearbox Fault Diagnosis.", Mathematical Problems in Engineering, vol. 2018, pp. 1-10, 2018.

[78] C. Zhang, et al. "Deep Sparse Autoencoder for Feature Extraction and Diagnosis of Locomotive Adhesion Status." Journal of Control Science and Engineering, Vol. 2018, pp. 1-9, 2018.

[79] A. Ashrafian, M. Rostami and G. B. Gharehpetian, "Hyperbolic S-transform-based method for classification of external faults, incipient faults, inrush currents and internal faults in power transformers,", IET Generation, Transmission & Distribution, vol. 6, no. 10, pp. 940-950, October 2012.

[80] N. R. Choudhury, S. S. Roy, A. Pal, S. Chatterjee and R. Bose, "Epileptic Seizure Detection Employing Cross-Hyperbolic Stockwell Transform," 2018 Fourth International Conference on Research in Computational Intelligence and Communication Networks (ICRCICN), Kolkata, India, 2018, pp. 70-74.

[81] https://in.mathworks.com/help/deeplearning/ref/trainautoencoder.html;jsessionid=27cf749c492279850cfcaf2984f9, "Train Auto encoder", Online document.

[82] R. Thirukovalluru, S. Dixit, R. K. Sevakula, N. K. Verma and A. Salour, "Generating feature sets for fault diagnosis using denoising stacked auto-encoder," 2016 IEEE International Conference on Prognostics and Health Management (ICPHM), Ottawa, ON, 2016, pp. 1-7.

[83] S. Wang and C. Manning, "Fast dropout training," in Proceedings of the International Conference on Machine Learning, JMLR.org, p. 118, 2013.

[84] M. Geng, W. Zhou, G. Liu, C. Li and Y. Zhang, "Epileptic Seizure Detection Based on Stockwell Transform and Bidirectional Long Short-Term Memory," in IEEE Transactions on Neural Systems and Rehabilitation Engineering, vol. 28, no. 3, pp. 573-580, March 2020.

[85] S. Singha Roy, K. Samanta, S. Modak, S. Chatterjee and R. Bose, "Cross Spectrum Aided Deep Feature Extraction Based Neuromuscular Disease

Detection Framework," in IEEE Sensors Letters, vol. 4, no. 6, pp. 1-4, June 2020.

[86] K. Kang, F. Gao and J. Feng, "A New Multi-Layer Classification Method Based on Logistic Regression," 2018 13th International Conference on Computer Science & Education (ICCSE), Colombo, 2018, pp. 1-4, doi: 10.1109/ICCSE.2018.8468725.

[87] F. F. Chamasemani and Y. P. Singh, "Multi-class Support Vector Machine (SVM) Classifiers -- An Application in Hypothyroid Detection and Classification," 2011 Sixth International Conference on Bio-Inspired Computing: Theories and Applications, Penang, pp. 351-356, 2011.

[88] A. K. Das, B. Ghosh, S. Dalai and B. Chatterjee, "Sensing surface contamination of Metal Oxide Surge Arrester through resistive leakage currentsignal analysis by Mathematical Morphology,", IEEE Sensors Journal, doi: 10.1109/JSEN.2020.2986677.

[89] J. Chen et al., “A parallel random forest algorithm for big data in a spark cloud computing environment,” IEEE Trans. Parallel Distrib. Syst., vol. 28, no. 4, pp. 919–933, Apr. 2017.

[90] I. Banerjee, S. S. Mullick, and S. Das, “On Convergence of the Class Membership Estimator in Fuzzy k-Nearest Neighbor Classifier,” IEEE Trans. Fuzzy Syst., vol. 27, no. 6, pp. 1226–1236, 2018.

[91] T. Zhong, S. Zhang, G. Cai, Y. Li, B. Yang and Y. Chen, "Power Quality Disturbance Recognition Based on Multiresolution S-Transform and Decision Tree," IEEE Access, vol. 7, pp. 88380-88392, 2019.

[92] I. L. Cherif and A. Kortebi, "On using eXtreme Gradient Boosting (XGBoost) Machine Learning algorithm for Home Network Traffic Classification," 2019 Wireless Days (WD), Manchester, United Kingdom, 2019, pp. 1-6, doi: 10.1109/WD.2019.8734193.

[93] C. W. N. F. C. W. Fadzal, W. Mansor, L. Y. Khuan and A. Zabidi, "Short-time Fourier Transform analysis of EEG signal from writing," 2012 IEEE 8th International Colloquium on Signal Processing and its Applications, Melaka, 2012, pp. 525-527, 2012.

[94] C.-C. Liao, H.-T. Yang, and H.-H. Chang, “Denoising techniques with a spatial noise-suppression method for wavelet-based power quality monitoring,” IEEE Trans. Instrum. Meas., vol. 60, no. 6, pp. 1986–1996, Jun. 2011.

[95] K. Thirumala, M. S. Prasad, T. Jain and A. C. Umarikar, "Tunable-Q Wavelet Transform and Dual Multiclass SVM for Online Automatic Detection of Power Quality Disturbances," in IEEE Transactions on Smart Grid, vol. 9, no. 4, pp. 3018-3028, July 2018.

[96] P. K. Mishra, U. Subudhi and S. Jain, "Power Quality Disturbances Classification with Deep Learning Approach," 2019 International Conference on Information Technology (ICIT), Bhubaneswar, India, 2019, pp. 273-278.

[97] Y. Wang and J. Orchard, "Fast Discrete Orthonormal Stockwell Transform." SIAM J. Scientific Computing. vol.31. pp. 4000-4012, 2009.

[98] S. S. Roy, S. Dey and S. Chatterjee, "Autocorrelation Aided Random Forest Classifier-Based Bearing Fault Detection Framework," in IEEE Sensors Journal, vol. 20, no. 18, pp. 10792-10800, 15 Sept.15, 2020.

[99] G. S. Chawda et al., "Comprehensive Review on Detection and Classification of Power Quality Disturbances in Utility Grid with Renewable Energy Penetration," IEEE Access, vol. 8, pp. 146807-146830, 2020.

[100] P. D. Achlerkar, S. R. Samantaray and M. S. Manikandan, "Variational Mode Decomposition and Decision Tree Based Detection and Classification of Power Quality Disturbances in Grid-Connected Distributed Generation System," IEEE Transactions on Smart Grid, vol. 9, no. 4, pp. 3122-3132, 2018.

[101] J. Liu, H. Song, H. Sun and H. Zhao, "High-Precision Identification of Power Quality Disturbances Under Strong Noise Environment Based on Fast ICA and Random Forest," IEEE Transactions on Industrial Informatics, vol. 17, no. 1, pp. 377-387, 2021.

[102] C. Zhao et al., "Novel Method Based on Variational Mode Decomposition and a Random Discriminative Projection Extreme Learning Machine for Multiple Power Quality Disturbance Recognition," IEEE Transactions on Industrial Informatics, vol. 15, no. 5, pp. 2915-2926, 2019.

[103] S. Dalai, B. Chatterjee, D. Dey, S. Chakravorti and K. Bhattacharya, "Rough-Set-Based Feature Selection and Classification for Power Quality Sensing Device Employing Correlation Techniques," IEEE Sensors Journal, vol. 13, no. 2, pp. 563-573, 2013.

[104] M. A. Rodriguez, J. F. Sotomonte, J. Cifuentes and M. Bueno-López, "Classification of Power Quality Disturbances using Hilbert Huang Transform and a Multilayer Perceptron Neural Network Model," Proceedings of International Conference on Smart Energy Systems and Technologies (SEST), Porto, Portugal, pp. 1-6, 2019.

[105] M. Sahani and P. K. Dash, "FPGA-Based Online Power Quality Disturbances Monitoring Using Reduced-Sample HHT and Class-Specific Weighted RVFLN," IEEE Transactions on Industrial Informatics, vol. 15, no. 8, pp. 4614-4623, Aug. 2019, doi: 10.1109/TII.2019.2892873.

[106] Wei Qiu, Qiu Tang, Jie Liu, Zhaosheng Teng, Wenxuan Yao,"Power Quality Disturbances Recognition Using Modified S Transform and Parallel Stack Sparse Auto-encoder," Electric Power Systems Research, vol. 174, 105876, 2019.

[107] G. Yu, Z. Wang, and P. Zhao, "Multisynchrosqueezing transform," IEEE Trans. Ind. Electron., vol. 66, no. 7, pp. 5441–5455, Jul. 2019.

[108] S. Meignen, T. Oberlin, and D.-H. Pham, "Synchrosqueezing transforms: From low-to high-frequency modulations and perspectives," Comp. Rendus Phys., vol. 20, no. 5, pp. 449–460, Jul. 2019.

[109] A. K. Das, S. Deb, D. Dey, B. Chatterjee and S. Dalai, "Multisynchrosqueezing Transform Based Improved Time-Frequency Representation for Automated Contamination Severity Estimation of Overhead Line Insulator," IEEE Sensors Journal, vol. 22, no. 12, pp. 12098-12106, 2022.

[110] S. K. Khare, V. Bajaj and U. R. Acharya, "SPWVD-CNN for Automated Detection of Schizophrenia Patients Using EEG Signals," IEEE Transactions on Instrumentation and Measurement, vol. 70, pp. 1-9, 2021.

[111] A. K. Das, D. Dey, B. Chatterjee and S. Dalai, "A Transfer Learning Approach to Sense the Degree of Surface Pollution for Metal Oxide Surge Arrester Employing Infrared Thermal Imaging," IEEE Sensors Journal, vol. 21, no. 15, pp. 16961-16968, 2021.

[112] A. Shamsi et al., "An Uncertainty-Aware Transfer Learning-Based Framework for COVID-19 Diagnosis," IEEE Transactions on Neural Networks and Learning Systems, vol. 32, no. 4, pp. 1408-1417, April 2021, doi: 10.1109/TNNLS.2021.3054306.

[113] S. Shao, S. McAleer, R. Yan and P. Baldi, "Highly Accurate Machine Fault Diagnosis Using Deep Transfer Learning," IEEE Transactions on Industrial Informatics, vol. 15, no. 4, pp. 2446-2455, April 2019, doi: 10.1109/TII.2018.2864759.

[114] C. Wang et al., "Pulmonary Image Classification Based on Inception-v3 Transfer Learning Model," IEEE Access, vol. 7, pp. 146533-146541, 2019, doi: 10.1109/ACCESS.2019.2946000.

Viron Qandi.
11.12.2025